SANDIA REPORT

SAND2003-8784
Unlimited Release
Printed November 2003

Assuring Ultra-Clean Environments in Microsystem Packages: Irreversible and Reversible Getters

L. Whinnery, J. McElhanon, G. Buffleben, T. Zifer, J. Hollenshead, B. Nilson

Prepared by
Sandia National Laboratories
Albuquerque, New Mexico 87185 and Livermore, California 94550

Sandia is a multiprogram laboratory operated by Sandia Corporation, a Lockheed Martin Company, for the United States Department of Energy under Contract DE-AC04-94AL85000.

Approved for public release; further dissemination unlimited.

Sandia National Laboratories

Issued by Sandia National Laboratories, operated for the United States Department of Energy by Sandia Corporation.

NOTICE: This report was prepared as an account of work sponsored by an agency of the United States Government. Neither the United States Government, nor any agency thereof, nor any of their employees, nor any of their contractors, subcontractors, or their employees, make any warranty, express or implied, or assume any legal liability or responsibility for the accuracy, completeness, or usefulness of any information, apparatus, product, or process disclosed, or represent that its use would not infringe privately owned rights. Reference herein to any specific commercial product, process, or service by trade name, trademark, manufacturer, or otherwise, does not necessarily constitute or imply its endorsement, recommendation, or favoring by the United States Government, any agency thereof, or any of their contractors or subcontractors. The views and opinions expressed herein do not necessarily state or reflect those of the United States Government, any agency thereof, or any of their contractors.

Printed in the United States of America. This report has been reproduced directly from the best available copy.

Available to DOE and DOE contractors from
U.S. Department of Energy
Office of Scientific and Technical Information
P.O. Box 62
Oak Ridge, TN 37831

Telephone: (865)576-8401
Facsimile: (865)576-5728
E-Mail: reports@adonis.osti.gov
Online ordering: http://www.osti.gov/bridge

Available to the public from
U.S. Department of Commerce
National Technical Information Service
5285 Port Royal Rd
Springfield, VA 22161

Telephone: (800)553-6847
Facsimile: (703)605-6900
E-Mail: orders@ntis.fedworld.gov
Online order: http://www.ntis.gov/ordering.htm

SAND2003-8784
Unlimited Release
Printed November 2003

Assuring Ultra-Clean Environments in Microsystem Packages: Irreversible and Reversible Getters

LeRoy Whinnery, Jim McElhanon, George Buffleben, Tom Zifer
Materials Chemistry Department

Jeromy Hollenshead and Bob Nilson
Fluid and Thermal Science Department
Sandia National Laboratories
P.O. Box 969
Livermore, CA 94551-0969

Abstract

A new generation of irreversible, chemically reacting getters specifically targeted toward assuring the integrity of the local environment within microsystem packages were developed and evaluated. These reactive getters incorporate volatile species into a polymer through covalent bonds, thus producing a non-volatile product. These reactive getters will be combined with getters that rely on absorption media (*e.g.* zeolites and high surface area carbon fibers) to scavenge non-reactive species, like solvents. Our getter systems will rely on device packaging to limit exchange between the microsystem and the global environment. Thus, the internal getters need only provide local environmental control within the microsystem package. A series of experiments were conducted to determine uptake rates and capacities absorption and reactive-based getters. Diffusion rates through the binder used to hold the getter particles together were also investigated. Getters were evaluated in environments with a saturated headspace and with a limited amount of the volatile species of interest.

One- and two-dimensional numerical models and analysis techniques have been developed and used to predict the transport of contaminant species within a representative microsystem package consisting of an open gas-filled volume adjacent to a polymer layer containing embedded particles of getter. The two-dimensional model features explicit representation of the individual getter particles while the one-dimensional treatment assumes a homogeneous distribution of getter material within the getter/polymer layer. Example calculations illustrate the dependence of getter performance on reaction rates, polymer diffusivity, and getter particle volume fraction. In addition, the model is used to deduce surface reaction rates, solid phase diffusivities, and maximum-loading densities by least-squares fitting of model predictions to measured histories of gas-phase contaminant concentration and getter weight gain.

This page intentionally left blank

Contents

ABSTRACT **3**

CONTENTS **5**

1. INTRODUCTION **7**

2. EXPERIMENTAL MATERIALS AND METHODS **9**

2.1 CHEMICALS AND MATERIALS 9
2.2 ABSORPTION-BASED GETTER STUDIES 9
2.3 REACTION-BASED GETTER STUDIES 9
2.4 BINDER DIFFUSION STUDIES 10
2.5 GETTER REACTIVITY AND CAPACITY IN SATURATED ENVIRONMENTS 10
2.6 GETTER REACTIVITY IN UNSATURATED ENVIRONMENTS – GAS PHASE IR STUDIES 10

3. EXPERIMENTAL RESULTS AND DISCUSSION **13**

3.1 ABSORPTION-BASED GETTER RESULTS 13
3.2 REACTION-BASED GETTER RESULTS 15
3.3 DIFFUSION THROUGH BINDER 19
3.4 GETTER REACTIVITY AND CAPACITY IN SATURATED ENVIRONMENTS 20
3.5 GETTER REACTIVITY IN UNSATURATED ENVIRONMENTS RESULTS – GAS PHASE IR STUDIES 23

4. MICROSYSTEM SIMULATION AND EXPERIMENTAL ANALYSIS **31**

4.1 PROBLEM DESCRIPTION AND MODELING APPROACH 32
4.2 ONE-DIMENSIONAL MODEL 34
4.3 ADVANCED TWO-DIMENSIONAL MODELING 44
4.4 ANALYSIS OF EXPERIMENTS 61

5. PROJECT SUMMARY AND FUTURE WORK **81**

6. ACKNOWLEDGEMENTS **85**

7. REFERENCES **87**

8. DISTRIBUTION **89**

This page intentionally left blank

1. Introduction

Microsystems are currently being evaluated as possible replacements for a number of weapon subsystems with the expectation of improved surety combined with reduced weight and volume. However, there is great concern that long periods of dormant storage[1] may impair the mechanical functioning of microdevices that are exposed to water, out gassing products (organics, solvents and silicones) and particulates (talc and dust). Low temperature operating environments and small moving parts in contact with stationary and mating structures, make capillary condensation, ice formation and corrosion true concerns for microsystems.

Contaminants are present from a variety of sources. Some contaminants are present from when the microsystem is first produced and others are introduced over time. Examples of contaminants initially present are cleaning solvents, particles, water and anything else present in the atmosphere of the microsystem at the time it is sealed. Additional water can diffuse out of packaging materials over time. Degradation of organic materials within the microsystem by a variety of aging mechanisms can also contribute contaminants. Finally, diffusion of species through packaging, joints and o-rings can be responsible for introduction of significant contaminants over time.

Water is not only a concern from a corrosion standpoint but can also cause mechanical components to become immobilized due to capillary condensation and freezing. Small particles (talc) are known to cause problems for micro electrical mechanical (MEM's) devices and steps are taken to minimize their presence. Even in the ideal case that no contaminants were present at the time of manufacture, diffusion, corrosion and aging can all lead to contamination. Getters tailored toward removing specific contaminants expected in a given microsystem can provide a great deal of protection. Absorbing these contaminants in a safe location with the microsystem is one approach to minimizing the effect that contaminants will have on the function of a MEM's device.

Past weapons experience provides little guidance, and the desiccants currently used to manage system-wide moisture levels cannot be relied on to provide the more stringent control needed to assure microsystem reliability. Existing getters generally rely on van der Waals attractive forces to reduce the availability of volatile species. While the equilibrium may be shifted toward the bound product, the dissociation is still accessible at room temperature. This is evidenced by the redistribution of absorbed water in a sieve-type desiccant bed over time. However, a more robust covalent attachment would effectively eliminate dissociation at lower temperatures. Our approach has been to make use of these covalent attachments by chemically reacting volatile species out of the local atmosphere of microsystems.

We have evaluated, through experiments and subsequent modeling analysis, the performance of several reactive and non-reactive getters to chemical species of interest. The experimental procedures and results are discussed first, followed by the mathematical descriptions of the gettering process where they are used to analyze the available experimental data, and make some estimates of getter performance in microsystem packages.

This page intentionally left blank

2. Experimental Materials and Methods

2.1 Chemicals and Materials

Isocyanate, polymer bound, poly(maleic anhydride-alt-1-octadecane), poly(ethylene-alt-maleic anhydride), hexamethyl disiloxane (HMDS), perfluorohexane (PFH), ethylbenzene (EB) and 1,1,1-trichloroethane (TCE) and 4-dimethylaminopyridine (DMAP) were obtained from Aldrich Chemical Co.. Each was placed on a vacuum line and dried for at least 24 hours before use. Ethanol (100%), iso-propanol, and potassium bromide were obtained from Aldrich and used as received. Deionized (18 Mega Ohm) water was produced in house using a Barnstead "NANOpure" ultra water system . ScavengePore Resin fibers were provided by Rapp Polymere. Ricon 130 was obtained from Sartomer. Ricon was prepared by vacuum stripping to remove any volatile components and mixed with anti-oxidant preservatives. Supelco supplied several different SPME fiber getter materials

2.2 Absorption-based Getter Studies

A glass vial fitted with a Teflon Mininert sampling valve served as the sample container. The container and valve assembly have a total volume of 39.2 ml. The sample mixture was prepared by first evacuating the container and then introducing the appropriate amounts of the liquid model compounds to obtain equimolar concentrations of each species. The liquid samples readily volatilized as the pressure in the system was below the saturation limit. The sample vials were then back filled with nitrogen to atmospheric pressure.

An SPME fiber was placed into the container containing the compounds where it was allowed to absorb the vapor phase mixture for 2 min at room temperature. The loaded fiber was then placed into the heated injector of an HP 5890 Gas Chromatograph where the chemicals were allowed to desorb for two minutes. The mixture was then separated on an HP-5MS capillary column. The column was kept at 45°C for two minutes then ramped at 10°C/min to 150°C. The carrier gas was hydrogen at 6 psi head pressure and the detector was a flame ionization detector (FID).

While the injector temperature was nominally at 150°C for much of the desorption analysis, additional fibers were also evaluated at injector temperatures ranging from 75°C to 250°C in order to estimate the retention of the compounds at these temperatures.

2.3 Reaction-based Getter Studies

The method selected for determining the maximum gettering capacity of isocyanates and anhydride polymers involved recording weight changes of the getter material upon reaction with an excess of reactive species (water, ethanol and iso-propanol). Experiments were performed in a Teflon sealed reaction chamber containing a known amount of polymeric getter and a large excess of water, ethanol, or iso-propanol. Typically, reaction/exposure times were on the order of days and up to a month. Weight change data was collected periodically. At the end of each experiment, the getter material was vacuum dried, the final weight changes were recorded and the getter materials were examined by infrared (IR) spectroscopy (BIORAD, model FTS-40). IR spectroscopy proved to be an ideal method for evaluating functional group changes that occurred in the getter materials upon reaction with water, ethanol and iso-propanol.

2.4 Binder Diffusion Studies

Ricon was prepared by vacuum stripping to remove any volatile components and mixed with anti-oxidant preservatives. The tacky polymer was used as the binder to help minimize the generation of particles, as well as, scavenge particles generated from other sources in the local environment of the microsystem.

Thick films of Ricon 130 (1mm, 5mm and 10mm) were placed in sealed chambers with a saturated gas headspace of either water or ethanol. The films were weighed periodically to determine the rate of water and ethanol absorption in the binder material. The containers used for the thick films were round straight walled aluminum containers with an internal diameter of 49.6 mm resulted in an exposed surface area of 19.32 cm^2 for the Ricon 130.

2.5 Getter Reactivity and Capacity in Saturated Environments

The procedure for determining the capacity of the isocyanate and anhydride polymer getters involved weighing several samples of identical weights (approx. 100-500 mg) of a getter into glass vials. The open vials were then placed into a Teflon sealed glass chamber which contained a large excess of either deionized water, ethanol, or iso-propanol. In some experiments, between 10-33 weight percent of a catalyst (*e.g.* Nafion®) was added to some getter samples for testing. Samples were allowed to react over a period of days to months in the sealed environments. Periodically, samples were removed from the chamber, weighed, and vacuum dried until a final, constant weight was obtained. Reactivity was also monitored by infrared spectroscopy (BIORAD, model FTS-40) of reacted getter samples (KBr pellets).

2.6 Getter Reactivity in Unsaturated Environments – Gas Phase IR Studies

While the results described in the previous section are observed when the gas phase concentrations are near saturation a more realistic evaluation of getter reactivity in microsystems can be performed using only limited quantities (ppm) of analyte. Here, a Fourier Transform Infrared Spectrometer (FTIR) (BIORAD, model FTS-40) was used to monitor analyte concentration changes in the vapor phase as either water or ethanol are removed by the getter in a closed experimental cell. Stainless steel gas IR cells with sapphire windows in Conflat flanges were used. The cells are 14.4 cm long with a 3.5 cm inner diameter. The getter material, typically placed into the cell on aluminum foil, was exposed to ethanol, ethanol-d_6, or D_2O in one of two ways.

In the first method, the cell is filled with air containing a known amount of solvent in the gas phase. The gas phase solvent concentration was controlled by flowing dry air through a dyna-calibrator (model 190) obtained from VICI Metronics containing a permeation tube (also from VICI Metronics) filled with the analyte of interest. The permeation tube has a known permeation rate of solvent at a given temperature. Changing the rate of airflow to the cell controls the concentration. In the second method, a series of 10 µl drops of the solvent were added to the cell using a syringe. The liquid solvent remained separated from the getter sample and evaporated into the cell at room temperature. The first method of introducing analytes lets us examine the getters ability to remove a limited amount of analyte and measure the lower bounds of its ability

to remove the analyte. The second method lets us examine the getters performance when exposed to a substantial percentage (10-20% per drop) of the getters capacity.

Four different getters were evaluated. The first two, poly (ethylene-alt-maleic anhydride) (PEMA) from Aldrich and 5 Å molecular sieves (W. A. Hammond Drierite Co.), were mixed in a polybutadiene binding matrix (either Ricon 130 or Ricon 156) by hand in a 1:1 ratio. The second two getters were commercially available: Staydry Hicap2000 and Staydry GA2000, both from Cookson Electronics.

The IR spectrometer was run in absorbance mode with a resolution of 4 wave numbers against a reference cell containing air. Peak heights were used to quantify the amount of a species present within the IR cell. All measurements were made at room temperature unless otherwise noted. D_2O and ethanol-d_6 are used in most of these experiments to eliminate background interferences from humidity and other contaminates.

This page intentionally left blank

3. Experimental Results and Discussion

With the expectation that microsystems would ultimately be used inside a weapon, we chose the W80, currently undergoing a Life Extension Program (LEP) as a model environment that a microsystem might experience. Thornberg and Borek have reported gas analysis of the internal environment of the W80 warhead.[2] Of the unreactive volatile species observed by Thornberg and Borek, we were able to group the major constituents into 4 groups (silicones, perfluoroalkanes, hydrocarbons and hydrochlorocarbons) and chose model compounds to represent these groups. The model compounds are hexamethyl disiloxane (HMDS), perfluorohexane (PFH), ethylbenzene (EB) and 1,1,1-trichloroethane (TCE). Both gas and liquid cocktails of these compounds were prepared and monitored as a function of time to ensure the integrity of the data.

3.1 Absorption-based Getter Results

Absorption based getters for non-reactive volatiles were evaluated by solid phase micro-extraction (SPME). The SPME fiber consists of a small glass rod coated with getter material and mounted onto a holder to aid the sampling procedures. Supelco supplies several different SPME fiber getter materials for use with a broad range of chemical species. For this work, we used two types, a PDMS (polydimethylsiloxane) fiber and a Carboxen/PDMS fiber. Carboxen is a high surface area carbon that is imbedded in a PDMS matrix on the glass fiber. The SPME fiber is exposed to a particular environment, followed by thermal desorption onto a GC column for analysis. The carbons on these fibers are available in bulk and have been designed to have selective affinities for particular classes of compounds.

Initially an equimolar mixture of the four analytes was characterized by taking a 200 μl gas sample of the headspace above the liquid in the container and introducing it directly into the GC. From this experiment we were able to identify the peaks and establish a reference by which we could evaluate the SPME fibers for this set of model compounds. The results in Figure 1 (top) shows the response expected for each analyte based on its population in the sample mixture. The chromatogram shown in the bottom of Figure 1 demonstrates the effectiveness of the Carboxen/PDMS fiber to absorb the individual analytes. In this Carboxen/PDMS experiment the fiber was exposed to the analyte mixture for two minutes at room temperature then desorbed in the GC injector at 150°C for two minutes. From these results it is clear that the Carboxen/PDMS fiber has the greatest affinity for ethyl benzene. A second desorption at 150°C of this same fiber yielded no additional evolution of the analytes, however when the desorption temperature was raised to 250°C an additional 10% of the ethyl benzene was liberated. This would indicate a reasonable affinity for ethyl benzene even at 150°C. There also appears to be little or no affinity for the perfluorohexane.

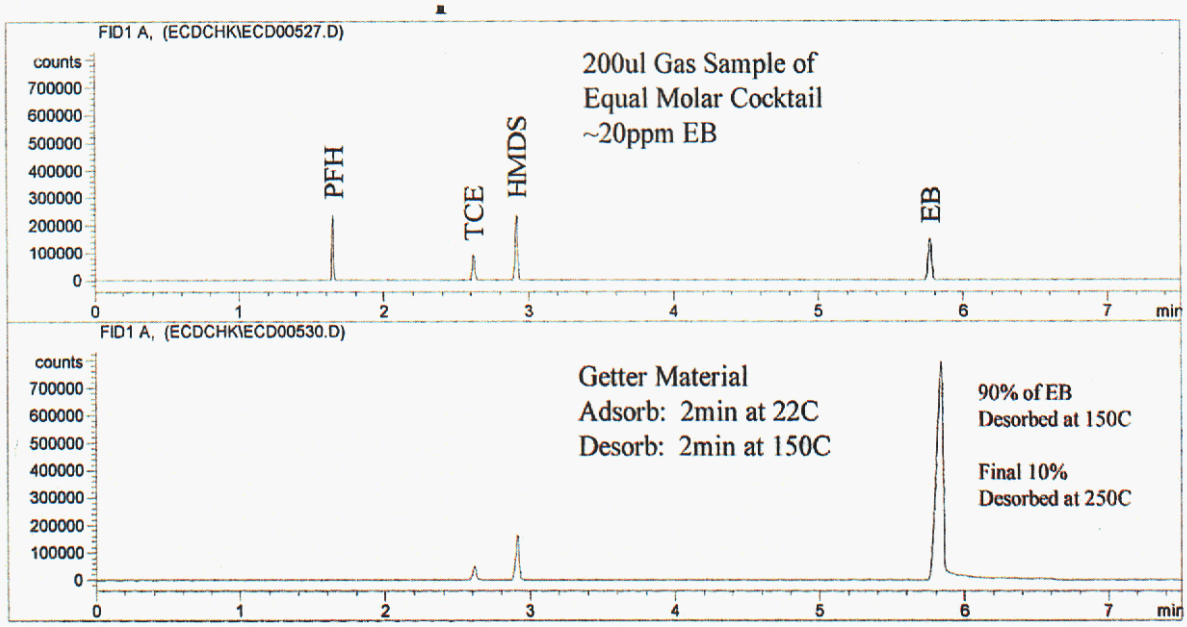

Figure 1. GC Analysis of the four analyte mix resulting from injection of a gas sample of the headspace (top) and desorption of a Carboxen/PDMS coated SPME fiber (bottom).

Figure 2 shows the ethylbenzene thermal desorption results of exposure of two different SPME fibers to an equal molar mixture of the four model compounds. One fiber was a Carboxen/PDMS and the other was only PDMS. In this experiment, the fiber was loaded by exposure to the sample mixture headspace for two minutes at room temperature. Then the loaded fiber was desorbed in the injector for two minutes at 75°C then removed. The fiber was stored at room temperature during the analysis of the desorption products. Then the injector temperature was increased to 100°C and the fiber was reintroduced into the injector for two minutes and removed for the analysis of the desorption species. This was repeated at 150°C, 200°C, and 250°C.

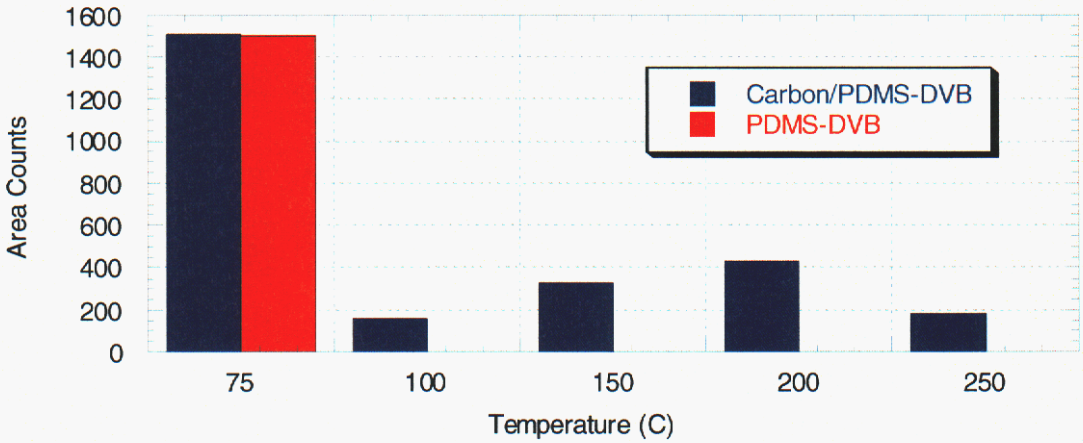

Figure 2. Thermal desorption profile of ethylbenzene on carbon/PDMS-DVB and PDMS-DVB.

Perfluorohexane was not observed from either fiber over the temperature range examined, 75-250°C. Hexamethyl disiloxane, 1,1,1-trichloroethane and ethylbenzene were observed upon

desorption from both fibers at 75°C with a much greater capacity for ethylbenzene. However, the carbon-loaded fiber showed continued desorption of ethylbenzene as the injection port temperature was raised, indicating a higher affinity or thermal stability for the carbon-ethylbenzene association. The temperatures required to desorb the ethylbenzene is a positive sign that this carbon, and possibly others, will hold on to hydrocarbons fairly well as part of a getter system.

3.2 Reaction-based Getter Results

For the two reactive volatile species, i.e. water and ethanol, we evaluated uptake with two different experimental set-ups. The first has the getter material in an open vial that is inside a larger closed vessel containing liquid ethanol or water and therefore a saturated vapor in the atmosphere. This method allows us to have several vials of materials and mixtures of materials in the same atmosphere at the same time for simultaneous evaluation, thus saving a significant amount of time and allowing for more reliable comparisons between materials. The uptake is monitored by mass of each vial as a function of time.

The second set-up involves liquid phase reactions with the getter material in direct contact with the alcohol or combination of alcohol and solvent. This method has a semi-infinite amount of the alcohol that should dramatically help the kinetics. It also allows us to take samples of the liquid for analysis on an NMR to monitor the progress with time.

Two reactions have been probed using the first experimental set-up (vapor phase). First, the acid catalyzed reaction of epoxides with water and alcohols to produce a hydroxy alkoxide and a dihydroxide, respectively.[3] The epoxide we used is tris (2,3-epoxypropyl) isocyanurate (TEPI), a non-volatile solid with a mass of 99 g/mole per epoxide functional group. The solid acid catalyst we chose was Nafion, a porous nanocomposite of 10-20% fluorosulfonic acid polymer on amorphous silica. Finally, the Nafion catalyst and the TEPI were mixed into a viscous oil of polybutadiene (PB), Ricon-130 or Ricon-150. The tacky polymer was used as the binder to help minimize the generation of particles, as well as, scavenge particles generated from other sources in the local environment of the microsystem. The results of exposing this combination and each of the individual components to ethanol vapor are shown in Figure 3.

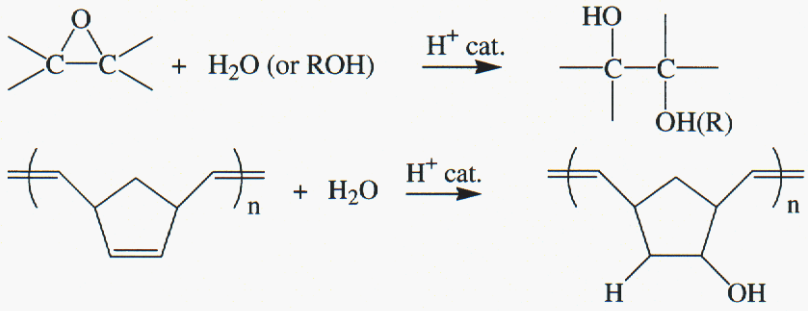

Figure 3. Reaction chemistries for the acid catalysis of water and alcohols reacting with epoxides and olefins.

The second reaction, also shown in Figure 3, is the acid catalyzed addition of ethanol across an olefin. The acid chosen is the same as above, Nafion. The olefin selected, polynorbornene, is a

non-volatile solid and contains a highly alkyl-substituted and strained ring olefin. The final product is expected to have less ring strain, thus providing driving force for the reaction and making the reverse reaction less likely.

The graph in Figure 4 shows an increase in mass for most of the vials (except for the epoxide and each of the polybutadienes) with time. Each of the materials appears to reach an equilibrium where the curves level out. After approximately 1100 hours, the vials were evacuated to remove adsorbed ethanol. Any remaining mass above the starting mass should be due to reacted ethanol. After evacuation, one vial had less mass and three vials had more mass than when they started. The vial with less mass may have had surface adsorbed water initially, that was removed under vacuum. Three materials, polynorbornene, polybutadiene/Nafion/polynorbornene and polybutadiene/Nafion/tris(2,3-epoxypropyl) isocyanurate, showed an increase in mass of 2-3 percent. Due to the loading fraction of the epoxide or olefin in the mixtures above, complete reaction would result in an increase of 7 and 14 percent, respectively.

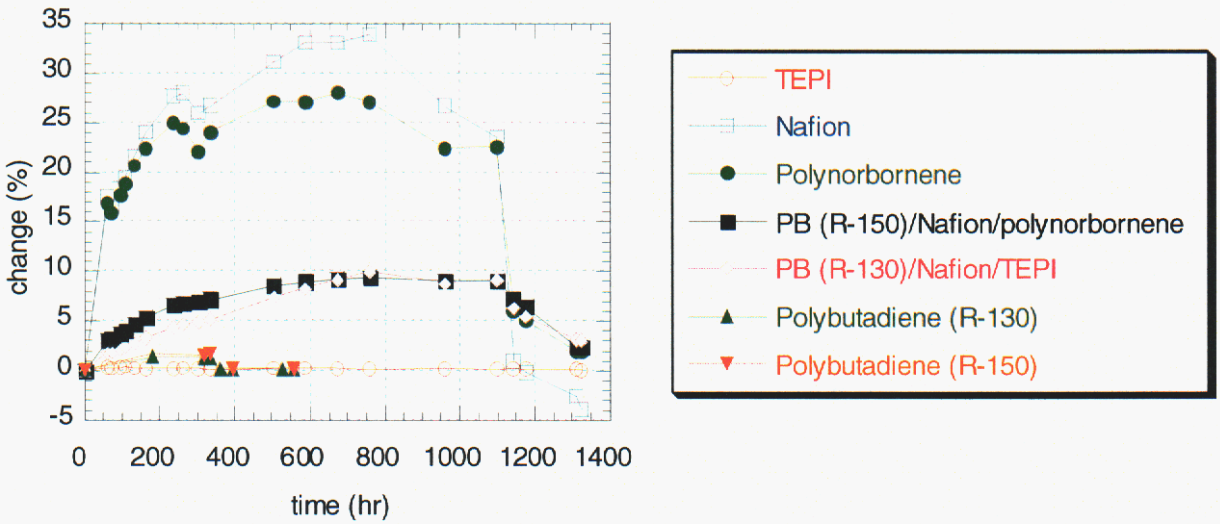

Figure 4. Mass change with time upon exposure to ethanol vapor.

Since the vapor phase tests outlined above are only indicative of mass changes, we also looked at these reactions in the liquid phase where we could monitor the reactions by NMR. ^{1}H NMR (Varian Gemini, 300 MHz) experiments examining the irreversible reaction of TEPI with iso-propanol and ethanol in the presence of Nafion acidic resin were examined. No evidence of ring opening of the epoxide by ethanol or iso-propanol has been found. It was later pointed out that the Nafion used in this experiment was most likely in a hydrated state (as an oxonium salt). The oxonium salts are known to be much less acidic than the hydrate-free sulfonic acid and could account for the poor reactivity observed. Recently, lanthanide ion exchange resins have been reported to catalyze ring opening of epoxides in quantitative yield.[4] A terbium ion exchange resin was prepared from Amberlyst 15, a sulfonic acid catalyst, as an alternative to the Nafion catalyst used in our initial studies. NMR experiments revealed complete reaction of TEPI with ethanol in the presence of the Yb ion exchange resin when the reaction was conducted in refluxing EtOH. Due to successes with other reaction chemistries, this approach was not explored further.

Additional chemistries were examined to irreversibly react with water and alcohols. The method selected for determining the maximum gettering capacity of isocyanates and anhydride polymers involved recording weight changes of the getter material upon reaction with an excess of reactive species (water, ethanol and iso-propanol). Experiments were performed in a Teflon sealed reaction chamber containing a known amount of polymeric getter and a large excess of water, ethanol, or iso-propanol. Typically, reaction/exposure times were on the order of days and up to a month. Weight change data was collected periodically. At the end of each experiment, the getter material was vacuum dried, the final weight changes were recorded and the getter materials were examined by infrared (IR) spectroscopy. IR spectroscopy proved to be an ideal method for evaluating functional group changes that occurred in the getter materials upon reaction with water, ethanol and iso-propanol.

One of the getter materials evaluated was a commercially available isocyanate polymer, Isocyanate, polymer bound (ICPB) (Aldrich), **1**. The polymer, as received, consisted of *ca.* 2 mmol isocyanate per gram of material. The theoretical percent weight change for this getter was determined to be -5.2, 9.2 and 12.0%, for water, ethanol and iso-propanol, respectively. For the reaction between isocyanate and water, weight loss occurs due to CO_2 emission during the course of the reaction (Figure 5). Treatment of this isocyanate polymer with the reactive species for one week as described above yielded experimental capacity values of –1.9, 2.7, and 2.7% for water, ethanol, and iso-propanol, respectively. It was postulated that the low capacity values and reactivity observed could be improved by addition of an amine catalyst. Accordingly, we performed analogous gettering experiments incorporating a 66/33 weight percent mixture of isocyanate polymer to ScavangePore phenethyl piperidine catalyst (Rapp Polymere). Even after two weeks of reaction, capacity values of –1.3, 2.0, and 5.5% for water, ethanol, and iso-propanol, respectively, were obtained. These results indicate that addition of this amine catalyst has little effect on enhancing the isocyanate's gettering ability.

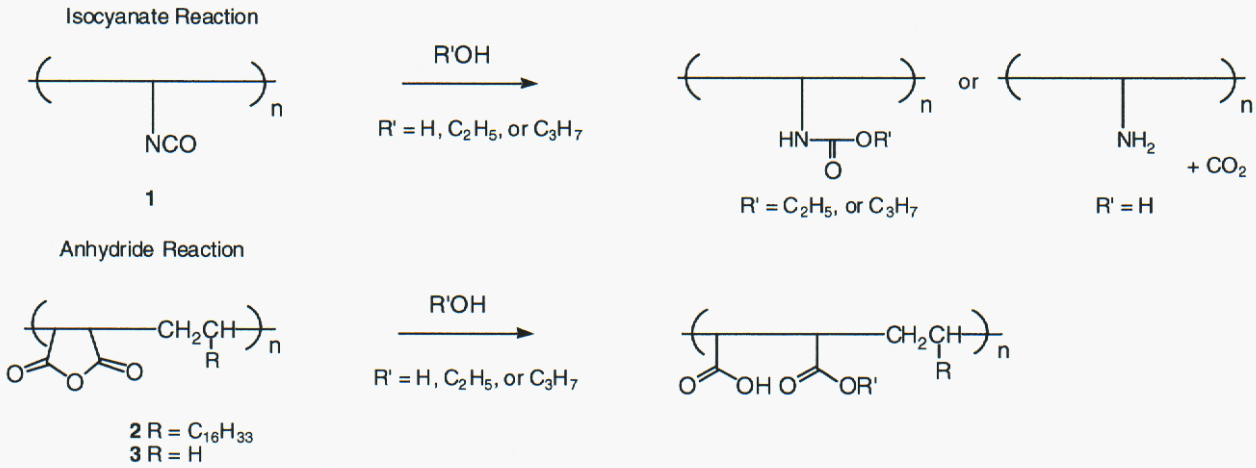

Figure 5. Reaction chemistries for gettering water and alcohols with isocyanates and anhydrides.

A second approach to covalently removing water and alcohols from local environments involved reacting these species with polymeric anhydrides. Anhydrides are well known to cleave or ring

open (for cyclic anhydrides) in the presence of water, alcohols, and amines. Reaction of cyclic anhydrides with water yields a dicarboxylic acid, while reaction with alcohols produces both an ester and carboxylic acid functional group (Figure 5). Two commercial maleic anhydride polymers, poly (maleic anhydride-*alt*-1-octadecane) **(PMA) 2** and poly (ethylene-*alt*-maleic anhydride) **(PEMA) 3** (Aldrich) were examined as getter materials. The primary difference between the two materials is that poly (maleic anhydride-*alt*-1-octadecane) **2** contains a long hydrophobic chain off of the polymer backbone while poly (ethylene-*alt*-maleic anhydride) **3** simply contains a hydrogen group at that position.

Similar gettering experiments were conducted for the anhydride polymers as described previously. For poly (maleic anhydride-*alt*-1-octadecane) **2**, the theoretical percent weight change was calculated to be 5.1, 13.1, and 17.1% for water, ethanol, and iso-propanol, respectively. The experimental values obtained for gettering of an excess amount of reactive species, weight change values of 0, 9.5, and 1.4% were obtained for water, ethanol, and iso-propanol, respectively. In an attempt to enhance the gettering reaction, experiments were performed using 4-dimethylaminopyridine (DMAP) as catalyst. Under catalytic conditions, weight change values of 4.0, 9.0, and 12% were obtained for water, ethanol, and iso-propanol, respectively. Addition of DMAP catalyst clearly has a pronounced effect on gettering of water and iso-propanol. Since the presence of a catalyst should only change the rate of the reaction, not the conversion, the changes we observed are likely due to changes in the polarity of the polymer/catalyst mixture. Gettering experiments were also conducted using a stoichiometric amount of reactive species in the presence of catalyst. Weight change values of 1.7, 6.1, and 10.1% were obtained for water, ethanol, and iso-propanol, respectively.

The low reactivity of water with poly (maleic anhydride-*alt*-1-octadecane) **2** may be due to the presence of the hydrophobic alkyl chain adjacent to the anhydride ring in the polymer backbone. To further elucidate this, we conducted gettering experiments with poly (ethylene-*alt*-maleic anhydride) **3,** which contains no hydrophobic chain in the polymer repeat unit. An additional benefit was that poly (ethylene-*alt*-maleic anhydride) **3** offered higher theoretical gettering capacity with calculated values of 14.3, 36.5, and 47.6% weight change for reaction with water, ethanol, and iso-propanol, respectively. Gettering experiments were conducted and monitored with an excess of these reactive species over a period of two months.

Table I shows weight gain percent of reacted PEMA **3** for each species after vacuum drying (to remove adsorbed, but not reacted species) until a constant weight was obtained. It must be noted that for all of these gettering experiments, a large excess of reactive species is also adsorbed on to the polymer material. Poly (ethylene-*alt*-maleic anhydride) **3** gettering of water yielded a 10.5% weight increase after only one week of reaction. The theoretical maximum weight gain, 14.3%, for reaction of water with PEMA **3** was achieved within one month of exposure. An experimental weight gain of 16% was observed for reaction with water. Hydrogen bonding of free water molecules to carboxylic acid groups of the reacted PEMA is probably responsible for the additional 2% weight gain observed in the experiment. Ethanol reacted slower than water over time with a 52.8 % increase in weight after two months. This large weight gain in excess of the theoretical maximum for ethanol is probably due to unreacted trapped ethanol in the polymer matrix. Indeed, the PEMA-ethanol getter sample was a hardened gel after high vacuum

treatment. Reaction of iso-propanol with PEMA **3** was the slowest reaction of the three species with a 12.8% weight gain after two months.

Reactive Species	1 Week (% Wt Gain)	1 Month (% Wt Gain)	2 Month (% Wt Gain)	Theoretical Maximum (%)
Water	10.5	16.0	15.6	14.3
Ethanol	4.6	22.9	52.8	36.5
Iso-propanol	0.0	4.1	12.8	47.6

Table I. Weight gain data for reaction of water, ethanol, and iso-propanol with PEMA **3**.

It is clear from these results that the reactivity of maleic anhydride polymers with molecules containing a free hydroxyl group is dependent on substituent group effects adjacent to the anhydride ring. The 18-carbon alkyl chain in poly (maleic anhydride-*alt*-1-octadecane) **2** inhibits its reaction with water due to the hydrophobicity surrounding the cyclic anhydride. For poly (ethylene-*alt*-maleic anhydride) **3** no such hydrophobic environment exists and water is able to readily react with the cyclic anhydride. In addition, no catalyst is required to enhance the reactivity of the polymer as was observed for poly (maleic anhydride-*alt*-1-octadecane) **2**.

Although our approach toward covalently removing reactive species from sealed environments using anhydride polymers was successful, it was realized early on that the reverse reaction may also occur at elevated temperatures. Specifically, at elevated temperature, the reacted ring-opened anhydride polymer may ring close or crosslink to reform an anhydride moiety and expel water or alcohol in the process. Both reacted poly (maleic anhydride-*alt*-1-octadecane) **2** and poly (ethylene-*alt*-maleic anhydride) **3**, exhibited no reversible reaction at 70 °C after approximately 16 hours of heating. However, both anhydride polymers exhibited some reversible behavior at temperatures above 80 °C after 24 hours of heating as evidenced by characteristic changes in the polymers infrared spectra.

3.3 Diffusion Through Binder

In an effort to provide more accurate diffusion data for the modeling aspects of this project, we investigated transport of water and ethanol in the polybutadiene binder, as well as mixtures of binder and the getter. This information is an important part of the overall gettering system because, depending on the loading fraction of the gettering material in the binder, diffusion through the binder can be the rate limiting step. A PEMA/Ricon 130 (50:50) blend formed our model getter/binder system. Ricon 130 is a viscous liquid used to hold the powdery PEMA into a castable semi-solid paste. Ricon 130 is a 1,4 – polybutadiene resin with a molecular weight of 2500 g/mol and when mixed with the PEMA getter a formable paste is generated. Thick films were prepared, placed in closed containers with water or ethanol saturated atmospheres and monitored for mass changes over time. The change in mass over time is shown in Figure 6 for water and Figure 7 for ethanol.

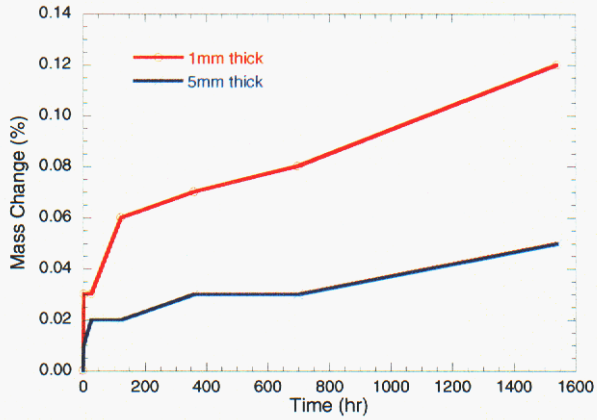

Figure 6. Water absorption in Ricon130 thin films exposed to 100% water humidity at room temperature and pressure.

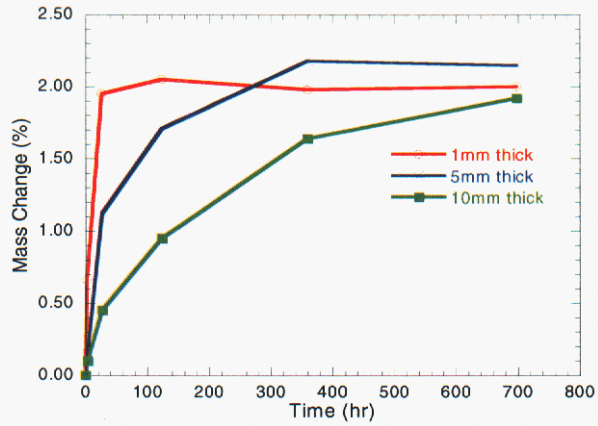

Figure 7. Ethanol absorption in Ricon130 thin films exposed to saturated gas phase headspace at room temperature and pressure.

Comparing Figure 6 and 7, one can see that the uptake rate of ethanol in Ricon 130 is much faster than that of water in Ricon 130. This is not surprising, considering Ricon 130 is a hydrophobic hydrocarbon polymer. At 1500 hours, the Ricon 130 is still taking up water. In the case of ethanol diffusion, the films reached saturation at 27 hours for the 1mm film, 360 hours for the 5mm film and 700 hours for the 10mm film. Water capacity cannot de determined from this data since the weight is still increasing over the time of the experiment.

3.4 Getter Reactivity and Capacity in Saturated Environments

Isocyanate, polymer bound (ICPB) **1**.

A characteristic absorption peak for isocyanates generally occurs around 2240 cm^{-1} and is a convenient handle for monitoring reaction of –NCO containing compounds as few other functional groups absorb in that region. Figure 8 shows the IR spectra of ICPB **1** and ICPB **1** after reaction with ethanol. IR spectroscopy revealed a slight decrease in isocyanate absorption at 2242 cm^{-1} and the appearance of new absorptions between 1723-1692 cm^{-1}, corresponding to urethane absorption due to the covalent gettering of ethanol and iso-propanol. That the isocyanate peak at 2242 cm^{-1} does not substantially decrease for reaction with ethanol or iso-propanol supports the weight change and capacity data reported above. For reaction with water, a new absorption appeared at 1692 cm^{-1} due to carboxylic C=O stretching.

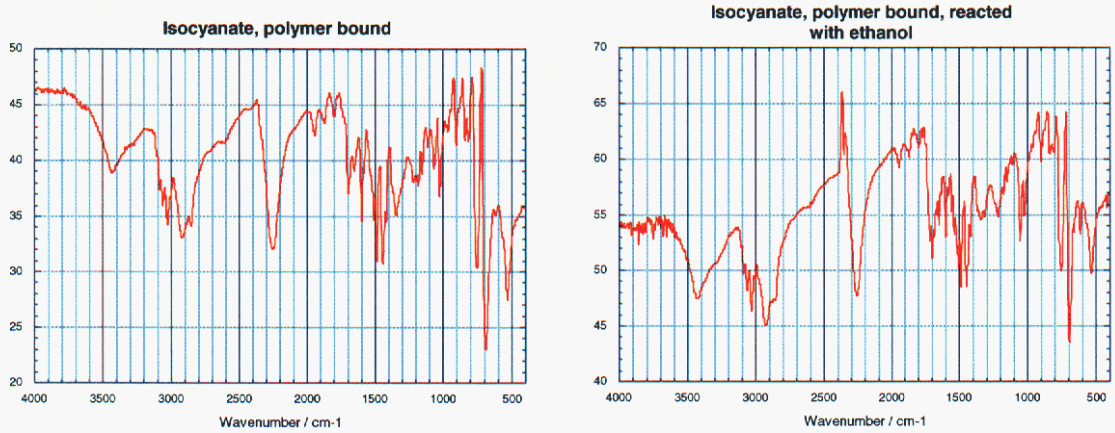

Figure 8. IR spectra of ICPB **1** and ICPB **1** after reaction with ethanol.

Poly(maleic anhydride-*alt*-1-octadecane) (PMA) **2**

IR spectroscopy showed characteristic functional group changes in poly (maleic anhydride-*alt*-1-octadecane) **2** that occurred during reaction. Poly(maleic anhydride-*alt*-1-octadecane) **2** has a prominent absorption at 1782 cm^{-1} which is characteristic of the strained anhydride C=O ring structure (Figure 9). Upon reaction with water, ethanol, or iso-propanol, this absorption is significantly reduced, and new absorbances occur between 1700-1750 cm^{-1} corresponding to ester carbonyl stretches (Figure 9). As expected, the reaction with water produces a new absorption at 3500 cm^{-1}, corresponding to the C-OH stretch of the dicarboxylic acid that is formed and loss of peak absorption at 1782 cm^{-1}.

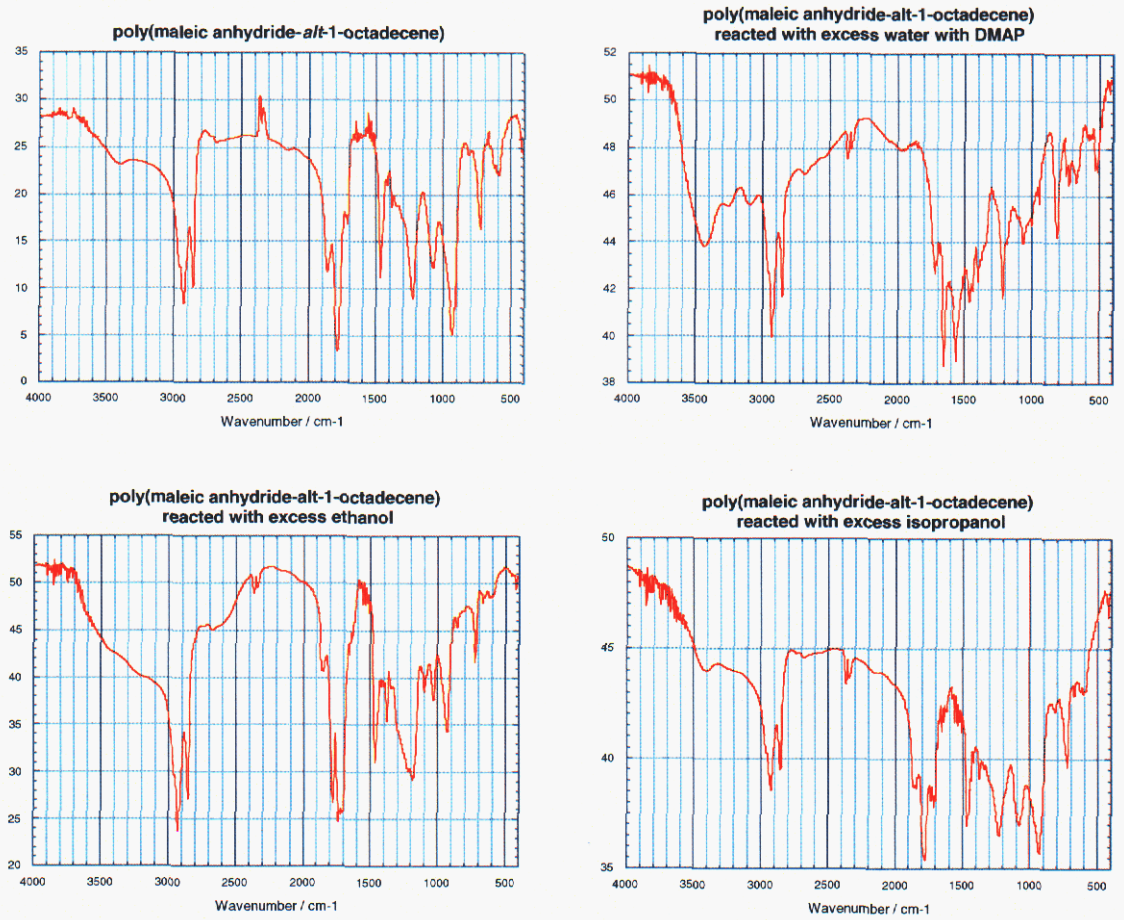

Figure 9. PMA **2** and reactions with water, ethanol and iso-propanol.

Poly (ethylene-*alt*-maleic anhydride) (PEMA) **3**

PEMA **3** exhibited practically identical IR spectroscopic behavior as observed for PMA **2**. Decrease in absorption at 1782 cm^{-1} is clearly evident for the anhydride functionality with new peaks appearing between 1700-1750 cm^{-1} due to formation of ester and carboxylic functional groups upon reaction. Water reaction with PEMA **3** shows complete conversion by IR spectroscopy as the anhydride functionality at 1782 cm^{-1} completely disappears while prominent –C-OH stretches are observed at approximately 3500 cm^{-1}.

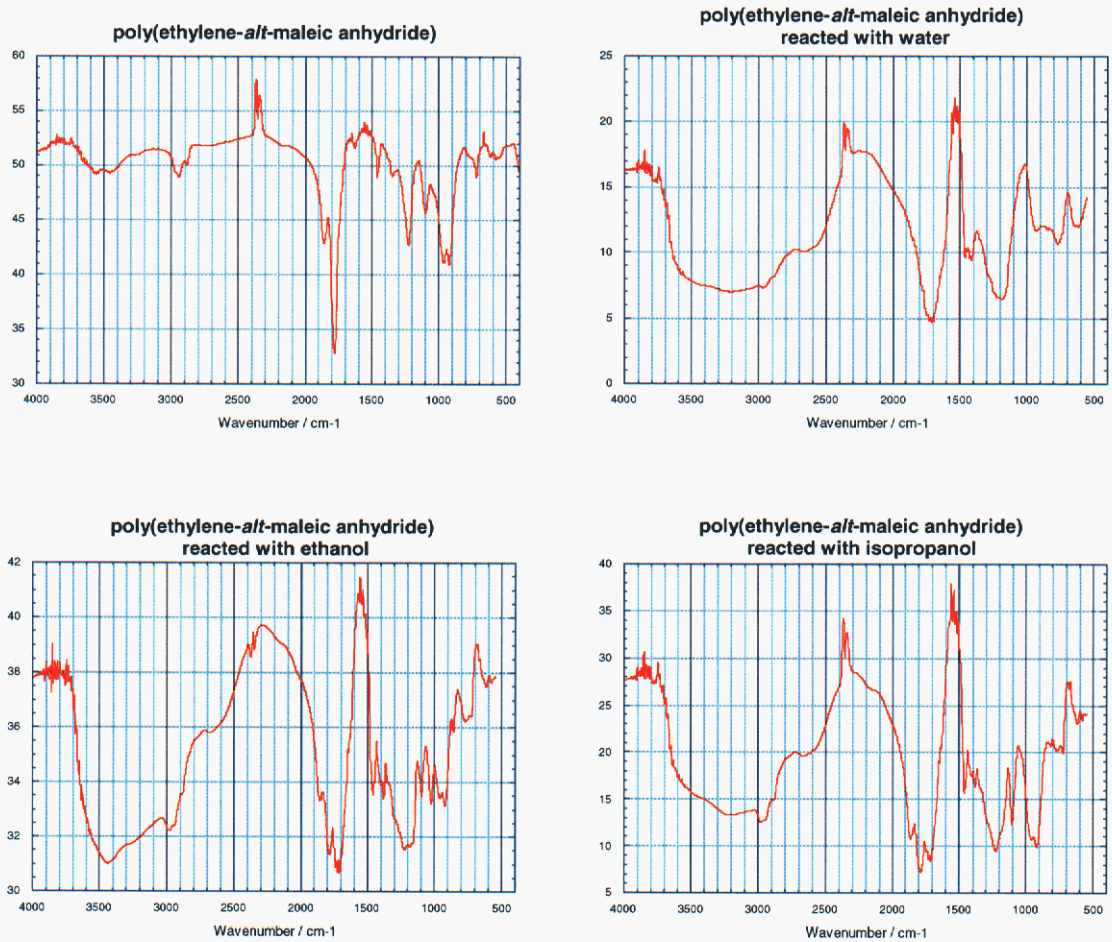

Figure 10. IR spectra of PEMA **3** and reactions with water, ethanol and iso-propanol.

3.5 Getter Reactivity in Unsaturated Environments Results – Gas Phase IR Studies

Deuterated compounds (D_2O and ethanol-d_8) were used instead of the protonated versions to provide an IR signal away from where other common absorbances are observed. Gas phase IR analysis experiments were conducted with two different methods for introducing the vapor of interest. In the first method, several 10 µl drops of D_2O or ethanol-d_6 are added to the IR cell by opening the cell and pippeting in the solvent. Depending on the amount of getter present, 10 µl is 10-20% of the getters capacity for these experiments. The second method introduces a smaller aliquot of the vapor in the gas phase generated by flowing dry air through a dynacalibrator containing a permeation tube filled with the solvent of interest and produces a known amount of solvent at a set temperature. In this method, the concentration is controlled by changing the rate of airflow and lets us examine the getters ability to remove a limited amount of solvent and measure the lower bounds of its ability to remove the solvent.

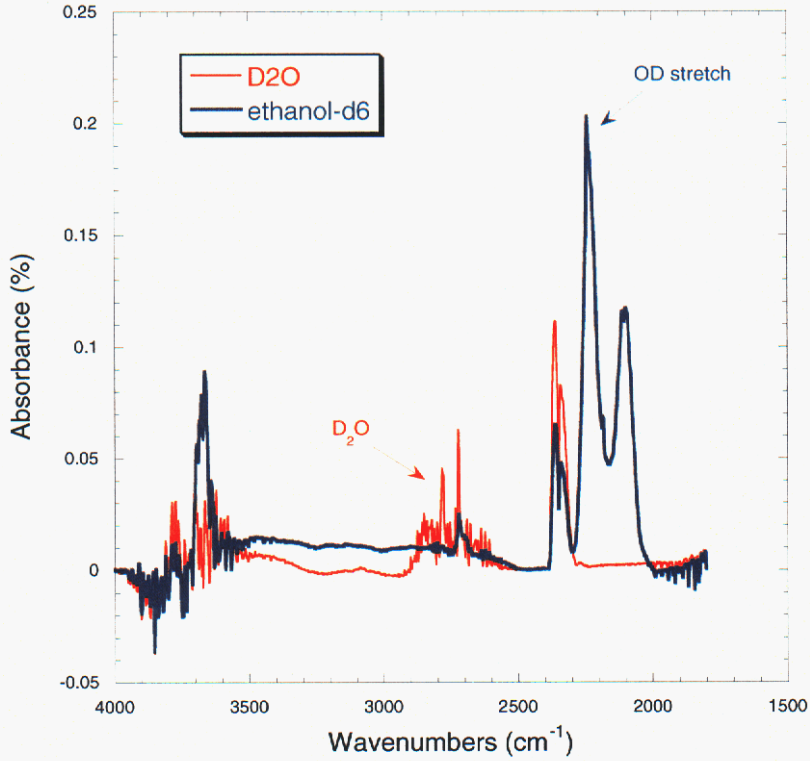

Figure 11. Examples of baseline corrected IR data.

Figure 11 shows examples of the baseline corrected IR data collected and used in this study. Solvent concentration is monitored by peak height. The peak at 2780 cm^{-1} for D_2O and 2242 cm^{-1} for the O-D stretch of ethanol-d_6 were used to follow the progress of the gettering reactions. These peaks were selected because there are no interfering peaks nearby that could complicate the interpretation of the data.

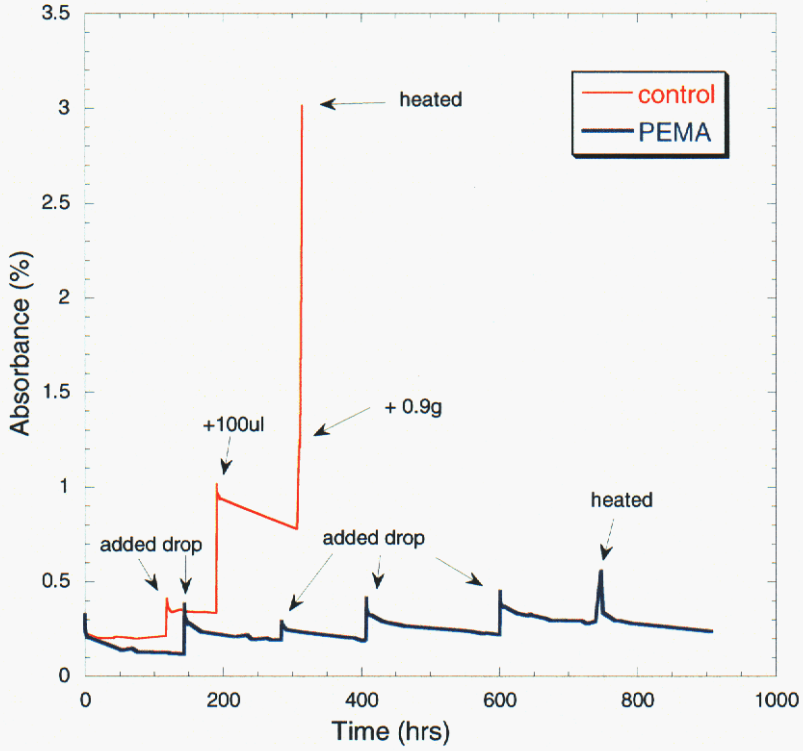

Figure 12. PEMA **3** exposed to a series of 10 µl drops of ethanol-d_6, and then heated to 50°C. A control cell with only ethanol-d_6 on foil is also shown with addition of a large excess of ethanol-d_6 followed by heating to 50°C.

Figure 12 shows the changes in concentration of ethanol-d_6 exposed to PEMA **3** powder. Four sequential aliquots (10 µl) of ethanol-d_6 were added to the cell over the length of the experiment. Absorption occurs quickly after each drop is added until equilibrium is reached with the excess of gas phase ethanol-d_6 and then gettering continues at a slower rate. Heating of the cell to 50°C at the end of the experiment produce a slight increase of ethanol in the cell indicating that some of the solvent had absorbed onto the getter and not yet reacted with it. Ethanol in the control cell came down to constant level after each drop was added. Some of this may be due to ethanol coating the IR cell walls. Two large amounts of solvent were added to determine the maximum signal (or concentration) at room temp. The cell was then heated to 50°C to determine maximum response at the elevated temperature. In both cases liquid solvent remained in the saturated cell.

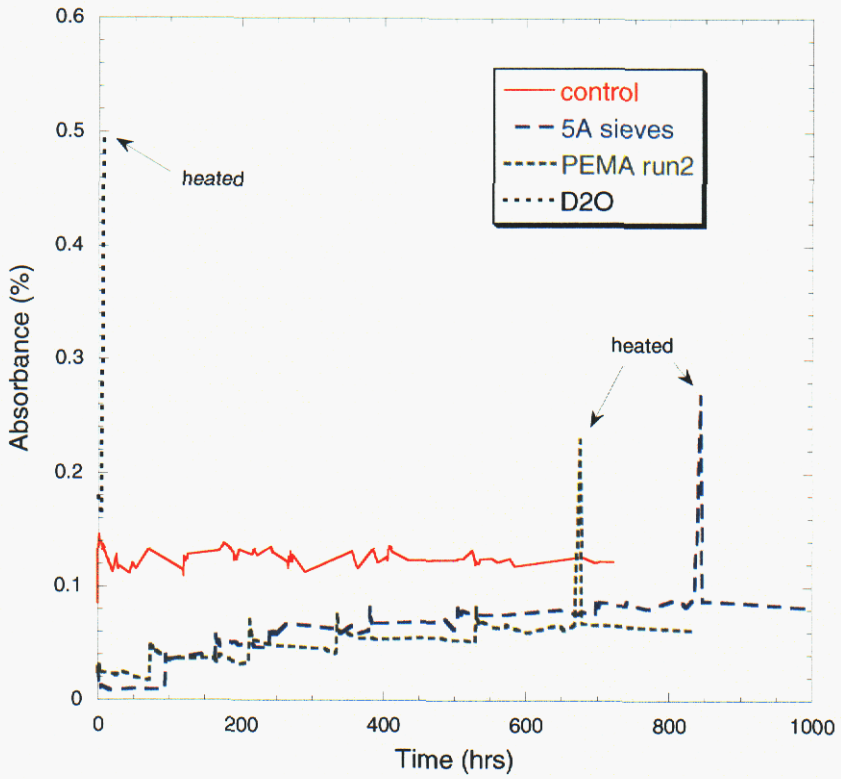

Figure 13. Absorption plots of D_2O with selected getters.

Using a similar procedure to that of Figure 12, Figure 13 shows the absorption behavior of adding a series of 10 µl drops of D_2O to cells containing PEMA powder, 5Å molecular sieves powder, and a control cell with aluminum foil. Again the getters absorbed the solvent quickly until equilibrium was reached. The concentration then continues to decrease at a slower rate. The amount of solvent in the gas phase increased with each drop added, slowly approaching that of the control. Heating the samples to 50°C at the end caused an increase of the vapor phase D_2O indicating that some of the solvent was absorbed onto the getter and walls of the IR cell and had not yet fully reacted. The IR absorbance decreased upon cooling back to room temperature indicating that the vapor was reabsorbed.

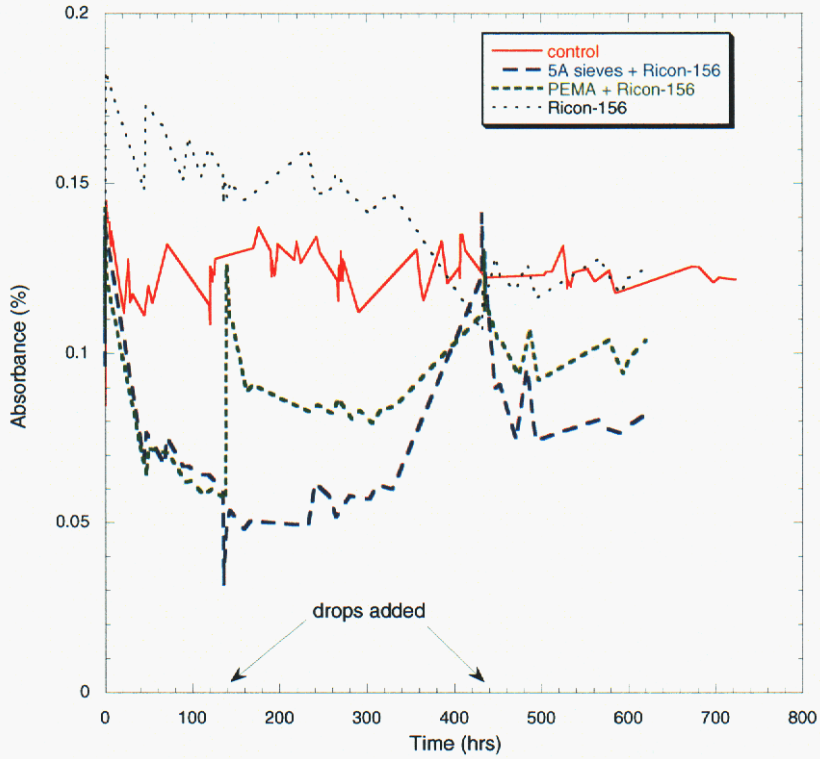

Figure 14. Absorption plots of D_2O with selected getters mixed with the Ricon binder.

The data shown in Figure 14 is for getter 3 immobilized in a sticky polybutadiene matrix, more closely representing the expected deployment conditions for this getter. Initial absorption after each drop reduced when compared to the neat getters in Figure 13. Reaction rates are slower as the solvent has a harder time accessing the getter through the binder. The slow rates will help in the deployment of the getter by increasing the working time for assembly of the microsystem without using up all of the getters capacity. The remaining capacity will help to ensure a clean environment over the life of the system.

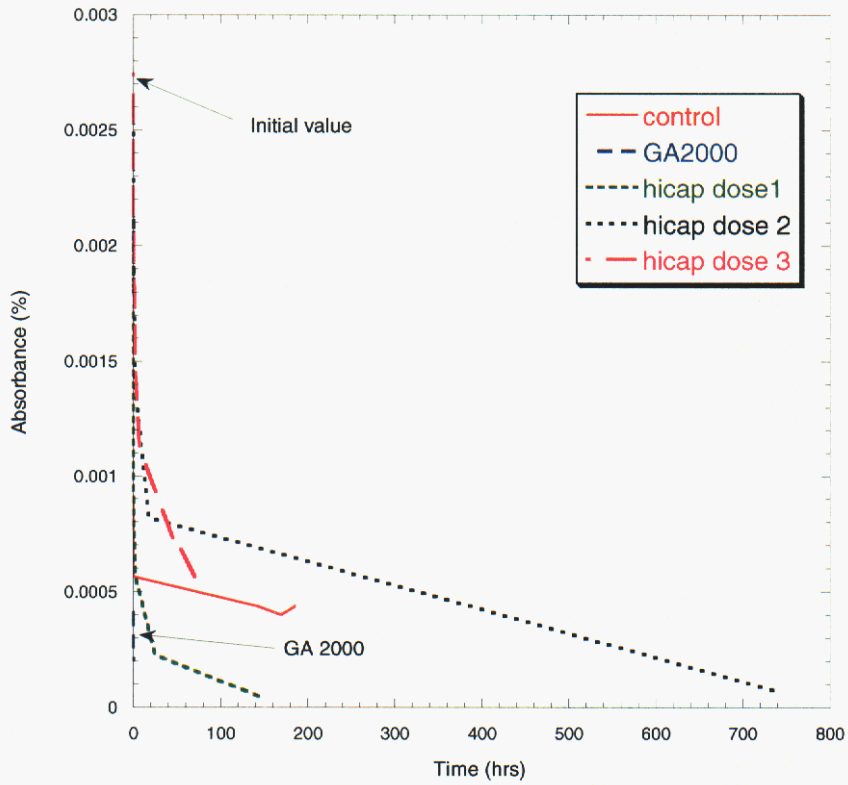

Figure 15. Commercial getters from Cookson electronics exposed to air containing D_2O.

The next series of experiments were conducted in the same gas phase IR cell, but used D_2O vapors generated from a dispersion tube in a dynacalibrator. Figure 15 shows the results of the two commercial getters, GA2000 and Hicap. The Hicap getter was exposed to three separate doses of D_2O. The rate of each subsequent absorption was a little slower than the previous. The D_2O absorption with GA2000 was extremely fast and would pose a problem (loss of usable capacity), if assembled out in the air. While these getters performed well, they only remove water and are therefore inadequate for use in microsystems with other solvents of concern. As shown by the control data in Figure 15, much of the initial decrease in IR absorbance in these experiments is due to the small solvent dose adhering to the cell walls and foil.

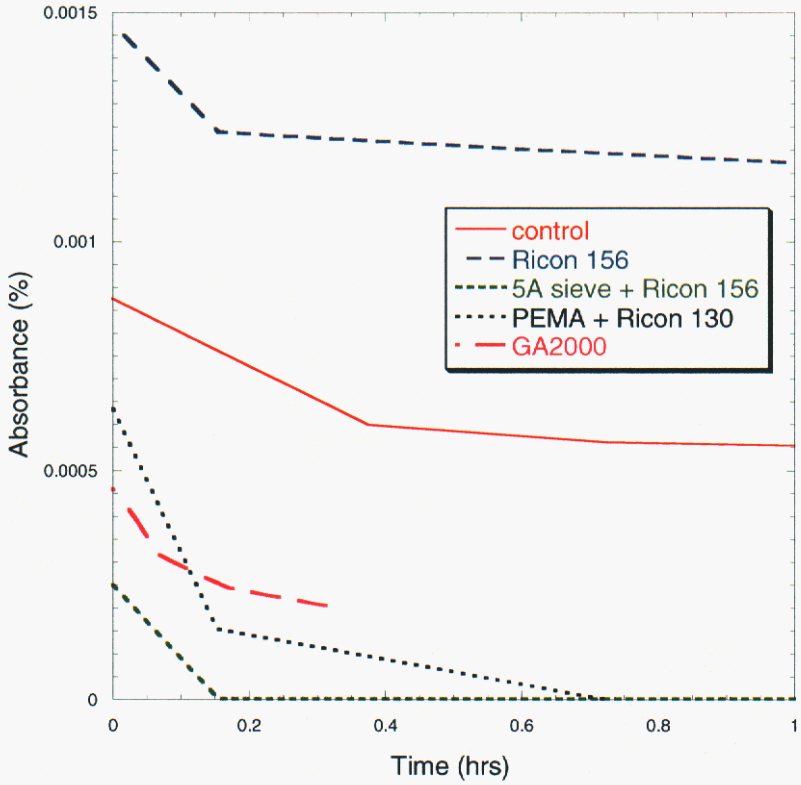

Figure 16. A comparison of different getter materials when exposed to a small amount of D_2O in air.

The data from Figure 16 shows that PEMA mixed with Ricon, and 5Å molecular sieves mixed with Ricon are both competitive with the commercially available getter and are capable of reducing D_2O below our detection limits in a short time. The sample containing only the Ricon binder is not capable of gettering any of the solvents, and being hydrophobic, blocks the D_2O from coating some of the foil surface, thereby increasing the gas phase concentration.

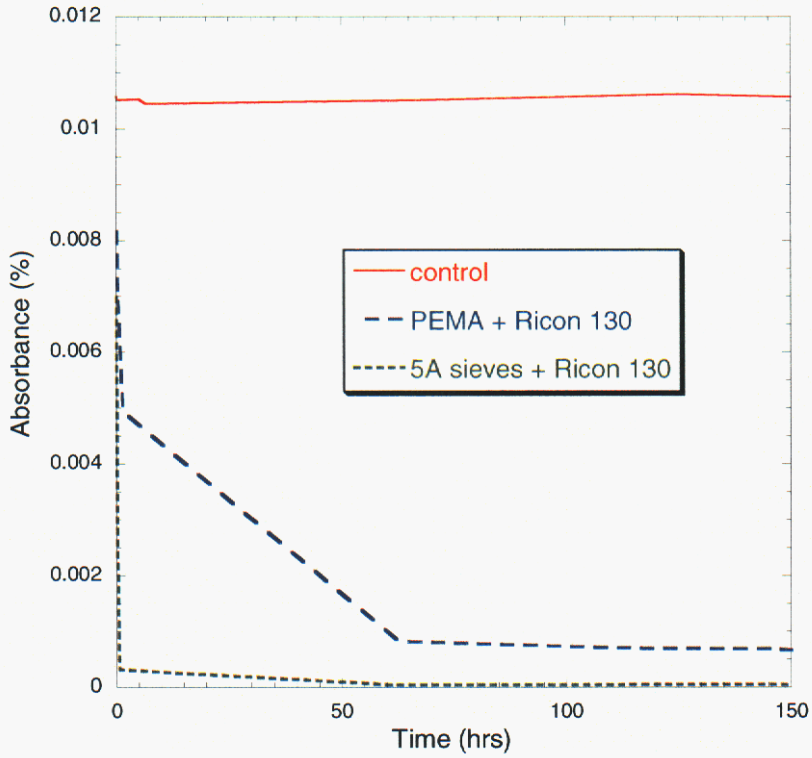

Figure 17. PEMA and 5Å sieves in Ricon binder exposed to a small dose of ethanol in air.

Figure 17 shows a small dose of gas phase ethanol being remove by PEMA and 5Å molecular sieves in Ricon 130 binder. These getters effectively removed the ethanol but did so more slowly than the removal of D_2O in Figure 16. This is consistent with water diffusion through the hydrophobic Ricon being slower than that for ethanol.

The data shown in the previous figures indicate that PEMA is effective at reacting with water and ethanol (and presumably other primary alcohols). The data also supports the desire to coat the particles with a binder that not only broadens the way the getter can be applied, but also slows the absorption, providing more assembly time for a given application.

It should be noted that, due to isotope effects, the rates shown here are to be considered lower limits of the rates for non-deuterated water and alcohol reactions. In general, the non-deuterated reactants are expected to react faster and could have an effect on the microsystem assembly time discussed earlier.

4. Microsystem Simulation and Experimental Analysis

The major goal of the project is to assess the overall capabilities of a new class of irreversible getters. To this end, the modeling portion of the work seeks to quantify the getter and system performance by developing a mathematical approach capable of predicting the environmental evolution over the lifetime of any microsystem of interest. Such models can be used to estimate the ingress of undesirable species, determine the amount of getter required for a particular microsystem package, and yield insight on the best location for the getter within the microsystem. These goals were accomplished by developing reaction and transport models describing the fate of chemical species within microsystems containing getter material. In the current work, the specific chemicals of interest include both water and ethanol.

An overview of the problem of interest and an introduction to the overall modeling approach is given in Section 4.1. Then in Section 4.2, a general one-dimensional numerical model is developed and used to describe the transport and reaction of chemical species in a microsystem package that includes a getter material encapsulated within a polymer matrix. The model is first developed in terms of dimensionless quantities that apply to all systems regardless of their system specific parameters. The simplest one-dimensional model helps to elucidate the relative importance of gas phase diffusion and diffusion within the binder material, and allows a quick estimate of the gas phase and polymer phase concentrations over time. Additionally, the relationship between diffusion and reaction in the polymer/getter material is examined in a generic manner.

The two-dimensional model developed in Section 4.3 extends the one-dimensional model by explicitly taking into account the location of individual grains of the getter material within the surrounding polymer matrix. Additionally, the disparate material properties of the getter and polymer matrix phases are explicitly represented whereas the one-dimensional model treats the getter/polymer mixture as a single material. Thus, the two-dimensional model incorporates the role of diffusion through the high-diffusivity getter phase and reveals the importance of particle-to-particle proximity in determining bulk transport properties.

Before these models can be used for any specific application, it is necessary to determine several system specific parameters. These include getter parameters such as the getter reaction rate, getter maximum capacity, and the getter equilibrium absorption curve. Additionally, since a polymer binding material surrounds the getter, the storage and transport properties of the chemical species of interest through this polymer must also be determined. Such properties include the diffusion coefficient of both water and ethanol through the polymer and additionally the equilibrium solubility/capacity of both species within the polymer itself. As explained in Section 4.4, these parameters have been estimated by analysis of the experimental data sets described in the first major section of this report.

Finally, once the system parameters are known, the developed model can be used to estimate the anticipated mass concentrations of chemical species within the microsystem environment over the lifetime of a specific system. The effects of changing the magnitude of interfacial leak rates (such as from diffusion through the side walls or through the bottom of the package) or sources arising from internal components (such as gasses trapped within organics or trapped spaces) can

be estimated along with the effects of different initial vapor phase environments and alternative gettering strategies. While discussion of these effects is found in Section 5, specific examples are not included in the current report.

4.1 Problem Description and Modeling Approach

The physical systems of interest consist of micro or nano-scale packages containing features or parts susceptible to various chemical species, such as water, that may infiltrate the package. Figure 18 shows a picture of a typical system having dimensions of 1 mm x 2 mm x 4 mm. The volume of a typical package is on the order of several mm^3.

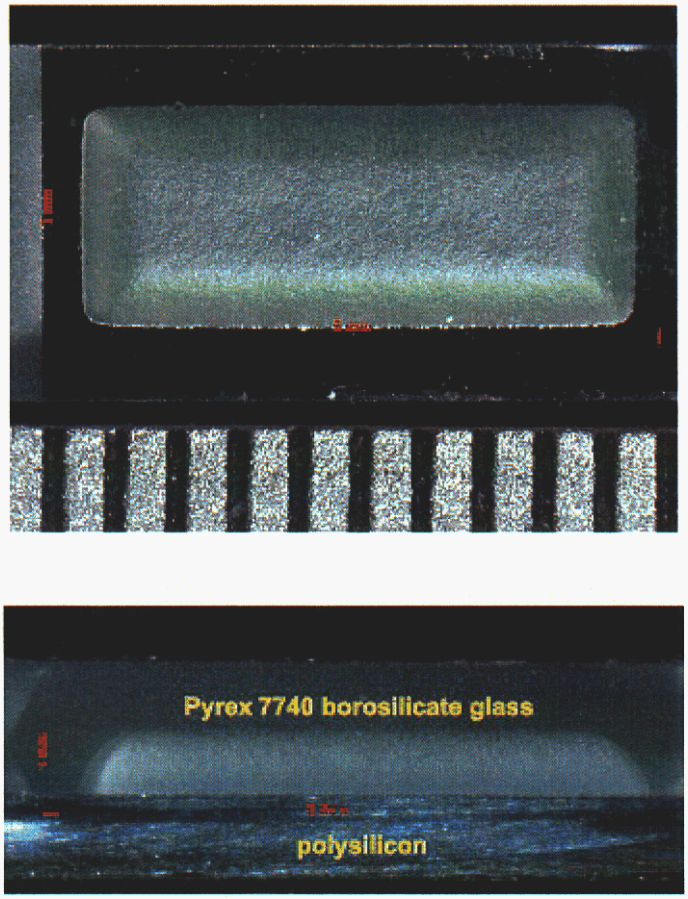

Figure 18. Photograph of a typical microsystem (1 mm x 2 mm x 4 mm)

In these systems, fragile key features are often attached to the top surface of a substrate, typically made of silicon. Such systems are typically packaged by placing a 'lid' over the features of interest to seal the vapor space above the components from the external environment. A number of different physical packaging processes are available to seal the package.[5] These processes may be performed in inert environments, such as a nitrogen fill, so that the initial packaged environment is free of potentially reactive species. However, since strict environmental controls are costly and time consuming, packaging sometimes takes place in non-inert environments. Here, the air exposure during packaging may quickly saturate a getter to capacity. This can severely shorten the overall lifetime of the microsystem.

Once the microsystem is sealed, the chance that potentially harmful chemicals could reach the fragile features is greatly diminished. However, several pathways exist that could allow ingress of harmful species. The most likely source of leaks from the external environment is the interface between the lid and the substrate itself.[6] Additional ingress pathways include pass-throughs needed for wires or other means of exchange between the microsystem and the external environment.[7]

Even if leaks could be completely eliminated, contaminants may originate from within the package itself. One potential source is species that are absorbed on free surfaces within the package during the fabrication and packaging processes. Additional contaminants may originate from gasses trapped within organic materials found within the package or from the chemical decomposition of the organic materials themselves. Such gas contaminants are gradually released over time. Microsystem packages may also contain trapped volumes that release undesirable species over the package lifetime. Experimental observations of vapors present in microsystems after packaging have been observed by Mack *et. al*[8] and Weber *et. al.*[9]

In general, the time required for equilibration of molecular sieves and other getters within the package environment will be on the order of hours to days. Since these times are short compared to the package lifetime, it will often be reasonable to assume instantaneous equilibrium between the getter and the package environment. However, several significant scenarios may occur where this assumption is not valid. For example, the getter material may be intentionally protected by a polymer layer intended to prevent getter loading during assembly. Here the contaminant must diffuse through the polymer before reacting with the getter. This greatly increases the time needed for the system to come to equilibrium and the transient effects can become important. Additionally, an abrupt rise in species concentration may occur due to any of the possible sources listed above. These concentration bursts or "puffs" may have consequences on a time scale that is much shorter than the getter response time. In these scenarios, modeling of the transient response is required. Modeling of water in sealed electronic packages has previously been conduced by Keenan.[10]

The modeling approach taken here is to solve the differential form of the equations describing mass conservation of relevant chemical species within each of the different regions of the domain (i.e. getter material, polymer material, vapor region). Transport of species between regions is incorporated through boundary conditions that account for surface kinetics (eg. surface gettering rates) as well as equilibrium considerations (eg. solubility). Thus, for each species, there will be one differential equation for each region of interest. In the absence of explicit convective forces, the species differential mass balance reduces to a simple diffusion equation with a reactive source/sink term:

$$\frac{\partial \rho_A^{(i)}}{\partial t} = \frac{\partial}{\partial x}\left[D_{AB}^{(i)} \frac{\partial \rho_A^{(i)}}{\partial x} \right] + r_A^{V(i)} . \qquad (1)$$

Here $\rho_A^{(i)}$ is the mass density of species A in the ith region or phase. $D_{AB}^{(i)}$ is the diffusion coefficient of species A through B in the ith region, and $r_A^{V(i)}$ is a reactive source or sink term

that describes the rate of transport of material between different regions. The exact form of $r_A^{V(i)}$ depends on the manner in which material is transferred between regions and must be specified.

Mass balance equations can be formulated mathematically in terms of several alternative dependent variables such as mass concentration, molar concentration, mass fraction, partial pressure, parts per million (by volume), and relative humidity (when discussing water). However, converting between these variables is straightforward, and we have chosen to work in terms of mass concentration in cgs units (grams / cm^3).

For convenience, the collective mass balance for all species is used to replace one of the species balance equation; here we eliminate the most prevalent species (eg. air or nitrogen) and treat all contaminant species as trace components of the mixture. Once suitable initial conditions and boundary conditions are specified, the equations describing chemical species transport can be solved.

We have chosen to solve the resulting differential equations in MATLAB, a widely used commercial software package. MATLAB provides a convenient framework for solving the transport equations and displaying the results. Before input into MATLAB, the equations are discretized by applying the mass balance equations to many small computational zones within each region of interest. The resulting system of nonlinear algebraic equations is placed into a matrix format that numerically specifies the problem. At each time step in the problem evolution, routines within MATLAB are used to solve the matrix equation for the instantaneous values of the species concentrations in all zones. The total amount of any species in a particular region, such as the getter or gas phase, is determined at any time by integrating the instantaneous mass density over all zones within that region.

4.2 One-Dimensional Model

This section describes the one-dimensional modeling approach used to estimate species transport within the microsystem. Similar descriptions of transport through polymeric systems have been presented by George.[11] First the computational domain and governing equations are discussed. Then the equations are converted into their dimensionless form and two important dimensionless parameters are identified. Finally, the results of the one-dimensional analysis are presented and some conclusions are made.

4.2.1 Computational Domain and Governing Equations

The microsystem can be divided up into three computational regions, shown in Figure 19. The first region consists of the internal headspace volume within the lid, the second consists of the polymer material that holds the getter material. The final region consists of the getter particles themselves. The getter material is viewed as a collection of permeable spheres that are suspended throughout a thick polymer and then attached to the upper portions of the package lid. For contaminant species to reach the getter where it is reacted and absorbed, the material in the vapor phase must first diffuse through the polymer. Thus, transport properties of the polymer material play an important role in the function of the getter.

In the current one-dimensional approach, the second and third regions are combined into a composite material that includes both the polymer and the getter particles. The getter material is

assumed to be uniformly distributed within the polymer matrix so that the getter reaction can be described as uniform over the getter/polymer region. In the two-dimensional approach described later on, the individual getter particles will be explicitly represented and the assumption of uniformity is not required. Although actual microsystems are anticipated to have much more complicated geometries, the current one-dimensional model contains the essential characteristics of these more complex systems.

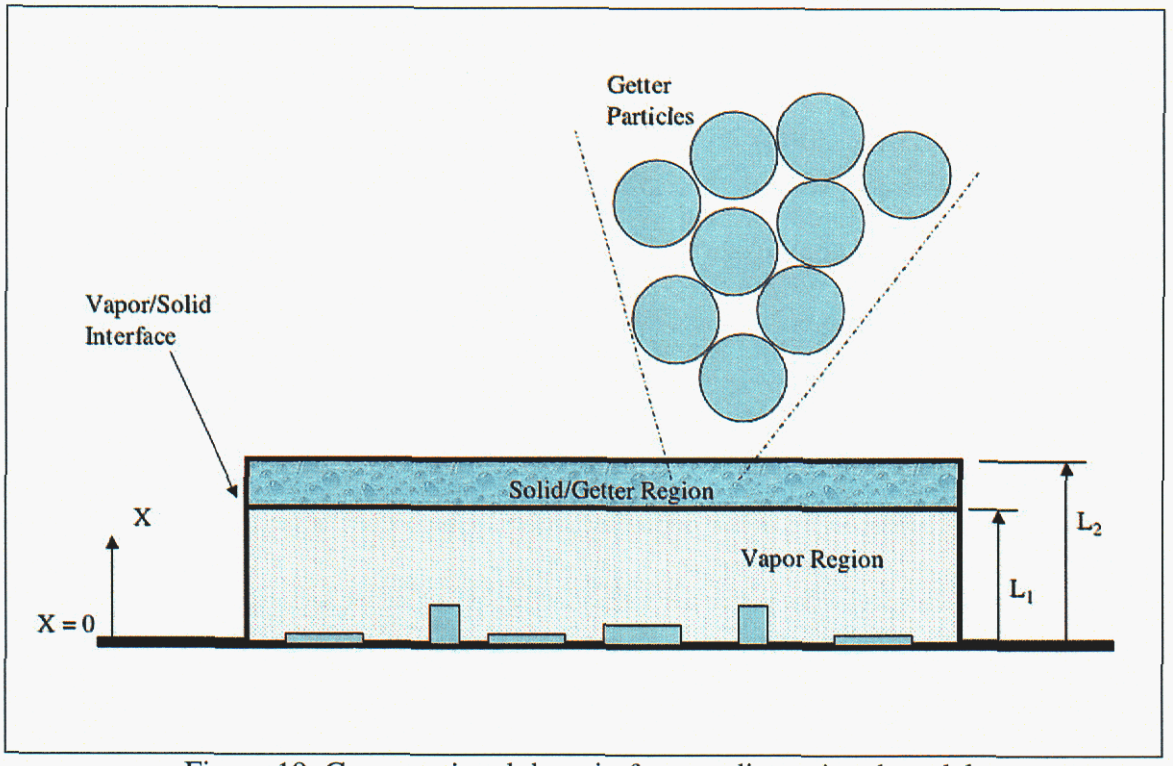

Figure 19. Computational domain for one-dimensional model.

In the current approach we model contaminant transport within the package using a coupled system of three one-dimensional equations; one for each of the regions described above. The transport of a chemical species A through the vapor (superscript v) headspace above the microsystem is mathematically described as

$$\frac{\partial \rho_A^{(v)}}{\partial t} = \frac{\partial}{\partial x}\left[D_{AB}^{(v)} \frac{\partial \rho_A^{(v)}}{\partial x} \right]. \tag{2}$$

For now, the initial condition is given to be:

$$t = 0 \quad \rho_A^{(v)} = 0, \tag{3}$$

indicating that the initial concentration of species A in the vapor phase is zero. The following boundary conditions are applied on lower and upper boundaries shown in Figure 19:

$$x=0 \quad \rho_A^{(v)} = \rho_A^{o} \tag{4}$$

$$x=L_1 \quad D_{AB}^{(v)} \frac{\partial \rho_A^{(v)}}{\partial x} = D_{AB}^{(s)} \frac{\partial \rho_A^{(s)}}{\partial x} . \tag{5}$$

The first condition specifies a mass concentration at the lid/substrate interface. In future studies, this boundary condition can be modified over time to simulate leaks from this interface. Since the model is one-dimensional, this boundary condition can also describe diffusion through the substrate. The second condition in Eq. (5) enforces continuity of the mass fluxes at the boundary between the vapor region and solid/getter region. The mass concentration gradients are related by the ratio of their respective diffusion coefficients.

A second equation describes contaminant transport within the composite material (superscript s) composed of the polymer binding material and the getter particles:

$$\frac{\partial \rho_A^{(s)}}{\partial t} = \frac{\partial}{\partial x}\left[D_{AB}^{(s)} \frac{\partial \rho_A^{(s)}}{\partial x} \right] + r_A^{V(s)} . \tag{6}$$

The homogeneous reaction term, $r_A^{V(s)}$, accounts for the reaction and absorption within the getter material that is assumed to be uniformly distributed throughout the polymer. Because the getter is surrounded by polymer, the contaminant within the vapor phase must diffuse through the polymer before it can react. This greatly reduces the effective reaction rate of the composite material compared to a directly exposed getter.

Similar to the vapor equation, we specify an initial condition of zero contaminant concentration within the polymer/getter material:

$$t=0 \quad \rho_A^{(s)} = 0. \tag{7}$$

Additionally, two boundary conditions are required and we specify the following:

$$x=L_1 \quad \rho_A^{(s)} = s\rho_A^{(v)} \tag{8}$$

$$x=L_2 \quad \frac{\partial \rho_A^{(s)}}{\partial x} = 0 \tag{9}$$

Equation (8), relates the contaminant concentration in the polymer/getter region to that in the vapor region. The proportionality constant, s, is the equilibrium solubility and is related to the Henry's Law constant. The second condition, Eq. (9), prevents contaminant from escaping through the top boundary.

The third and final mass balance equation describes the amount of water that has been reacted and is retained within the getter/polymer composite material:

$$\frac{\partial \rho_A^{(G)}}{\partial t} = -r_A^{V(s)}. \tag{10}$$

As before, the mass concentration of chemical species A within the getter is initially zero:

$$t = 0 \quad \rho_A^{(G)} = 0. \tag{11}$$

Both Eq. (6) and Eq. (10) have been expressed in terms of a general reaction rate, $r_A^{V(s)}$. The volumetric reaction rate, $r_A^{V(s)}$, is assumed to be proportional to the local density of unreacted contaminant within the getter/polymer composite:

$$r_A^{V(s)} = -k_A \rho_A^{(s)}. \tag{12}$$

We expect k_A to be proportional to the getters surface area per unit of composite volume, SA/V, the average impingement velocity of gas molecules within the getter pores, and some sticking or reaction probability, f:

$$k_A^{V(s)} \propto \frac{\mathrm{SA}^{(G)}}{\mathrm{V}^{(G)}} \cdot \bar{v} \cdot f. \tag{13}$$

Further, the sticking probability can be written in terms of an initial probability and a term that accounts for the diminished capacity of the getter to react/absorb as it reaches its capacity:

$$f = f_0 \left[1 - \frac{\rho_A^{(G)}}{\rho_A^{(G)\max}} \right]. \tag{14}$$

However, since we have no direct knowledge of the getter surface area, we choose to write the proportionality factor k in terms of experimentally observable quantities as:

$$k_A^{V(s)} = \hat{k}_A \frac{\mathrm{M}^{(G)}}{\mathrm{V}^{(G)}} \cdot \left[1 - \frac{\rho_A^{(G)}}{\rho_A^{(G)\max}} \right]. \tag{15}$$

where $\frac{\mathrm{M}^{(G)}}{\mathrm{V}^{(G)}}$ is the mass of getter material per unit of getter/polymer volume and $\hat{k}_A$ includes a number of constants that cannot be independently determined by the experiments described earlier. Thus, the reaction/absorption of contaminant by the getter is evaluated as:

$$r_A^{V(S)} = \hat{k}_A \cdot \frac{M^{(G)}}{V^{(G)}}\left[1 - \frac{\rho_A^{(G)}}{\rho_A^{(G)\max}}\right]\rho_A^{(s)} . \tag{16}$$

The constant parameters appearing here are determined in Section 4.4.2 by using this equation to analyze the experimental data described in preceding sections.

4.2.2 Dimensionless Governing Equations

To identify key parameters of interest and to minimize the number of parameters, it is useful to put the equations into a dimensionless form. This yields insight into the relative importance of various processes and parameters. Defining characteristic length, density, diffusivity, and time values allows us to define the following dimensionless variables:

$$t^* = \frac{tD_{AB}^{(s)}}{L_2^2} \qquad \rho_A^{*(v)} = \frac{\rho_A^{(v)}}{\rho_A^{o}} \tag{17}$$

$$x^* = \frac{x}{L_2} \qquad D_{AB}^* = \frac{D_{AB}}{D_{AB}^{(s)}} \tag{18}$$

The vapor phase differential mass balance in Eq. (2) is now expressed as:

$$\frac{\partial \rho_A^{*(v)}}{\partial t^*} = \varepsilon \frac{\partial}{\partial x^*}\left[\frac{\partial \rho_A^{*(v)}}{\partial x^*}\right], \tag{19}$$

with initial condition

$$t^* = 0 \quad \rho_A^{*(v)} = 0, \tag{20}$$

and boundary conditions:

$$x^* = 0 \quad \rho_A^{*(v)} = 1 \tag{21}$$

$$x^* = \frac{L_1}{L_2} \quad \varepsilon \frac{\partial \rho_A^{*(v)}}{\partial x^*} = \frac{\partial \rho_A^{*(s)}}{\partial x^*} . \tag{22}$$

The dimensionless diffusion coefficients now take the following form:

$$D_{AB}^{*(v)} = \frac{D_{AB}^{(v)}}{D_{AB}^{(s)}} = \varepsilon \tag{23}$$

$$D_{AB}^{*(s)} = \frac{D_{AB}^{(s)}}{D_{AB}^{(s)}} = 1 . \tag{24}$$

Transport of contaminant into the composite material composed of the polymer binding material and the getter, Eq. (6), is now described as:

$$\frac{\partial \rho^{*(s)}_A}{\partial t^*} = \frac{\partial}{\partial x^*}\left[\frac{\partial \rho^{*(s)}_A}{\partial x^*}\right] - N\left[1-\rho^{*(G)}_A\right]\rho^{*(s)}_A, \tag{25}$$

where the homogeneous reaction rate has been replaced with the expression developed in Eq. (16). The dimensionless mass concentration of species A in the getter is defined in terms of the capacity of the getter, $\rho^{(G)\max}_A$:

$$\rho^{*(G)}_A = \frac{\rho^{(G)}_A}{\rho^{(G)\max}_A}. \tag{26}$$

A new dimensionless quantity, N, that appears in Eq. (25) describes the ratio of the reaction rate in the polymer/getter region to the nominal diffusion rate of species A through the polymer/getter region:

$$N = \frac{k_o L_2^2}{D^{(s)}_{AB}}. \tag{27}$$

This parameter may also be viewed as the time required for diffusion across the polymer/getter, $\frac{L_2^2}{D^{(s)}_{AB}}$, relative to the characteristic reaction time, $\frac{1}{k_o}$. The dimensionless initial condition becomes:

$$t^* = 0 \quad \rho^{*(s)}_A = 0, \tag{28}$$

while the dimensionless boundary conditions are expressed as:

$$x^* = \frac{L_1}{L_2} \quad \rho^{*(s)}_A = s\rho^{*(v)}_A \tag{29}$$

$$x^* = 1 \quad \frac{\partial \rho^{*(s)}_A}{\partial x^*} = 0 \tag{30}$$

The last dimensionless expression is derived from Eq. (10) and is the differential species mass balance in the getter:

$$\frac{\partial \rho^{*(G)}_A}{\partial t^*} = \alpha N\left[1-\rho^{*(G)}_A\right]\rho^{*(s)}_A, \tag{31}$$

Where

$$\alpha = \frac{\rho_A^o}{\rho_A^{(G)\max}}, \tag{32}$$

characterizes the ratio of the characteristic mass concentration in the vapor phase to the mass concentration of species A in the getter at capacity. Additionally, the initial condition is:

$$t^* = 0 \quad \rho_A^{*(G)} = 0. \tag{33}$$

In deriving these equations, two important dimensionless parameters have arisen. These are:

$$N = \frac{k_o L_2^2}{D_{AB}^{(s)}}, \tag{34}$$

the ratio of the reaction rate in the polymer/getter region to the diffusion of species A through the polymer/getter region and:

$$\varepsilon = \frac{D_{AB}^{(v)}}{D_{AB}^{(s)}}, \tag{35}$$

the ratio of the diffusion coefficient in the vapor region to that in the polymer/getter region. For the current set of equations describing the transport of material throughout the microsystem, we need only to vary these two parameters over a wide range of parameters to completely characterize the system response. The values of these parameters can be determined from the property data relevant to a particular system; usually this data is derived from experimental data like that presented earlier.

4.2.3 One-Dimensional Results and Discussion

Performance of a general getter system is now examined by solving the preceding dimensionless equations. Since we are interested in the performance of a specific system, we can readily make an estimate of ε, the ratio of the diffusion coefficient in the vapor phase to that in the polymer/getter material. Typical values of the diffusion coefficient of water in the gas phase are on the order of 10^{-1} cm^2/sec, while values in polymer materials are approximately 10^{-7} cm^2/sec. This results in an epsilon value of 10^6. With one of the dimensionless quantities set, it is now only necessary to vary the other, N, over a large range of values to completely characterize the system. Additionally, the above equations require a value for the equilibrium solubility of species A in the polymer/getter region. For the time being, we use value of s = 0.02.[12] These simulations also assume that there is a continuous source of contaminant available from the vapor phase. In more realistic simulations, the contaminant would not be continuous and would instead be released in shorter duration bursts or puffs whose duration and magnitude vary.

Simulations of the system response were performed for five values of the normalized reaction rate N (10^5, 10^4, 10^3, 10^2, and 0). Larger values of N correspond to larger/faster reaction rates in the getter. Results are shown for three dimensionless times. The first is a relatively short time where the getter has not been filled to capacity for any of the specified reaction rates (values of N). The second is an intermediate time where the getter has been filled to capacity for some values of N, and finally, a relatively long time where the getter has been filled for all N. For each case, we show the dimensionless concentration profile in the solid/getter region as a function of dimensionless position (the polymer region is defined within the region x/L = 0.95 thru x/L = 1.0). Additionally, we show the dimensionless concentration of the contaminant adsorbed in the getter/polymer as a function of dimensionless time. These results are shown in Figure 20 – Figure 24. For each of the simulations performed, the contaminant concentration in the vapor phase was effectively uniform and the results are not shown.

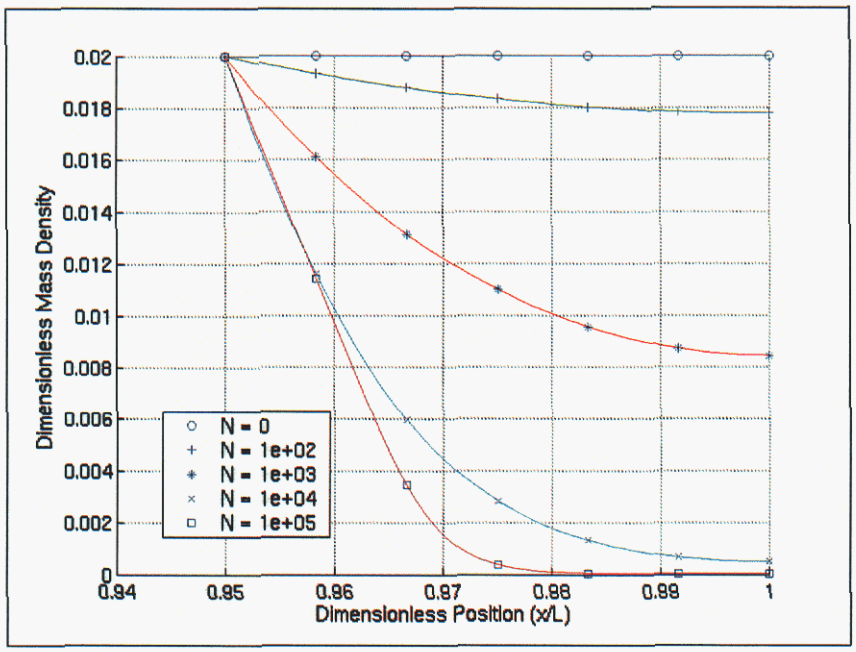

Figure 20. Concentration of unreacted contaminant in the polymer/getter region (early time)

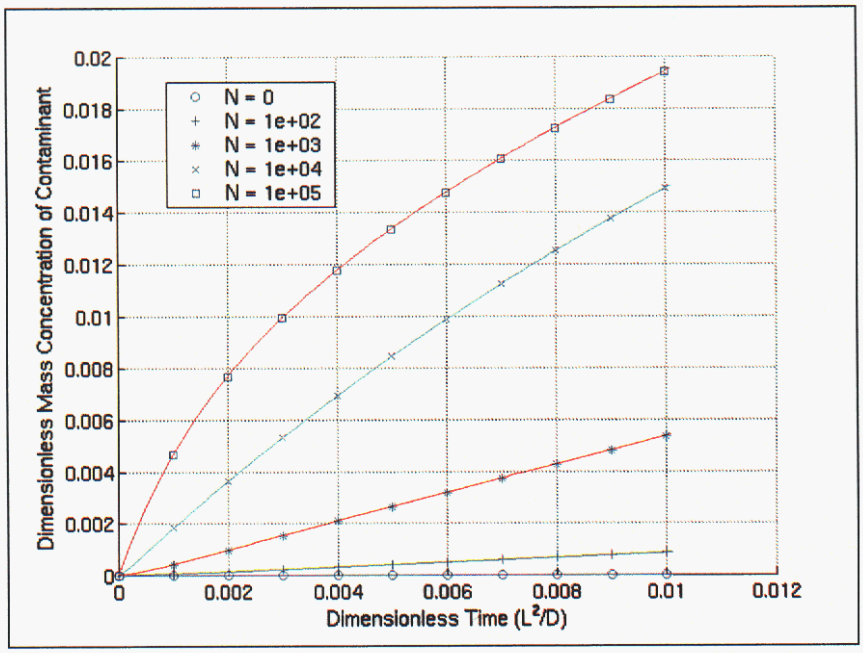

Figure 21. Concentration of contaminant reacted in getter (early time)

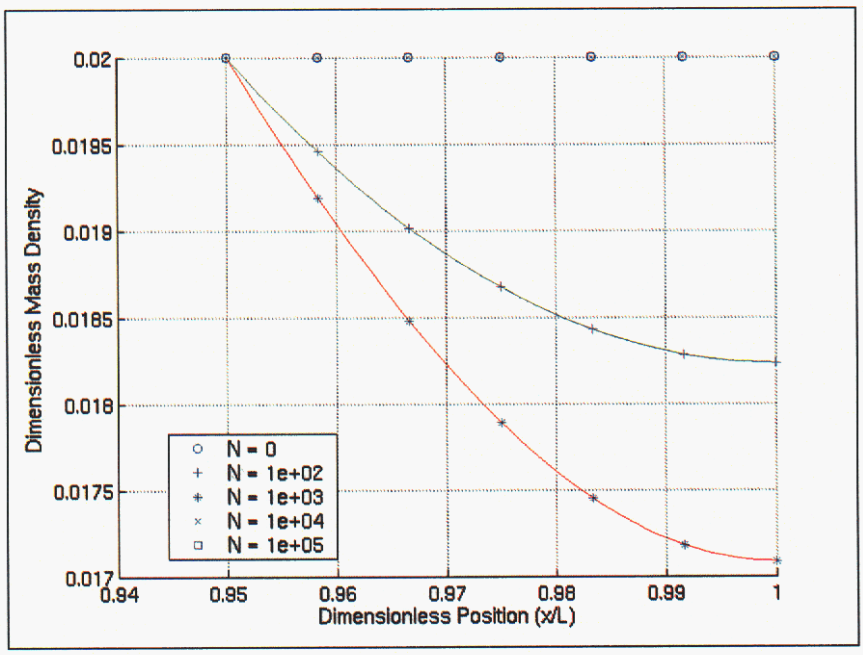

Figure 22. Concentration of unreacted contaminant in the polymer/getter region (intermediate time)

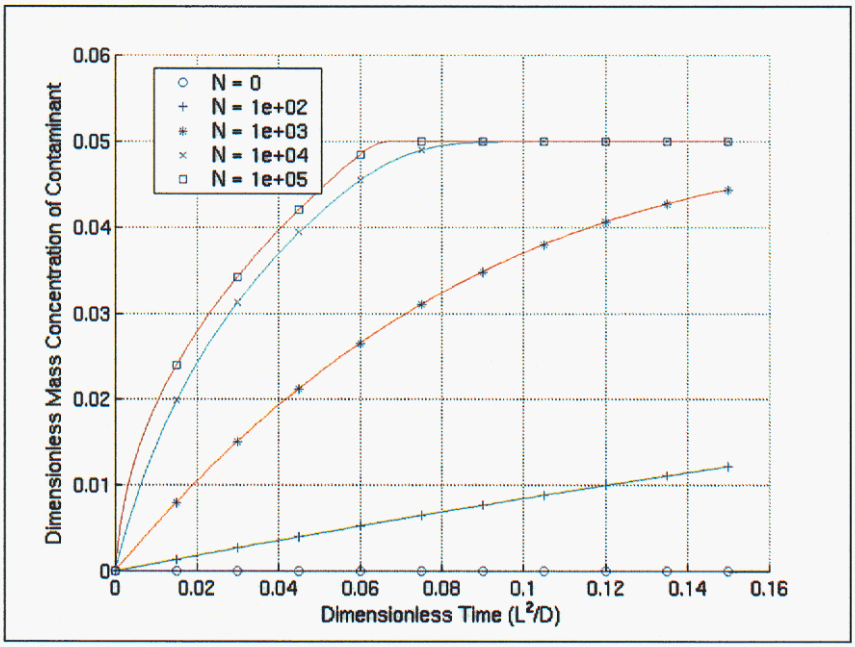

Figure 23. Concentration of contaminant reacted in getter (intermediate time)

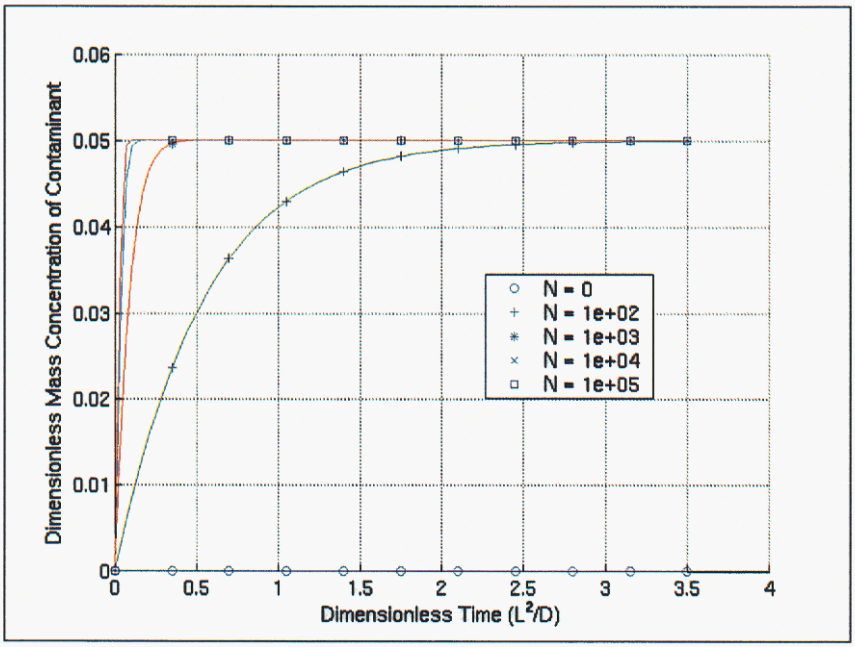

Figure 24. Concentration of contaminant reacted in getter (long time)

From these results we can make several observations. For each of the figures, the maximum contaminant concentration predicted is 0.02. This corresponds to the prescribed solubility, s, of the contaminant in the polymer/getter phase at the boundary x/L = 0.95. As the contaminant diffuses through the polymer towards the outer boundary at x/L = 1, its concentration decreases due to reaction/adsorption by the getter material.

Figure 20 shows the simulation results for the shortest time examined. Here the fastest gettering rate, corresponding to $N = 1x10^5$, reduces the unreacted contaminant concentration to zero within the polymer region. As the getter rate (N) decreases, the unreacted contaminant concentration within the polymer increases. For the case of no reaction (N=0), the concentration remains uniform at the solubility condition. Figure 21 shows the concentration of contaminant absorbed in the getter material at this same relatively short time. Here, none of the gettering rates are fast enough to fill the getter to capacity ($\rho = 0.05$) and the amount of contaminant reacted/absorbed is seen to be directly proportional to the gettering rate (N). For the case where no getter is present (N = 0), the concentration remains zero.

Figure 22 shows the contaminant concentration profile in the polymer at an intermediate time. Here, some of the reaction rates (N) are fast enough to have completely filled the getter to capacity. For the gettering rates of $N=1x10^5$ and $N=1x10^4$, we see that the contaminant concentration in the getter is uniform and at the solubility condition. In these cases, the getter has absorbed as much contaminant as it can and the system behaves as though no getter is present. Figure 23 shows the mass concentration history in the getter for each of the five gettering rates examined. Here it is apparent that the getter has reached its concentration capacity (0.05) for the two fastest gettering rates and the getter is filled. It is observed that as the getter rate decreases, the time to reach totally capacity increases. This trend is also observed for the relatively long time simulation results shown in Figure 24. Here, all of the reaction rates have had the opportunity to fill the getter and mass concentration of the getter within the polymer remains uniform at the solubility condition.

Additionally the study shows that for all values of N, the contaminant concentration is essentially constant throughout the entire vapor phase when using an estimated ε of 10^6. This indicates that diffusion in the vapor region is so fast compared to diffusion in the getter/polymer that the gas volume can be viewed as a bulk volume of uniform concentration. However, depending upon the system geometry, there may sometimes be restricted gas volumes that are slow to reach equilibration with the bulk internal volume. In addition, it may be of interest to simulate the distribution of contaminant in the vapor phase if a getter is intentionally co-located with an expected source of contamination. As a general rule, such placement seems desirable, but the magnitude of the benefit will depend on system parameters.

4.3 Advanced Two-Dimensional Modeling

Two-dimensional modeling was undertaken to better understand the role of diffusion through a composite material consisting of getter particles surrounded by a polymer matrix. In these simulations, the getter particles are explicitly modeled. First, in section 4.3.1, the two dimensional computational domain and governing differential equations are developed. Next, in Section 4.3.2, the methodology used to explicitly construct and represent the getter particles

within the polymer region is put forth. Several computations are then performed. The results are discussed in Section 4.3.3.

4.3.1. Computational Domain and Governing Equations

The domain is the same as described previously in the one-dimensional analysis. Again we view the system as being comprised of the three different regions, shown in Figure 25. The first being the internal headspace volume above the features, the second is the polymer material that surrounds the getter material, and the third being the getter particles themselves. In contrast to the previous the one dimensional model, the getter material is now modeled as a collection of permeable spheres suspended within a polymer layer that is attached to the package lid. In this approach we compute the lateral transport across the width as well as the longitudinal transport modeled previously.

The getter is now represented explicitly as a collection of non-overlapping circles of a specified radius randomly distributed throughout the polymer layer. Such an approach is often used to describe dual media or dual porosity systems.[13] Here, the contaminant species A is allowed to diffuse through the polymer region, but upon reaching the getter region, does not automatically react, but instead is allowed to diffuse (Knudsen diffusion) into the getter microspores where it may react. Because of the large aspect ratio between the width and height of the polymer phase, we chose to model a representative cell taken from an array that is assumed to be spatially periodic in the transverse direction. This greatly reduces the computational work with little reduction in fidelity.

As in the one-dimensional approach, we model the transport within the package by coupling a system of differential equations together, one for each region. However, since the results of the one-dimensional simulations indicated that transport through the vapor region is much faster than that through the polymer, we now assume that the vapor phase mass concentration is uniform. Again, three differential mass balance equations are required. The first describes the transport of contaminant through the polymer region surrounding the getter, the second describes the diffusion of contaminant into and through the getter, and the third describes the amount of contaminant that has been adsorbed/reacted within the getter.

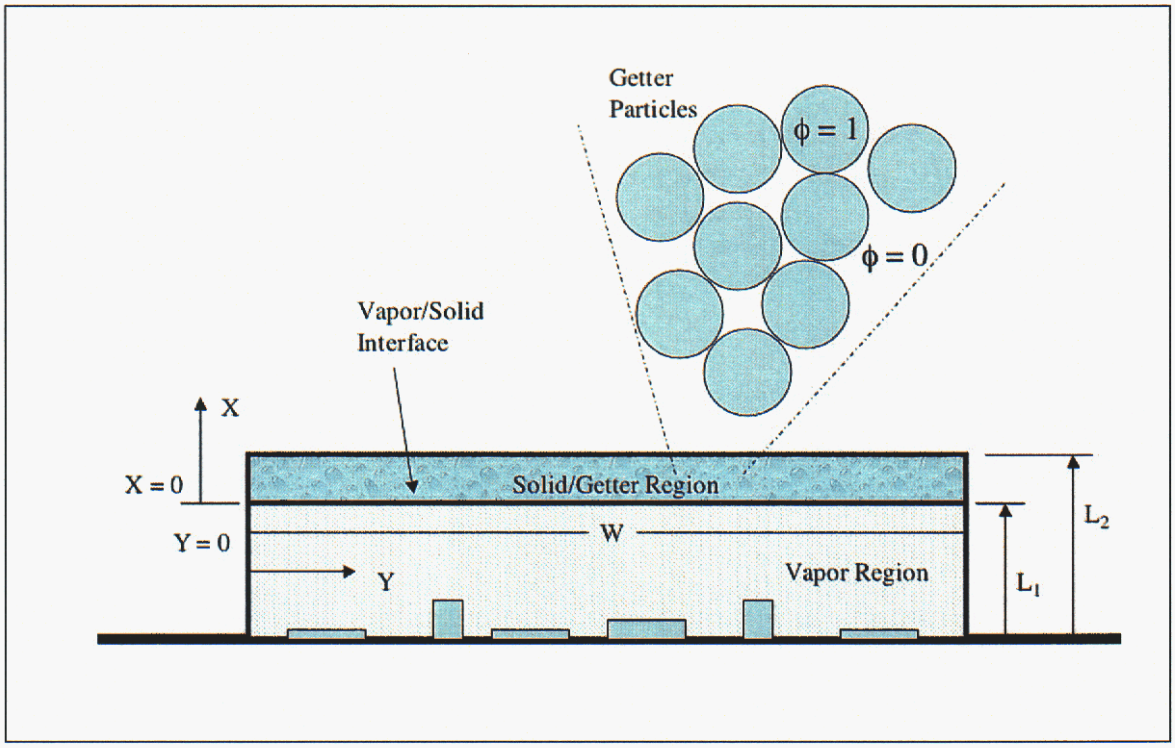

Figure 25. Computational domain for two-dimensional model.

The equation describing two-dimensional transport of contaminant through the solid polymer (superscript s) is:

$$\frac{\partial \rho_A^{(s)}}{\partial t} = \frac{\partial}{\partial x}\left[D_{AB}^{(s)} \frac{\partial \rho_A^{(s)}}{\partial x}\right] + \frac{\partial}{\partial y}\left[D_{AB}^{(s)} \frac{\partial \rho_A^{(s)}}{\partial y}\right]. \tag{36}$$

As before, the initial concentration within the polymer region is taken to be zero and the boundary conditions in the x direction are the same as in the one-dimensional case. In addition, we now apply no flux boundary conditions on the sides of the microsystem lid (y-direction):

$$y = 0 \quad \frac{\partial \rho_A^{(s)}}{\partial y} = 0 \tag{37}$$

$$y = W \quad \frac{\partial \rho_A^{(s)}}{\partial y} = 0 \tag{38}$$

The diffusion of contaminant through the getter material is described using the following equation:

$$\frac{\partial \rho_A^{(G)}}{\partial t} = \frac{\partial}{\partial x}\left[D_{AB}^{(G)} \frac{\partial \rho_A^{(G)}}{\partial x}\right] + \frac{\partial}{\partial y}\left[D_{AB}^{(G)} \frac{\partial \rho_A^{(G)}}{\partial y}\right] + r_A^{V(G)}, \tag{39}$$

where $r_A^{V(G)}$ is evaluated using Eq. (16). The initial condition assumes that the getter initially contains no contaminant. At the boundary of the polymer and getter regions, it is assumed that the mass concentrations are in equilibrium so that:

$$\rho_A^{(G)} = \frac{\rho_A^{(S)}}{s}. \tag{40}$$

In the computational approach explained below, however, there is no need to explicitly apply the boundary condition between the getter and the polymer along the very complex interfacial boundary.

Finally, the accumulation of contaminant within the getter material is modeled by the following initial value problem:

$$\frac{\partial \rho_B^{(G)}}{\partial t} = -r_A^{V(G)}, \tag{41}$$

where again the reaction rate is given by Eq. (16). The initial condition assumes that initially the getter contains no reacted species.

To circumvent the complexity of the getter/polymer interface, we define a function ϕ, that takes on discrete values of either one, for a location in a getter particle, or zero, for a location in the polymer region. Based on this definition, we write a single differential equation describing transport of contaminant within both the polymer and getter regions.

$$\frac{\partial \rho(\phi)}{\partial t} = \frac{\partial}{\partial x}\left[D(\phi)\frac{\partial \rho(\phi)}{\partial x}\right] + \frac{\partial}{\partial y}\left[D(\phi)\frac{\partial \rho(\phi)}{\partial y}\right] + r(\phi), \tag{42}$$

where

$$\rho(\phi) = \phi\, s\rho_A^{(G)} + (1-\phi)\rho_A^{(S)} \tag{43}$$

$$D(\phi) = \phi D_{AB}^{(G)} + (1-\phi) D_{AB}^{(S)} \tag{44}$$

$$r(\phi) = \phi \hat{k}_A^{V(G)} \cdot \frac{\mathrm{M}^{(G)}}{\mathrm{V}^{(G)}}\left[1 - \frac{\rho_B^{(G)}}{\rho_B^{(G)\max}}\right]\rho_A^{(G)}. \tag{45}$$

This equation reduces to the previous equations, Eq. (36) and Eq. (39), within their respective domains of application and it implicitly satisfies the equilibrium matching condition, Eq. (40),

which applies at getter/polymer interfaces. The expression for the reaction rate developed in Eq. (16) still applies and the initial concentration is still taken as zero. The boundary conditions for the x-direction are:

$$x=0 \quad \rho=\phi s\rho_{Ao}^{(v)}+(1-\phi)s\rho_{Ao}^{(v)} \tag{46}$$

$$x=L \quad \frac{\partial\rho}{\partial x}=0 \tag{47}$$

No flux conditions are still applicable at the symmetry boundaries of a unit cell:

$$y=0 \quad \frac{\partial\rho}{\partial y}=0 \tag{48}$$

$$y=W \quad \frac{\partial\rho}{\partial y}=0 \tag{49}$$

Once these equations are solved for ρ, the contaminant concentrations in the getter and the polymer phase are determined as follows:

$$\rho_A^{(S)}=\rho \quad \text{where } \phi=0 \tag{50}$$

$$\rho_A^{(G)}=\frac{\rho}{s} \quad \text{where } \phi=1 \tag{51}$$

This approach effectively switches between the two independent equations describing the diffusion and reaction of the contaminant in the polymer and getter regions. Although this technique assumes local equilibrium at all getter/polymer interfaces, this is expected to be a good approximation.

4.3.2. Explicit Getter Representation

For the two-dimensional analysis described above, it is necessary to create a computational domain that explicitly represents the getter material. The thickness of the polymer layer is expected to be about 1/20th of the microsystem height. Thus, for a 2 mm thick microsystem, the polymer layer is expected to be approximately .4 mm or 400 microns. The particle diameter of the getter is approximately 50 micron. Therefore, if packed perfectly and touching, we expect a maximum of eight particles across the depth of the polymer material; in practice we would expect a number closer to six particles at a volume fraction of around 35%. The width of the system is expected to be 1 mm – 5 mm, which corresponds to approximately 1000-5000 getter particles stacked side by side. Because of this large difference in length scales, there are two options. The first is to view the polymer material as a composite material, as done for the one-dimensional work, or second, create an explicit representation of the getter as a spatially periodic structure. The second approach is demonstrated below. In these calculations a unit cell is used to examine the character of diffusion within the getter/polymer material; this behavior is then

extrapolated over the full width of the getter/polymer material to simulate the entire microsystem.

In the example calculations the getter is represented as a collection of non-overlapping circles, having a diameter of 50 microns. These circles are randomly distributed throughout the thin polymer unit cell region that we specify as having a width of about five times its depth. For the project, we developed a MATLAB code to create the required getter structure. Within the code, the desired domain size, circle diameter and desired volume fraction of getter is first specified. A pair of random numbers is then generated and used to define the center coordinates of the new candidate circle. Using the specified radius, a test circle is created at these coordinates. Since the getter representation must be spatially periodic, we must first determine if the circle crosses any of the external boundaries. If so, we must generate an additional center point that corresponds to the center of the reflected circle. This check is done for all four boundaries. We now evaluate the test circle and all of its boundary reflections, if any, to see if they overlap with the current set of 'good' circles. If not, we add the test circle to the set of good circles and calculate a new volume fraction of getter relative to the overall volume of the getter/polymer composite. Since it is possible to specify a particle diameter, domain size, and volume fraction, that cannot be physically constructed, we also keep track of the number of failed attempts where a test circle is not added to the good circles. The process continues until the desired volume fraction or the maximum number of iterations is reached.

Examples of the unit cells computed by the developed algorithm are shown in Figures 26 and 27. A dimensionless domain is utilized where the width is five times the height. The circles are intended to represent the getter phase distributed randomly through the polymer phase. The difference between the figures is that the desired volume fraction of getter to polymer is 40 percent in Figure 26 while in Figure 27 it is 20 percent. These explicit representations of the getter material can be used to evaluate the importance of particle-to-particle diffusion in getter/polymer composite materials.

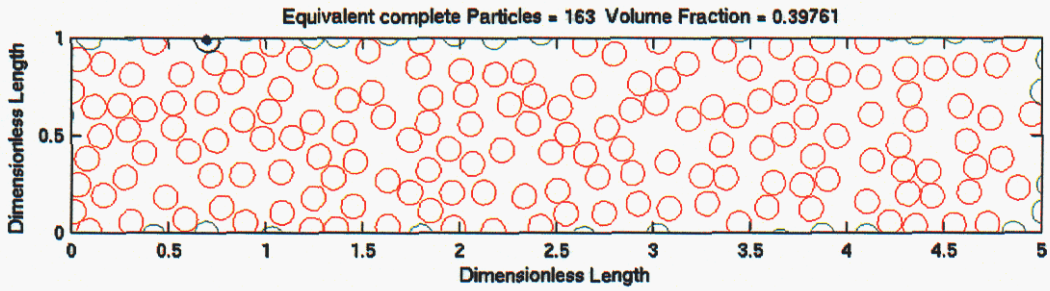

Figure 26. Computational domain (unit cell) for two-dimensional model - Explicit getter representation having a volume fraction of 40% getter to polymer.

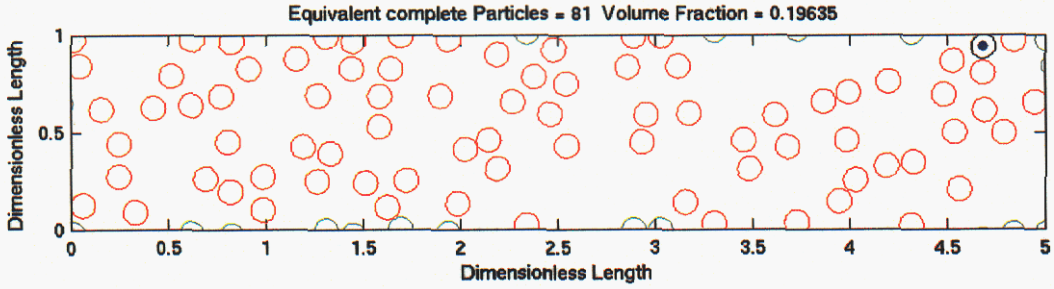

Figure 27. Computational domain (unit cell) for two-dimensional model - Explicit getter representation having a volume fraction of 20% getter to polymer.

Since the getter regions are defined by a family of circles, we can readily determine whether a computational zone lies within a getter circle and, if so, assign the appropriate value of ϕ. Once these assignments have been made it is only necessary to solve the discretized form of the differential, Eq. (42).

4.3.3. Two Dimensional Results and Discussion

As in the one-dimensional case, the equations developed above are first discretized and then solved using MATLAB. The results are the mass concentrations of the contaminant in the polymer region, the concentration of the contaminant diffusing throughout the getter particles, and the amount of contaminant reacted with the getter as a function of space and time. Again, we may determine the total amount of species A (water or ethanol in our case) in any particular region by integrating the dimensionless mass density over the volume of the region:

In the two-dimensional work, we are primarily interesting in understanding the effects of the diffusion through the getter material and the possible influence of particle-particle contact. Therefore, we simulate the process for two getter geometries: the first having a volume fraction of 0.40 and the second having a volume fraction of 0.20. We solve the problem on a dimensionless domain where the width of the unit cell is five times the height. The boundaries along the domain correspond to the lid of the microsystem and are sealed so that no contaminant can enter or leave. The bottom boundary corresponds to the vapor/polymer interface in the microsystem and it is assumed that we have a constant and uniform concentration of contaminant at this surface at all times. In an actual microsystem, the assumption of uniformity is expected to hold because of the high diffusivity in the vapor phase. Although the interfacial boundary condition will generally vary as a function of time, it is instructive to initially examine the fundamental case of a constant contaminant concentration in the open gas volume of the package.

Estimates of the diffusion coefficients of the contaminant in both the polymer material and the getter are now required. Literature values for diffusion of water through a number of different polymers are in the range of $1\text{x}10^{-11}$ m^2/s, whereas a much larger diffusivity of $1\text{x}10^{-7}$ m^2/s is appropriate to the micro porous spheres of getter material. As in the one-dimensional case, we use an equilibrium contaminant solubility of s = 0.02. Before simulations can be performed, it is also necessary to specify a reaction rate constant, $\hat{k}_A^{V(G)}$, and the capacity of the getter, $\rho_B^{(G)\max}$, in Eq. (45). Since these quantities are getter specific, we utilize the same set of representative

values in both of the simulations performed. Based on experimental evidence, the reaction rate coefficient of the getter is set to a large value corresponding to a fast reaction. The maximum getter capacity, $\rho_B^{(G)\max}$, is set to an intermediate value that reaches saturation in a reasonable timeframe. While such values are suitable for the current analysis, more system specific parameters may be determined and used when required, as in Section 4.4.2.

Computed two-dimensional concentration profiles are illustrated in the next sequence of figures; each contains three vertically stacked frames. In each, the top frame shows the amount of contaminant that has reacted in the getter as a fraction of its total capacity, the middle frame shows the concentration profile in the polymer material relative to its equilibrium solubility, and the bottom frame shows the normalized concentration profile of the contaminant diffusing through the getter material and the polymer. For each simulation, three different times are shown in a series of figures: early, intermediate, and late. Finally, for each of the simulations, the average contaminant concentration reacted in the getter phase and absorbed by the polymer is displayed as a function of dimensionless simulation time.

The first set of results is for a volume fraction of 40%. Figure 28 shows the two-dimensional concentration profiles for an early time. The top profile reveals that most of the getter particles have absorbed little to no contaminant. Only those particles near the source of the contaminant have started to react and adsorb material. The middle frame shows the concentration profile of the contaminant in the polymer material. The concentration front is seen to be fairly uniform, but variations due to diffusion of material through the high diffusivity getter particles are seen. The bottom frame in Figure 28 shows that the getter material near the source has reached a maximum concentration and that as the distance from the source increases so does the concentration of the contaminant adsorbed in the getter.

Figure 29 shows the two-dimensional profiles at an intermediate time later than Figure 28. Here, the top frame shows that most of the getter particles near the source have reached capacity while those at the top of the system have absorbed about 50% of their capacity. The middle frame shows that although the getter has continued to react and absorb the contaminant, the concentration in the polymer has only increased slightly. Thus, it seems that while the getter is reacting, the concentration profile in the polymer phase varies only slightly. Again the bottom profile shows only a slight change in the amount of contaminant that is diffusing through the getter and polymer.

The last set of three frames in Figure 30 show a dramatic change for a time much later in the simulation. Here, in the top profile, we see that all of the getter has nearly reached capacity. The getter material is no longer able to absorb any incremental contaminant near the surface. Because of this, the middle profile shows that that the contaminant has continued diffusing deeper into the interior of the polymer. Soon, all of the getter will have reached capacity and the entire polymer will be at its saturation limit. The bottom profile in this figure shows that the contaminant is diffusing fairly uniformly across the polymer/getter region.

Finally, in Figure 31, we see the time histories of the mean concentrations of contaminant in the polymer and in the getter, averaged over the entire getter/polymer region. Each of these concentrations is normalized by either the equilibrium concentration in the case of the polymer,

or the maximum capacity, in the case of the getter. The figure shows that initially the average polymer concentration rises quickly to a value of about 27% of its equilibrium level. The getter regions near the source of the contaminant react somewhat slower than the surface polymer regions, thereafter increasing, monotonically toward capacity. As more and more of the getter is filled, the contaminant in the polymer region travels further and further from the source before it is captured by the getter. Thus, the concentration in the polymer region slowly increases as the getter concentration increases. Finally, as all of the getter reaches its capacity, the contaminant concentration in the polymer phase quickly rises to its equilibrium concentration. At this point, the getter and polymer are full and no more contaminant can enter the system.

Simulations for a getter volume fraction of 20% are illustrated in Figure 32 through Figure 35. Figure 32 shows the two-dimensional profiles near the beginning of the simulation. As immediately evident, there are now about half as many getter particles as before. The results are similar to those for the 40% volume fraction. In the top profile, only the getter particles near the contaminant source have started to fill. The middle profile shows that the contaminant concentration in the polymer is fairly uniform, although diffusion through the getter does play a role.

As in the 40% scenario, the top profile in Figure 33 shows that for an intermediate time that the getter particles near the source are almost full while those near the top of the system have reached only 20% of capacity. The middle profile shows that the concentration in the polymer has continued to advance, but only slightly. In the late-time profiles of Figure 34 most of the getter material has reached capacity and the concentration front of the polymer, shown in the middle profile, has begun to advance towards the top edge of the getter/polymer region as seen earlier in the results for a 40% volume fraction.

Finally, Figure 35 shows the average contaminant concentration in the getter and the polymer respectively normalized by the equilibrium saturation and total capacity. The profiles are very similar to those in Figure 31 for a 40% getter volume fraction. As before, the amount of contaminant reacted in the getter increases monotonically until reaching capacity. The contaminant concentration in the polymer quickly jumps to approximately 29% of its equilibrium value. It is also observed that the concentrations for a 40% volume fraction reach maximum values at an earlier time than the 20% case, but the difference in filling times is remarkably small.

In the present example, there are surprisingly few differences in the time response of systems having getter volume fractions of 20% and 40%. One important difference in properties is that the 40% system can hold more contaminant since more getter material is available. Despite this factor of two difference in the capacitance, the required filling time is nearly the same. A probable explanation is that a doubling of the amount of high-diffusivity getter material has essentially doubled the diffusivity of the composite material, a claim made plausible by examination of the particle configurations in Figure 26 and Figure 27. A doubling of both the bulk capacitance and the bulk diffusivity would leave the filling time unchanged. However, it is quite certain that this simple linear scaling argument will fail in other ranges of relative volume fractions, requiring further calculations to reliably predict system response.

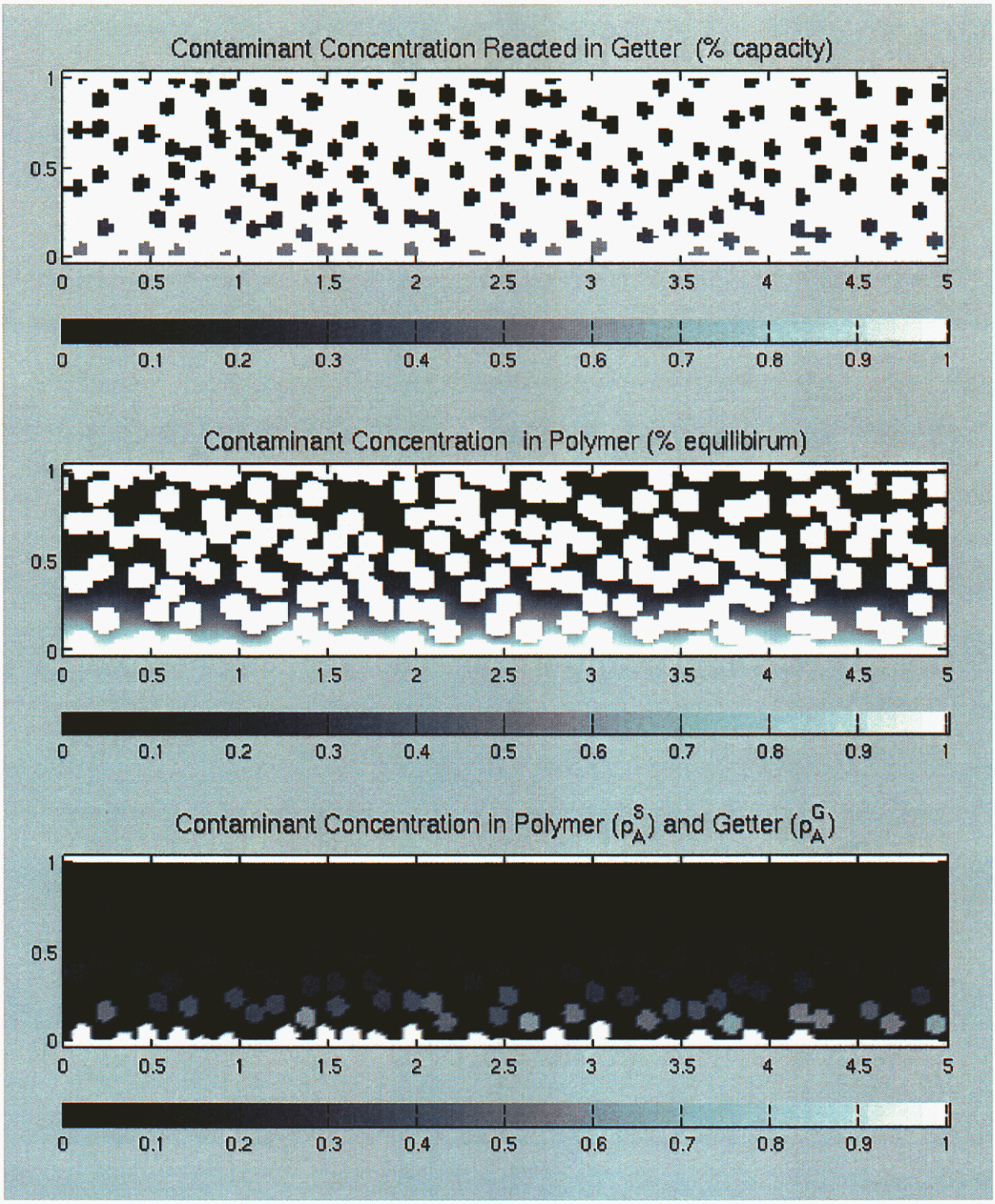

Figure 28: Two-dimensional simulation results (40% volume fraction) (early time)

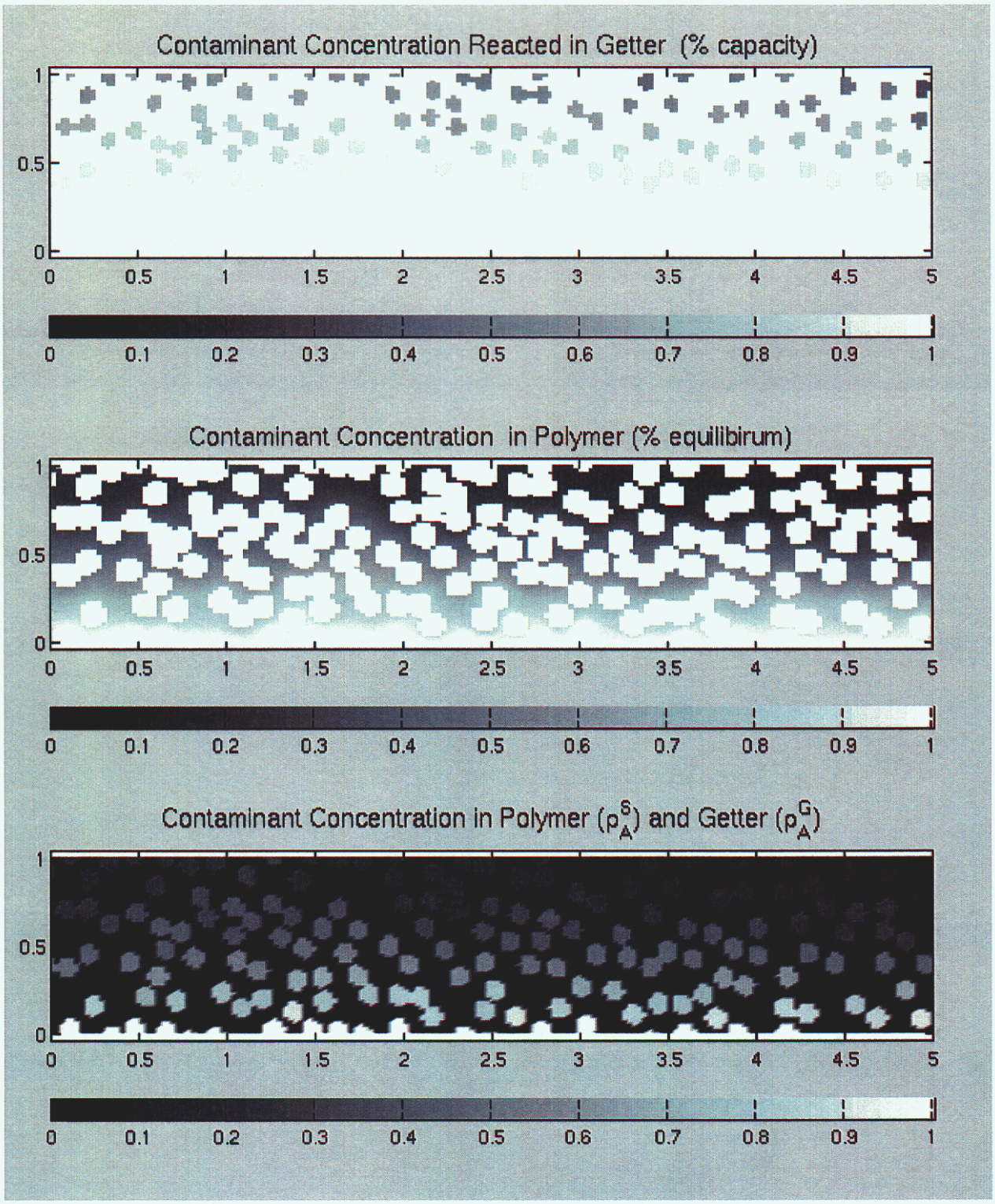

Figure 29: Two-dimensional simulation results (40% volume fraction) (intermediate time)

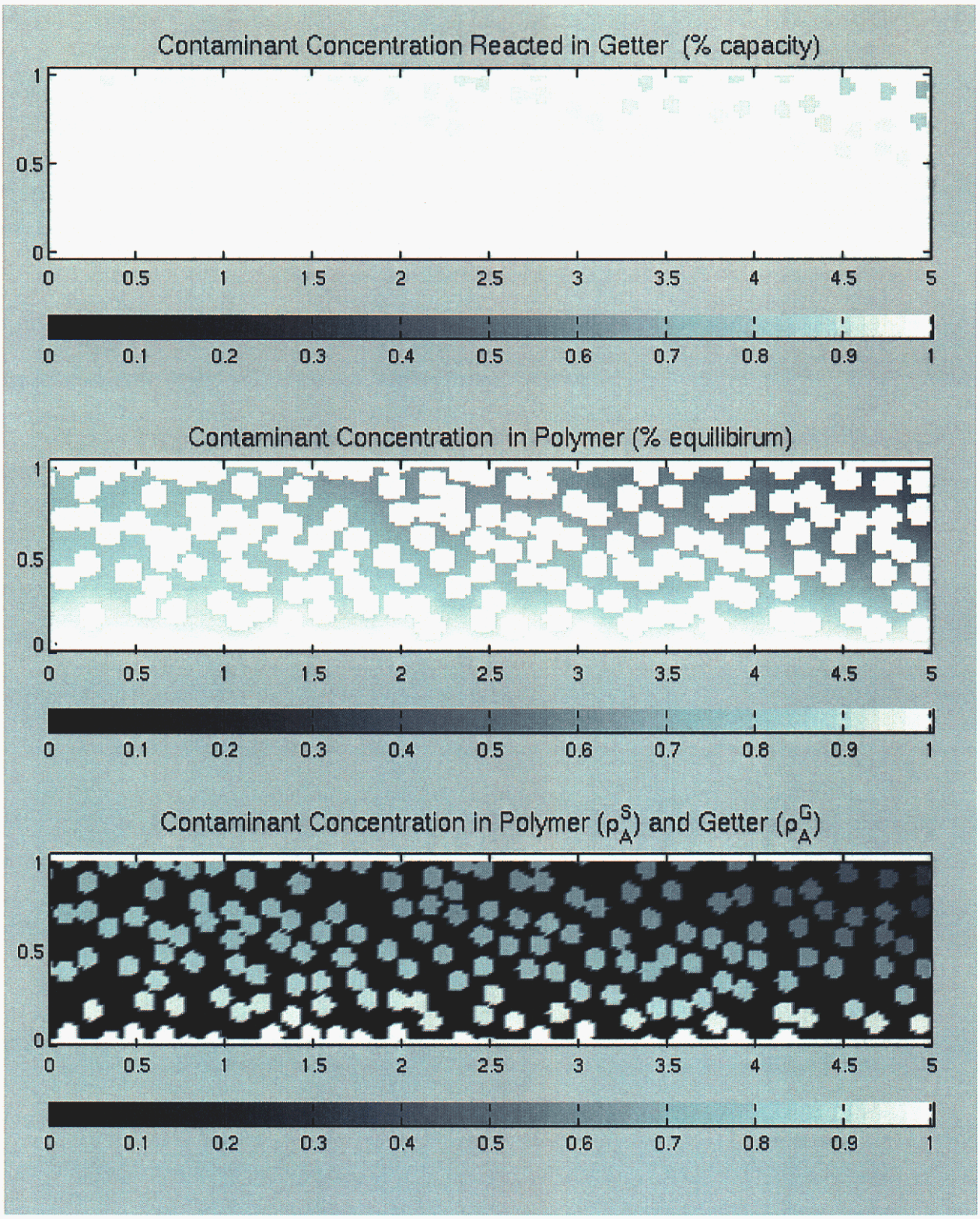

Figure 30: Two-dimensional simulation results (40% volume fraction) (long time)

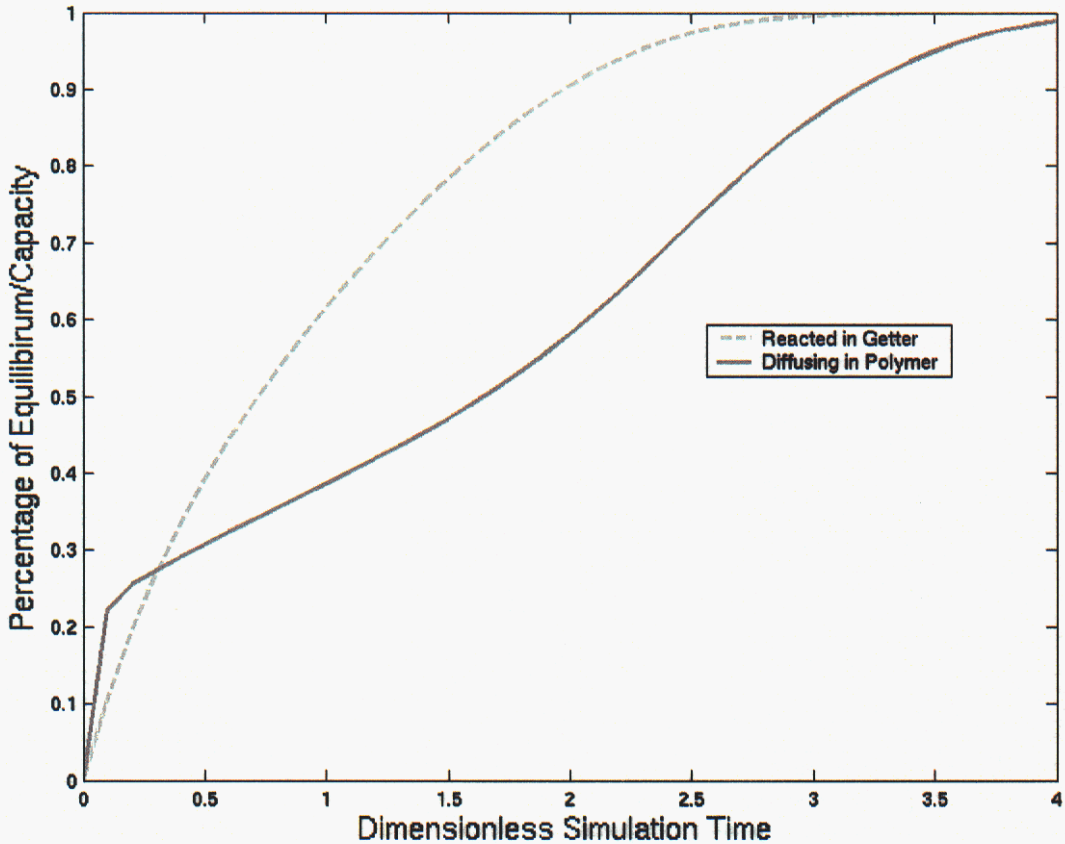

Figure 31: Mean contaminant concentration in getter and polymer regions (40% volume fraction)

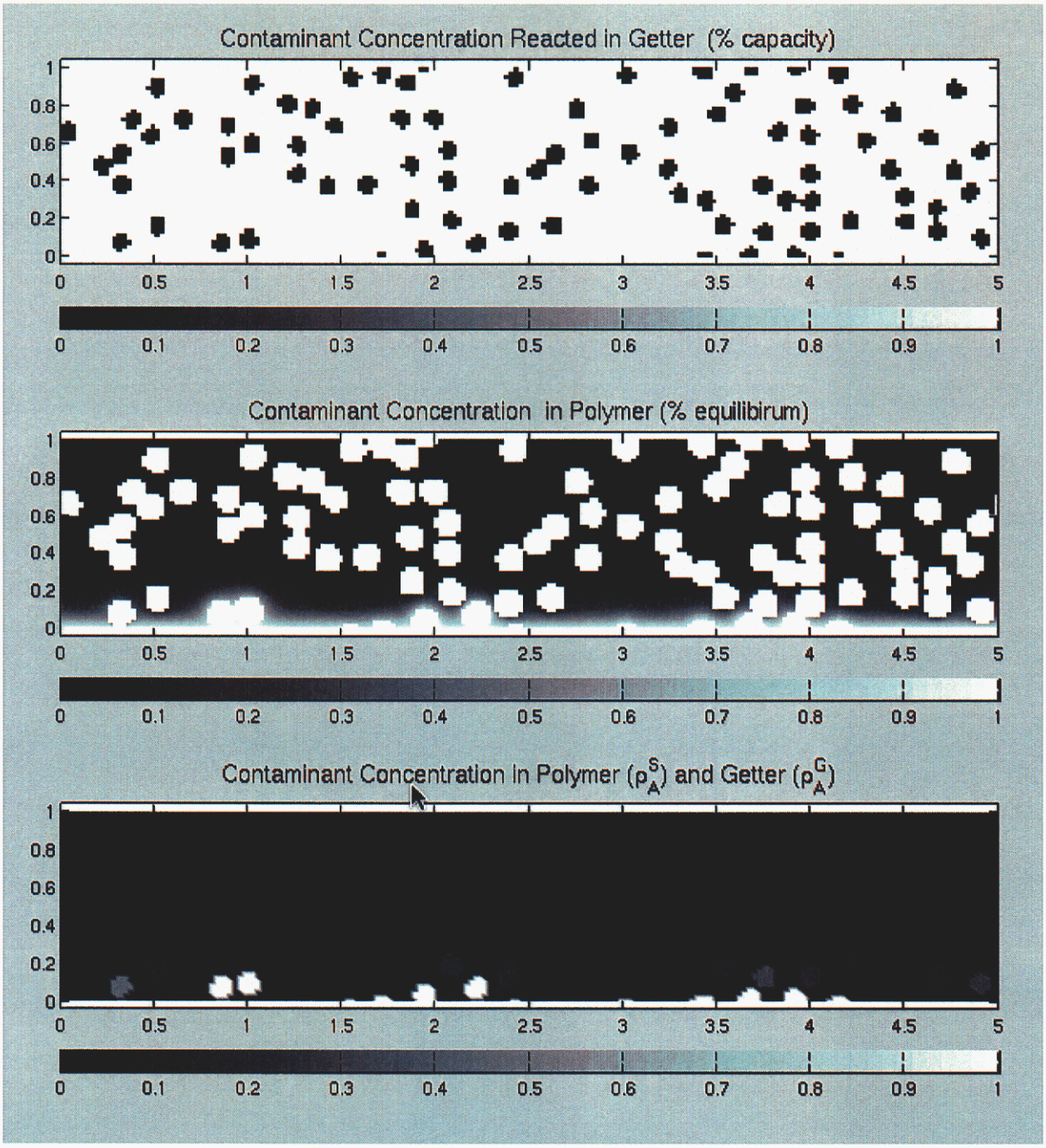

Figure 32: Two-dimensional simulation results (20% volume fraction) (early time)

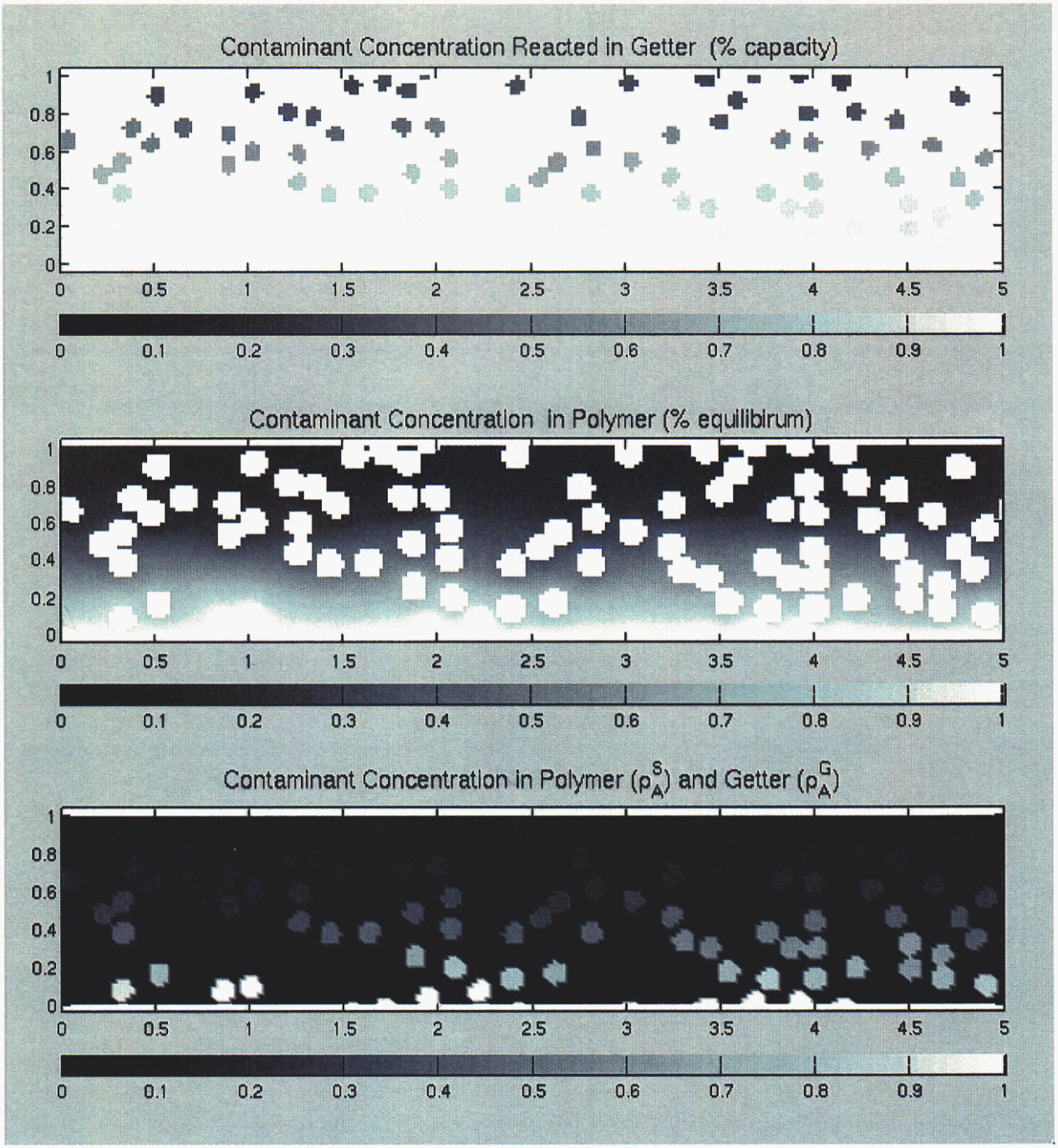

Figure 33: Two-dimensional simulation results (20% volume fraction) (intermediate time)

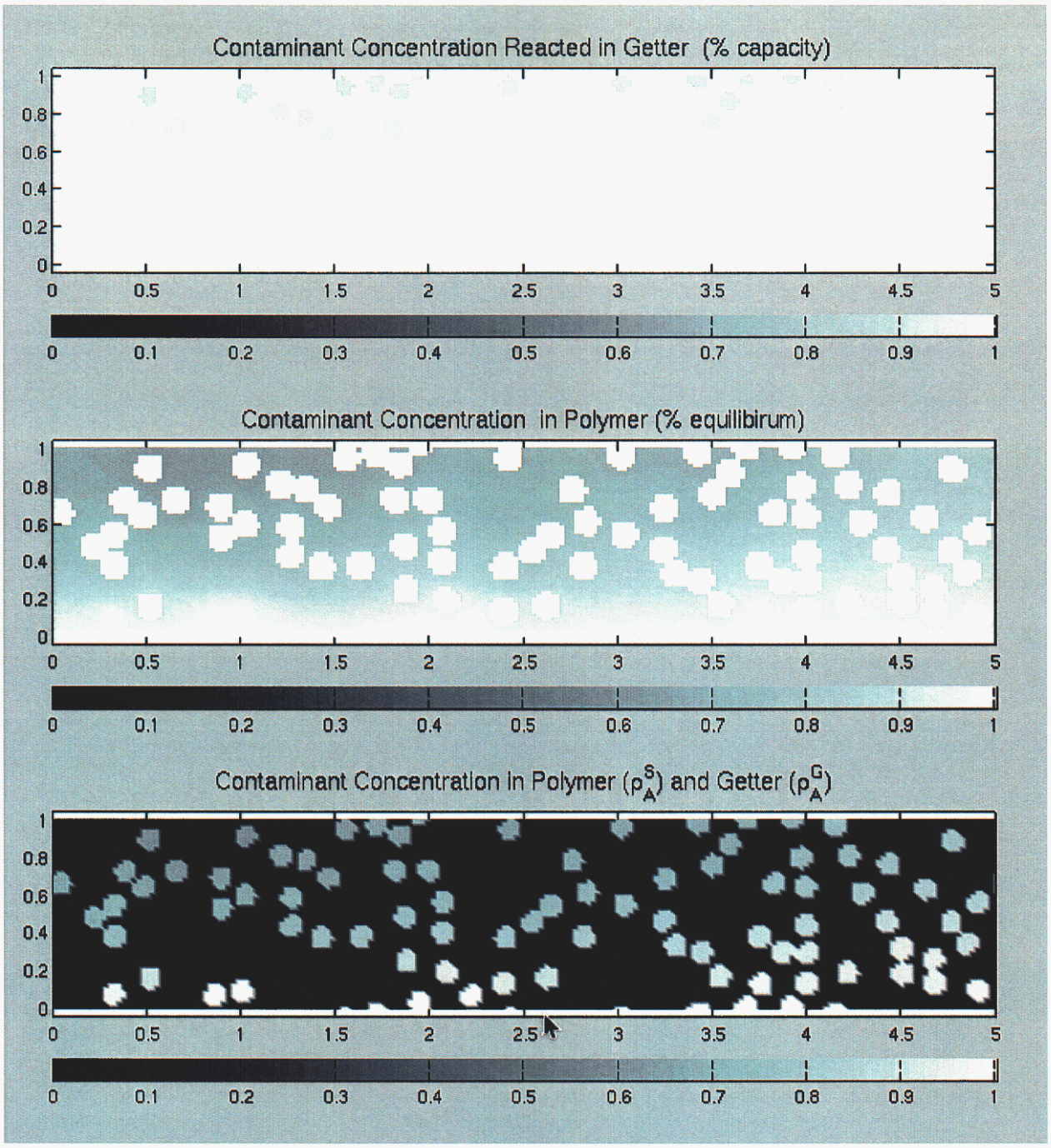

Figure 34: Two-dimensional simulation results (20% volume fraction) (long time)

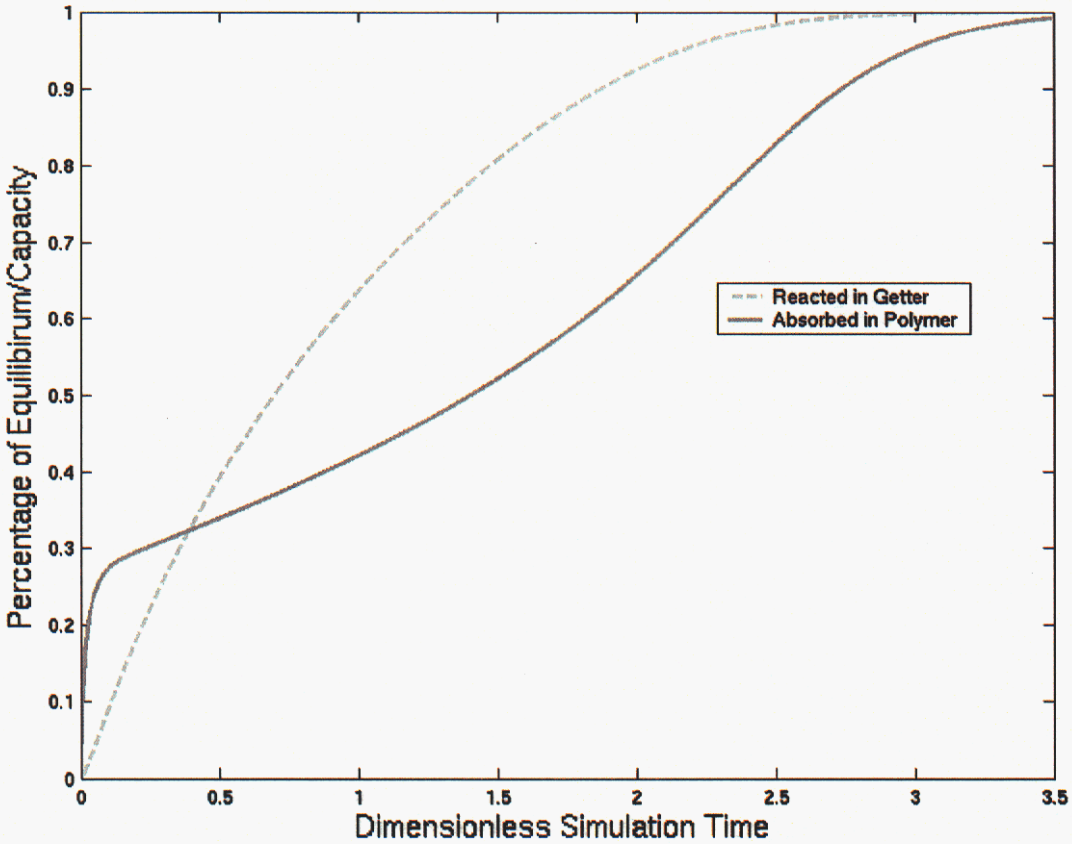

Figure 35: Mean contaminant concentration in getter and polymer regions (20% volume fraction)

4.4 Analysis of Experiments

Before the models developed above can be used for any specific application, it is necessary to determine several system specific parameters. These include getter parameters such as the getter reaction rate, maximum capacity, and the getter equilibrium absorption curve. Additionally, since a polymer binding material surrounds the getter, the properties describing storage and transport of contaminant species within the polymer must also be determined. Such properties include the diffusion coefficient of both water and ethanol through the polymer and additionally the equilibrium solubility/capacity of both species within the polymer itself.

Several experiments were performed to determine these system specific parameters as described earlier in this report. These experimental results are now analyzed to determine the relevant material properties. For situations where experiments could not be performed, or the experimental data was inconclusive, values obtained from the literature are reported.

Two different sets of data are analyzed in the present section. The first sets of experiments, analyzed in Section 4.4.1, were performed in a saturated vapor environment. These experiments, conducted for both H_2O and EtOH, were designed to estimate the important transport (diffusion coefficients) and storage properties (maximum equilibrium saturation) of the polymer binder used to hold the getter particles within the microsystem.

The second set of experiments was designed to estimate the getter reaction rate in environments that are similar to what is expected in actual microsystems. Here ppm quantities of contaminant are introduced into a sealed vessel and IR spectroscopy is used to observe the time history of vapor phase concentration. These experiments are analyzed in Section 4.4.2.

4.4.1 Diffusion/Solubility experiments

Because a polymer binder material surrounds the getter, the transport of contaminants through the polymer plays an important role in controlling the overall rate of gettering. In order to estimate the diffusion coefficient associated with contaminant transport through the polymer material, several experiments were conducted. While details of the experiment are discussed in Section 3.3, an overview of the procedure is included here.

The experiment is designed to observe the amount of mass absorbed by a given volume of Ricon polymer material as a function of time. A total of twelve samples were investigated; six to evaluate the transport of water and six to evaluate the transport of ethanol. For each sample, a cylindrical stainless steel dish was filled with polymer at one of three thicknesses: 1 mm, 5 mm, and 10 mm. Thus two samples at each thickness were created for each contaminant.

First, the initial weight of each sample was recorded. Then each set of samples was placed into a saturated vapor phase environment of either water or ethanol, where they were allowed to absorb mass by diffusion from the exposed sample face into the interior. At several times during the experiment, the samples were removed and weighed to determine the amount of contaminant that had been absorbed.

This mass uptake history observed for each sample was used to estimate the diffusion coefficient of the contaminant within the sample. Additionally, after a relatively long time within the

saturated vapor environment, the corresponding equilibrium value of the contaminant concentration within the polymer was also estimated.

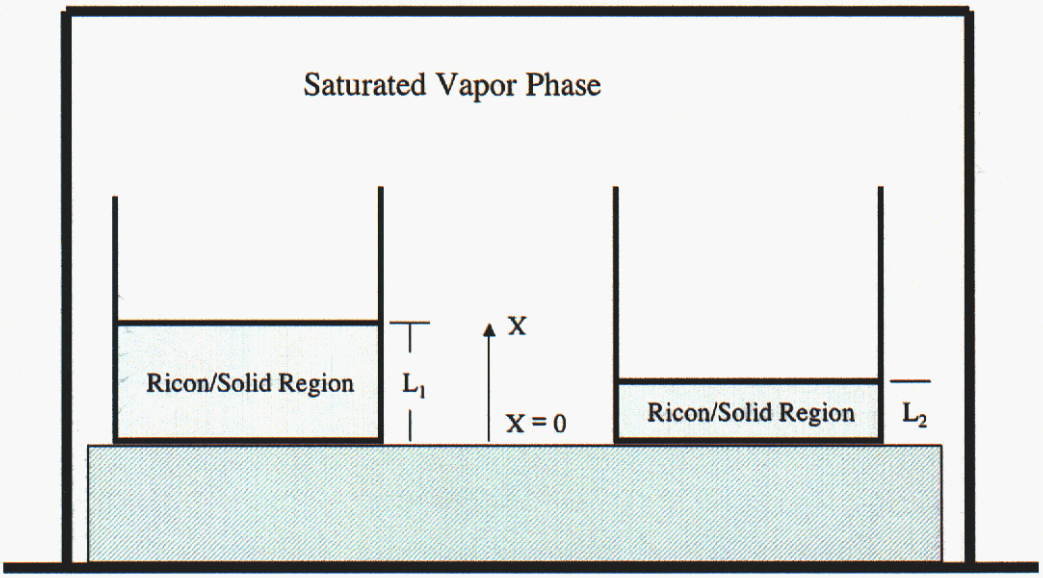

Figure 36: Computational domain used for diffusion analysis

Using the computational domain shown in Figure 36, we can describe the uptake of contaminant in the polymer using the following one-dimensional diffusion equation. Here, the diffusion coefficient is assumed to be independent of the contaminant concentration within the polymer (Fickian diffusion):

$$\frac{\partial \rho_A^{(s)}}{\partial t} = \frac{\partial}{\partial x}\left[D_{AB}^{(s)} \frac{\partial \rho_A^{(s)}}{\partial x} \right]. \tag{52}$$

The required boundary conditions assume that no contaminant leaves the bottom of the dish, and that the top surface of the polymer layer is equilibrium with the adjacent saturated vapor:

$$x = 0 \quad \frac{\partial \rho_A^{(s)}}{\partial x} = 0 \tag{53}$$

$$x = L \quad \rho_A^{(s)} = s\rho_A^{o} \tag{54}$$

For such a simple geometry, Equation 52 can be solved analytically. The total uptake of contaminant within the polymer can then be determined by integrating over the polymer volume

$$M^{(S)}{}_A = \int_{V^{(S)}} \rho_A^{(S)} dV^{(S)}. \tag{55}$$

The total uptake of mass within the polymer at any time can therefore be written in terms of the diffusion coefficient and the maximum capacity of the contaminant in the polymer as:

$$M_A^{(S)}(t) = M_A^{\infty}\left[1 - \sum_{n=0}^{\infty} \frac{8e^{-\lambda_n^2 \mathbf{D} t}}{\left[(2n+1)\pi\right]^2}\right], \tag{56}$$

where λ_n is defined as:

$$\lambda_n = \frac{(2n+1)\pi}{2L}. \tag{57}$$

The maximum capacity is readily related to the equilibrium concentration and solubility,

$$M_A^{\infty} = \int_{V^{(S)}} \rho_A^{\infty(S)} dV^{(S)}. \tag{58}$$

Its value can be estimated by observing the amount of absorbed mass at long experimental times. If an estimate of the equilibrium concentration in the polymer is not known, its value may also be estimated from least squares analysis of the data.

A least squares optimization is used to determine the diffusion coefficient appearing in Eq. (56). The analysis is accomplished by forming an objective function; a measure of the error between the experimentally observed mass uptake and the theoretically predicted value:

$$\underset{\min}{J} = \sum_{i=1}^{N_D} \left[M_A^{(S)}(t_i, D) - M(t_i)\right]^2. \tag{59}$$

This expression is a function of the diffusion coefficient, and, if necessary, the equilibrium saturation concentration. The analysis, which is performed in MATLAB seeks to determine the value of the diffusion coefficient that minimizes this function. Salazar[12] estimated diffusion coefficients in polymers using a similar technique.

Case	Thickness (mm)	Diffusivity (cm^2 / s)	Equilibrium % Capacity (g H2O/ g polymer)*100%
(A1)	1	1.0034E-8	2.3000E-3
(A2)	1	3.4514E-8	9.3042E-2
(A1+A2)	1	1.6234E-8	9.3042E-2
(B1)	5	1.1864E-7	5.2340E-2
(B2)	5	5.0484E-8	4.7684E-2
(B1+B2)	5	7.8381E-8	4.7687E-2

Table II: Estimated diffusivity and equilibrium capacity for water in Ricon polymer

Case	Thickness (mm)	Diffusivity (cm^2 / s)	Equilibrium % Capacity (g EtOH / g polymer)*100%
(A1)	1	6.9709E-7	2.0000
(A2)	1	3.596E-6	2.0178
(A1+A2)	1	3.594E-6	2.0178
(B1)	5	3.9296E-7	2.150
(B2)	5	2.6211E-7	2.145
(B1+B2)	5	3.5467E-7	2.146
(C1)	10	4.942E-7	1.926
(C2)	10	4.8433E-7	1.906
(C1+C2)	10	4.8283E-7	1.926

Table III: Estimated diffusivity and equilibrium capacity for EtOH in Ricon polymer

The results of the analyses tabulated in Table II show that the diffusion coefficient of water through the Ricon polymer seems to vary as function of the the polymer thickness. As the thickness of the polymer increases, so does the diffusion coefficient. Previous studies have shown that a concentration-dependent diffusion coefficients can be used to describe transport in various polymers and copolymers.[14] Because of experimental complications, neither of the 10 mm samples in the saturated water experiment could be analyzed. Additionally, because of the limited accuracy of the balance, and the relatively small amount of water that could be absorbed by the polymer, the error in the water calculation is larger than in the EtOH experiment, where more contaminant was absorbed. As is evident from Table II, the observed equilibirum capacity of water in the polymer was only about 0.03%, making it difficult to estimate the diffusion coefficient. However, the estimated value of approx 2.5×10^{-7} cm^2/s for the 5 mm case agrees nicely with values found in the literature for the diffusion of water through a number of different polymers.[12] Here values of 1.1×10^{-7} cm^2/s were reported for the diffusion of water through a poly(ester urethane). Also, for a wide number of polymers, diffusion coeffcients ranging from 1.5×10^{-10} cm^2/s to 1.04×10^{-6} cm^2/s were observed at external water vapor pressures of 0.072 atm

and at an elevated temperture of 36.5°C.[15] With these values in mind, our results seem reasonable. Additionally, literature values for the equilibrium water content in the polymers were found to range from 0.0071 to 0.014.[15] Our observed values are about an order of magnitude less than those previous observations.

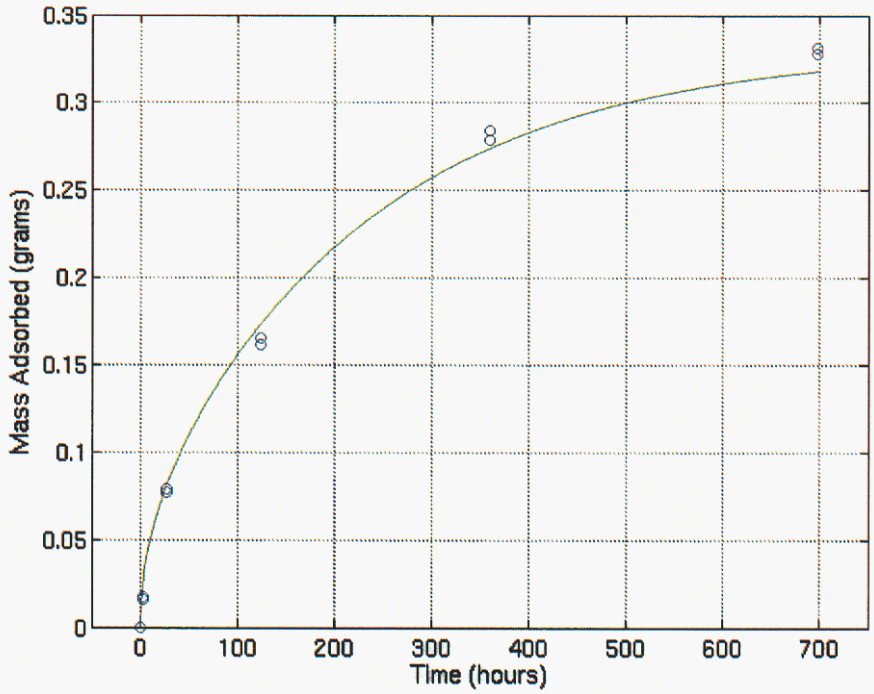

Figure 37: Observed and predicted mass absorbance for 10 mm thick polymer sample in a saturated EtOH gas phase environment.

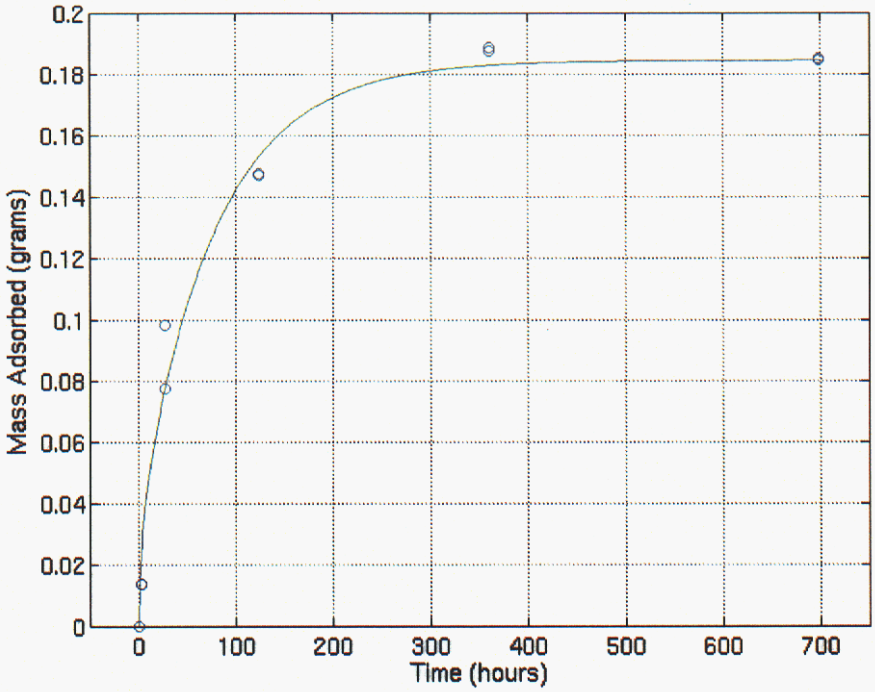

Figure 38: Observed and predicted mass absorbance for 5 mm thick polymer sample in a saturated EtOH gas phase environment.

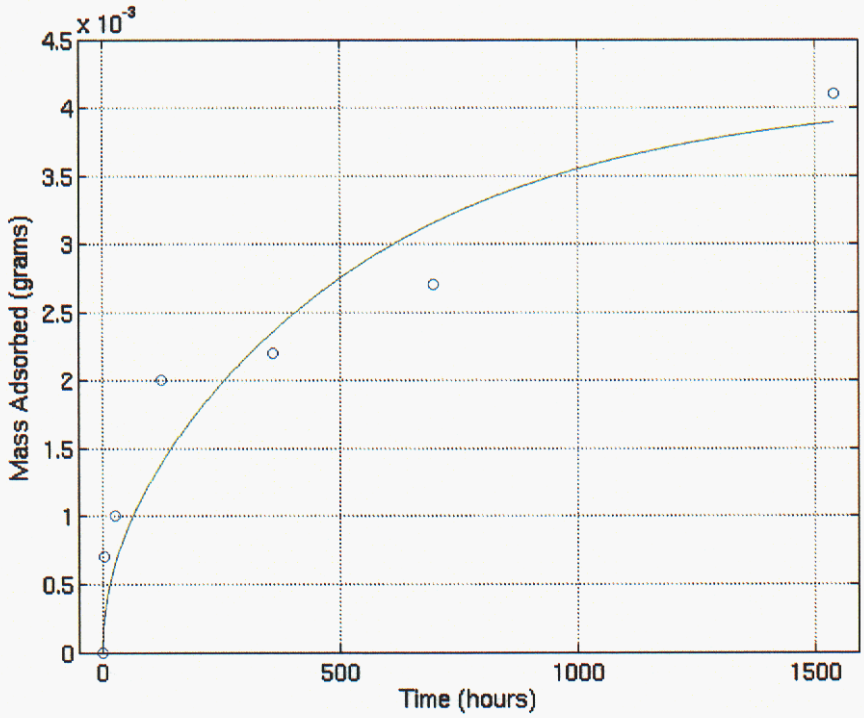

Figure 39: Observed and predicted mass absorbance for 5 mm thick polymer sample in a saturated H_2O gas phase environment.

The results for the ethanol samples are shown in Table III. The same general trends found in the water samples are seen. As the thickness of the polymer sample increases, so does the estimated diffusion coefficient. Perhaps this could result from relatively slow absorption kinetics at the surface, causing a time delay before the surface concentration reaches the equilibrium value that is applied instanteously in the model. The estimated value for the diffusion coefficient of ethanol through the polymer is approximately 3.5×10^{-7} cm^2/s for the 5 mm sample. More accuracy is expected in these measurements and calculations since a larger amount of ethanol, around 2%, could be absorbed when compared to the absorption of water.

Figure 37 through Figure 39 show a comparison of measured data with our model predictions of the weight gain histories for three representative experiments. The fit seems quite good, given the apparent scatter in the data, suggesting that the inferred diffusivities are more than adequate for present purposes.

Overall, we believe that the estimated storage and transport properties of ethanol through the Ricon polymer are very reasonable. However, more work could be done to better estimate the transport and storage properties of water in the Ricon polymer. For example, we might obtain a better estimate for the diffusion coefficient by differentiating the theoretical expression for the M and perform a least squares analysis on the mass absorption rate instead of the mass itself:

$$J_{\min} = \sum_{i=1}^{N_D-1} \left[\frac{\partial M_A^{(S)}(t_i, D)}{\partial t} - \frac{\Delta M(t_i)}{\Delta t} \right]^2. \tag{60}$$

Additionally, we could make allowance for surface kinetics in the modeling or pursue a more accurate method for measuring the mass of the samples. However, for the current endeavor, the determined values appear adequate.

4.4.2 Determination of Getter Properties

In the last section, we analyzed experiments performed to estimate the transport and storage properties of the polymer binder material used to hold the getter particles in the microsystem. In the current section, we analyze a group of experiments that are intended to determine the getter reaction rate in environments that are similar to those expected in actual microsystem applications. These experiments are described in Section 3.5 and are designed to determine the gettering rate of ppm quantities of both ethanol and water using infra-red (IR) spectroscopy to observe the time history of the vapor phase concentration.

In these experiments, the getter is exposed directly to the contaminant in the vapor phase. Thus, the transport of the contaminant through the polymer is not a factor in the current analysis. However, additional experiments for a polymer surrounded the getter were conducted and may be analyzed at a later date. In summary, a small amount of getter material and a drop of water are introduced into a cylindrical chamber having a volume of around 125 ml. The vapor phase composition in the vessel is monitored using IR spectroscopy through transparent windows on the ends of the cylinder. These measurements are used to construct a time history of the water or

ethanol concentration in the vapor phase within the cylinder. After a chosen time, typically around two days, the vessel is briefly opened and another drop is introduced. The process continues until four to five drops have been added. Additionally, a control experiment is also performed. The control contains no gettering material, and drops are added in a manner similar to the experiment containing getter material.

A sample of the data obtained for the control experiment is shown in Figure 40. Here we see an initial quick rise in concentration and then a relatively slow decrease to some steady amount. We attribute this initial rise to the evaporation of the fluid drop into the vessel. The slow decay that follows in this control group is assumed to represent the absorption of the contaminant by a sheet of foil (used to support the getter material in subsequent experiments) and the internal walls of the test chamber. Before the gettering data can be evaluated, these effects must be eliminated to properly identify the effects of the getter. To this end, we model the process using a system of mass balance equations that contain only reaction terms.

There are three regions where contaminant can be present: within the chemical drop itself, within the vapor phase volume of the chamber, or adsorbed on the foil and/or inside walls of the vessel. Balance equations are developed to describe the accumulation within these regions. The mass concentration in the drop is described by the following equation:

$$\frac{\partial \rho_A^{(D)}}{\partial t} = -k_A^{(D)} \left[1 - \frac{\rho_A^{(V)}}{\rho_A^{(V)\max}} \right] \rho_A^{(D)} . \tag{61}$$

The corresponding initial condition is given by the initial mass of the droplet divided by the chamber volume:

$$t = 0 \qquad \rho_A^{(D)} = \rho_{Ao}^{(D)} . \tag{62}$$

In Eq. (61), $\rho_A^{(V)\max}$ is the saturation value of the concentration corresponding to the maximum vapor pressure of the chemical species in the vapor phase. In this equation, and all equations to follow, we define the mass concentration of species A in terms of the volume of the entire vessel region. Using this definition, there is no need to calculate the volume of the water drop as it shrinks. Instead as the drop evaporates, the defined mass concentration will monotonically decrease to zero (if the drop disappears). The reaction rate in Eq. (61), indicates that the contaminant will evaporate until the drop is gone, or the vapor phase concentration reaches its saturated value.

A second equation used to analyze the control experiment describes the amount of mass absorbed by the aluminum foil and other absorption surfaces such as vessel walls that may also physically adsorb contaminants. This equation is:

$$\frac{\partial \rho_A^{(F)}}{\partial t} = k_A^{(F)}\left[1 - \frac{\rho_A^{(F)}}{\rho_A^{(F)\max}}\right]\rho_A^{(V)}, \tag{63}$$

where now $\rho_A^{(F)\max}$ is the maximum concentration of the contaminant on the absorption surfaces. This expression shows that the amount of contaminant adsorbed on the foil and walls is proportional to the concentration of contaminant in the vapor region. However, the rate slows with increasing surface coverage approaching zero as the foil/walls reach their maximum capacity. The initial condition assumes that the foil/walls are initially void of any contaminant.

Finally, a mass balance over the vapor phase can be developed by noting that any mass leaving the droplet enters the vapor phase whereas any mass gain by the foil/walls is lost from the vapor phase:

$$\frac{\partial \rho_A^{(V)}}{\partial t} = k_A^{(D)}\left[1 - \frac{\rho_A^{(V)}}{\rho_A^{(V)\max}}\right]\rho_A^{(D)} - k_A^{(F)}\left[1 - \frac{\rho_A^{(F)}}{\rho_A^{(F)\max}}\right]\rho_A^{(V)}. \tag{64}$$

The initial mass concentration of contaminants within the vapor phase is assumed to be zero.

These three equations are simultaneously solved to obtain the contaminant mass concentration history within each of the three regions. Since the system is closed, we can use an overall mass balance to reduce the number of differential equations that must be solved. The overall material balance for the contaminant is:

$$\rho_A^{(D)} + \rho_A^{(V)} + \rho_A^{(F)} = \rho_A^{o(D)} + \rho_A^{o(V)} + \rho_A^{o(F)}. \tag{65}$$

Using the initial conditions specified above, the mass concentration of the contaminant in the vapor region is written in terms of the concentrations in the other two regions:

$$\rho_A^{(V)} = \rho_A^{o(D)} - \rho_A^{(D)} - \rho_A^{(F)} \tag{66}$$

Substituting this expression back into Eq. (61) and Eq. (63) yields:

$$\frac{\partial \rho_A^{(D)}}{\partial t} = -k_A^{(D)}\left[1 - \frac{\rho_A^{o(D)} - \rho_A^{(D)} - \rho_A^{(F)}}{\rho_A^{(V)\max}}\right]\rho_A^{(D)} \tag{67}$$

$$\frac{\partial \rho_A^{(F)}}{\partial t} = k_A^{(F)}\left[1 - \frac{\rho_A^{(F)}}{\rho_A^{(F)\max}}\right]\left(\rho_A^{o(D)} - \rho_A^{(D)} - \rho_A^{(F)}\right). \tag{68}$$

The system of equations has now been reduced to two differential equations to be solved simultaneously. Once values for $\rho_A^{(D)}$ and $\rho_A^{(F)}$ are known, the vapor phase mass concentration is calculated from Eq. (66).

The experimentally observable quantity is the IR absorption intensity. This value is converted into a mass concentration by identifying the largest IR absorption peak and assuming that this value corresponds to the mass concentration of the chemical species at its vapor pressure. Once the vapor pressure of the chemical is known at experimental conditions the ideal gas law can be used to determine the mass concentration.

$$\rho^{sat(V)}_{A} = \frac{MW_A\, n}{V} = \frac{MW_A\, P^{sat(V)}_{A}}{R\,T}. \tag{69}$$

Using this relationship between IR absorption and mass concentration allows the remaining experimental data to be scaled properly in terms of the value predicted by Eq. (66).

The unknown parameters in Eq. (67) and Eq. (68) are the rate coefficient describing the evaporation of the drop ($k_A^{(D)}$) and the absorption onto the foil/walls ($k_A^{(F)}$). These values can now be estimated using a least squares technique that minimizes the difference between the experimentally observed mass concentration and the theoretically predicted value:

$$\underset{\min}{J} = \sum_{i=1}^{N_D}\left[\rho_A^{(V)}\left(t_i, k_A^{(F)}, k_A^{(D)}, \rho_A^{(F)\max}\right) - \rho_A^{(V)(\exp)}(t_i)\right]^2. \tag{70}$$

Using a value of $\rho_A^{(V)\max}$ calculated from Eq. (69), the methodology allows values of the remaining system parameters in Eq. (67) and Eq. (68) to be estimated.

This procedure was used to analyze the experimental data described in Section 3.5. In these experiments, up to five drops of fluid were added to the cell over the course of the experiment. For each drop, we re-initialized the time scale to the starting time of each individual drop. Thus, each drop is analyzed separately. Once the system comes to steady state after the addition of the first drop, the cell is opened up and another drop is placed on top of the previous drop. Since the system is no longer closed, vapor may leave the system and some contaminant molecules may desorb from the foil/walls. Thus, considering the uncertainty in the initial conditions for subsequent drops, we estimate the required parameters using only the first drop. The results are shown in Figure 40 and Figure 41 for water and ethanol respectively and the results are tabulated in Table IV.

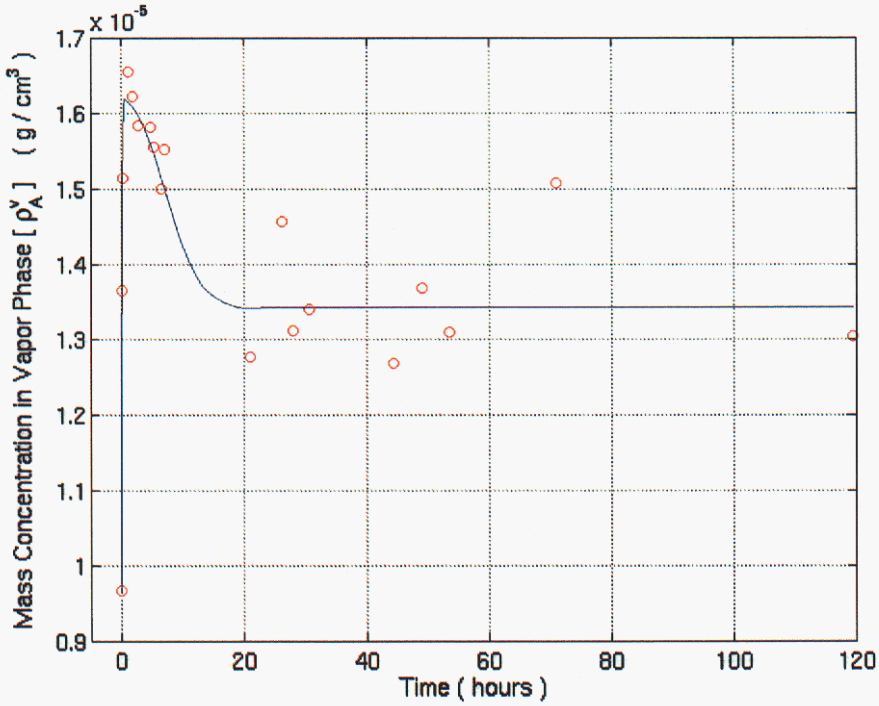

Figure 40: Observed and predicted vapor phase concentration in calibration step using one drop of H_2O

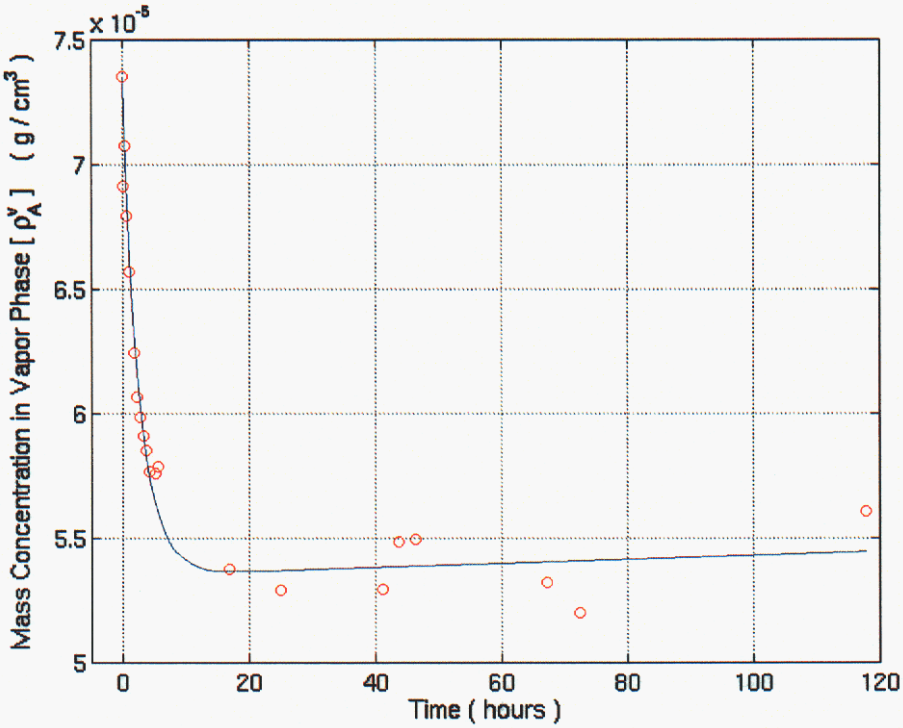

Figure 41: Observed and predicted vapor phase concentration in calibration step using one drop of EtOH

Experiment	$k_A^{(D)}$ hr $^{-1}$	$k_A^{(F)}$ hr $^{-1}$	$\rho_A^{(F)\max}$ g / cm^3
H_2O (1 drop)	1.56	2.28	8.4E-5
H_2O (5 drops)	1.182	2.57	8.6E-5
EtOH (1 drop)	3.17E-4	1.374E-1	1.86E-5
EtOH (2 drops)	1.02E-5	1.177E-1	1.93E-5

Table IV: Estimated evaporation rate ($k_A^{(D)}$), surface adsorption rate ($k_A^{(F)}$), and surface adsorption capacity ($\rho_A^{(F)\max}$) for the control experiments.

Figure 40 shows the observed and predicted responses for the vapor phase concentration as a function of time. The data shows the initial concentration increase due to the evaporation of water molecules from the water droplet. The observed concentration then slowly decays due to adsorption of water molecules on the cell walls and aluminum foil. The concentration then remains constant. The mathematical model does a suitable job in predicting the system response. The scatter in the data at later times is an indication of the level of error present in the measurements. The evaporation of water from the drop and the adsorption of water by the system surfaces are seen to have similar rate coefficients; 1.56 hr $^{-1}$ for evaporation and 2.28 hr $^{-1}$ for absorption. The walls have an inferred maximum capacity of approximately 8.4x10^{-5} g / cm^3 of water.

In the case of the ethanol experiment, Figure 41, the initial evaporation of the ethanol drop happens so quickly that it is not captured in the experimental data. Instead, the ethanol concentration decreases fairly monotonically. Because of this, the estimated value of the rate coefficient for the evaporation process is not expected to be accurate. Nevertheless, the predicted value of the absorption rate should be reasonable since the two processes occur on widely disparate time scales. However, since the goal of analyzing the control data is to isolate the effects of the getter in later experiments, any inaccuracy in the rate coefficient for the evaporation process may affect the inferred gettering coefficient since the evaporation and gettering processes happen on similar time scales.

Table IV shows that the estimated maximum concentration of ethanol on adsorbent surfaces is 1.86E-5 g / cm^3. This value is smaller than the value of 8.4x10^{-5} g / cm^3 estimated for the water experiment. The rate coefficient for the absorption of ethanol on system surfaces is 1.37x10^{-1} hr $^{-1}$ which is approximately an order of magnitude less than for the water system. The decrease in both of these quantities may be a result of the difference between water and ethanol's attraction to the cell surfaces.

In each of the experiments, multiple droplets were added to the chamber. The above analysis has been limited to the initial drop because the initial concentrations for the first drop are known

fairly accurately. When adding an additional drop, the cell is opened and it is no longer possible to explicitly track the movement of vapor components within the system. However, if one is willing to make some assumptions regarding the percentage components leaving the cell during replenishment, it is possible to estimate system parameters by analyzing the entire series of drops.

For the analysis of the sequential drops, the initial conditions/concentrations in Eq. (62) and the corresponding initial conditions for the surface concentrations and the getter region must be modified. As a first estimate, we set the initial concentrations to some fraction of the steady state value obtained during the previous drop. For example, the concentration and size of the fluid drop must now incorporate the 10 microliter drop that is added, plus any residual fluid remaining from previous drops. Therefore, when analyzing the kth drop, the initial condition can now be written as:

$$t^k = 0 \qquad \rho^{k\,(D)}_{A} = \rho^{k\,(D)}_{Ao} + \rho^{(k-1)\,(D)}_{A-SS}, \tag{71}$$

where $\rho^{(k-1)\,(D)}_{A-SS}$ is the steady state value obtained in the previous drop (k-1):. Similarly, the initial condition for the foil region can be written as a percentage of the previous drops steady state:

$$t^k = 0 \qquad \rho^{k\,(F)}_{A} = A^{(F)}_{A}\, \rho^{(k-1)\,(F)}_{A-SS}. \tag{72}$$

Performing the same least squares analysis as before, but using the experimental data from all available drops and the new initial conditions, we can again estimate the desired system parameters. In the analysis, a value of 0.5 was used for $A^{(F)}_{A}$, which implies that once the cell is opened, approximately half of the contaminant adsorbed onto the system walls is desorbed. The results are shown for the water experiments in Figure 42 and for the ethanol experiments in Figure 43. The determined parameters are tabulated in Table IV where they can be compared to the values obtained from the analysis of a single drop.

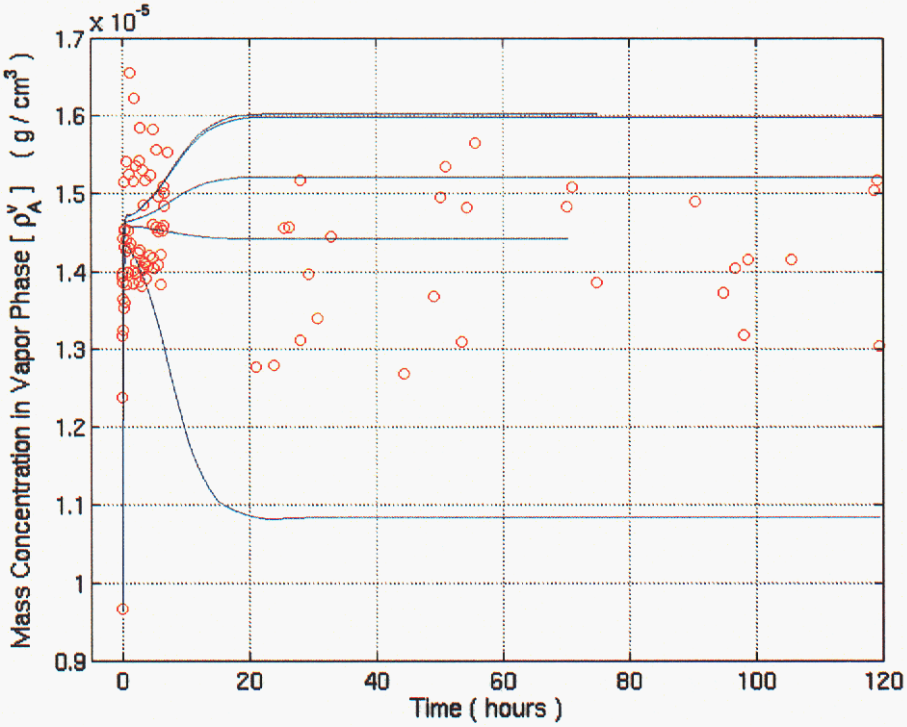

Figure 42: Observed and predicted vapor phase concentration in calibration step using five drops of H_2O

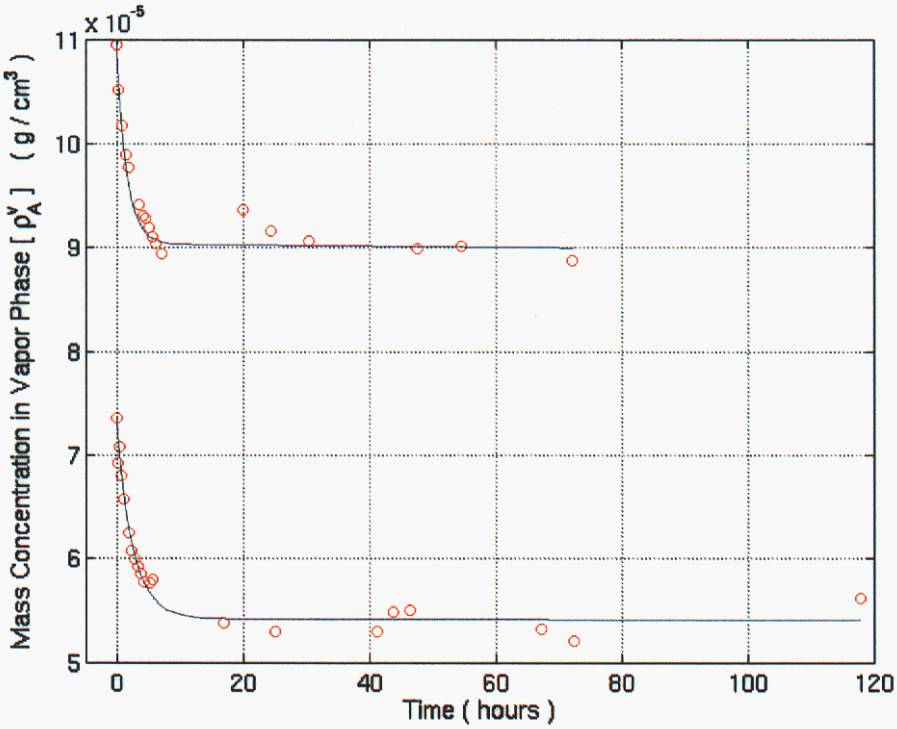

Figure 43: Observed and predicted vapor phase concentration in calibration step using two drops of EtOH

Figure 42 shows the results for the water drop control experiment. Here, five drops were added over the course of the experiment. A single set of parameters was estimated to describe all five data sets. Trends in the predicted responses are much easier to identify than in the experimental data itself. The lowest line describes the predictions of the initial drop. Each additional line represents another drop. The scatter in the data itself makes it difficult to assess the results other than to say that the predicted values do a good job of bounding the experimentally observed values. The initial evaporation effects seen in the later drops between one and two hours are not observed in the predicted values. It is believed this is due to our inability to specify accurate initial conditions for all the drops after the first. This being said, the agreement between the rate constants inferred from one drop and five drops is remarkably good. The estimated rate coefficient for the evaporation effects is determined to be 1.182 hr^{-1} compared to the value of 1.56 hr^{-1} obtained in the single drop case. Additionally, the estimated parameters for the adsorption coefficient and maximum adsorption capacity concentration are even closer.

The results for the ethanol drop experiments are easier to evaluate. Figure 43 shows that both of the drops in the EtOH experiments are predicted well. As noted before, the initial evaporation of the EtOH drop is not captured by the experiment and so the inferred value of the evaporation coefficient is expected to be unreliable but inconsequential. Moreover, the value obtained for the adsorption rate coefficient and the maximum capacity of the cell walls and foil are very consistent with the results obtained from the analysis of the single drop (See Table IV).

Having estimated the relevant system parameters in the control experiments, we are now in a position to describe a new experimental system that additionally includes getter material. The effects of evaporation and absorption that are present in the control experiments can be accounted for in the remaining experiments so that the response of the getter can be isolated and analyzed separately.

To this end, we now analyze a second set of experiments where a known amount of getter material was included within the vessel in addition to the foil and contaminant drop. An additional equation is required to describe the uptake of the contaminant by the getter. This expression is similar to the one used to describe the adsorption of contaminant by the system surfaces/foil (Eq. (63)):

$$\frac{\partial \rho_A^{(G)}}{\partial t} = k_A^{(G)} \left[1 - \frac{\rho_A^{(G)}}{\rho_A^{(G)\max}} \right] \rho_A^{(V)} . \tag{73}$$

For simplicity, it is assumed that the getter is initially free of any contaminant. Equation (73) is written in terms of $\rho_A^{(G)\max}$, the total capacity of contaminant that the getter is capable of holding at a specified loading. This quantity, which varies with the contaminant concentration in the adjacent region, must be determined by experimental analysis. In the current model, we represent $\rho_A^{(G)\max}$ as a linear function of $\rho_A^{(V)}$ in a manner similar to the solubility function used to describe the maximum or equilibrium concentration in the polymer material

$$\rho_A^{(G)\max} = A\rho_A^{(V)} + B . \tag{74}$$

While more complicated forms may be used, the linear approach appears reasonable. The additional parameters, A and B, will be estimated in the least squares analysis.

As in the previous analysis, we use an overall mass balance to reduce the number of differential equations that must be solved simultaneously. This balance is expressed as:

$$\rho_A^{(D)} + \rho_A^{(V)} + \rho_A^{(F)} + \rho_A^{(G)} = \rho_A^{o(D)} + \rho_A^{o(V)} + \rho_A^{o(F)} + \rho_A^{o(G)} , \tag{75}$$

which is reduced to the following form when using the specified initial conditions:

$$\rho_A^{(V)} = \rho_A^{o(D)} - \rho_A^{(D)} - \rho_A^{(F)} - \rho_A^{(G)} . \tag{76}$$

Substituting this expression back into the reaction equations yields:

$$\frac{\partial \rho_A^{(D)}}{\partial t} = -k_A^{(D)}\left[1 - \frac{\rho_A^{o(D)} - \rho_A^{(D)} - \rho_A^{(F)} - \rho_A^{(G)}}{\rho_A^{(V)\max}}\right]\rho_A^{(D)} \tag{77}$$

$$\frac{\partial \rho_A^{(F)}}{\partial t} = k_A^{(F)}\left[1 - \frac{\rho_A^{(F)}}{\rho_A^{(F)\max}}\right]\left(\rho_A^{o(D)} - \rho_A^{(D)} - \rho_A^{(F)} - \rho_A^{(G)}\right). \tag{78}$$

$$\frac{\partial \rho_A^{(G)}}{\partial t} = k_A^{(G)}\left[1 - \frac{\rho_A^{(G)}}{\rho_A^{(G)\max}}\right]\left(\rho_A^{o(D)} - \rho_A^{(D)} - \rho_A^{(F)} - \rho_A^{(G)}\right). \tag{79}$$

Using the system parameters determined in the analysis of the control experiment (Table IV), Eq. (77) – Eq. (79) are solved simultaneously to obtain concentrations in the drop, getter, and foil regions. Equation (76) is used to predict the gas phase vapor concentration, $\rho_A^{(V)}$. These predictions are then used in a least squares analysis to estimate values of $\rho_A^{(G)\max}$ and $k_A^{(G)}$ using an objective function similar to the one in Eq. (70):

$$\underset{\min}{J} = \sum_{i=1}^{N_D}\left[\rho_A^{(V)}\left(t_i, k_A^{(G)}, \rho_A^{(G)\max}\right) - \rho_A^{(V)(\exp)}(t_i)\right]^2. \tag{80}$$

This analysis is now applied to the experimental data obtained in Section 3.5. Here, getter material is included within the cell/vessel. The results, using only the first drop for both water and ethanol experiments are shown in Figure 44 and Figure 45. The estimated parameters are reported in Table V.

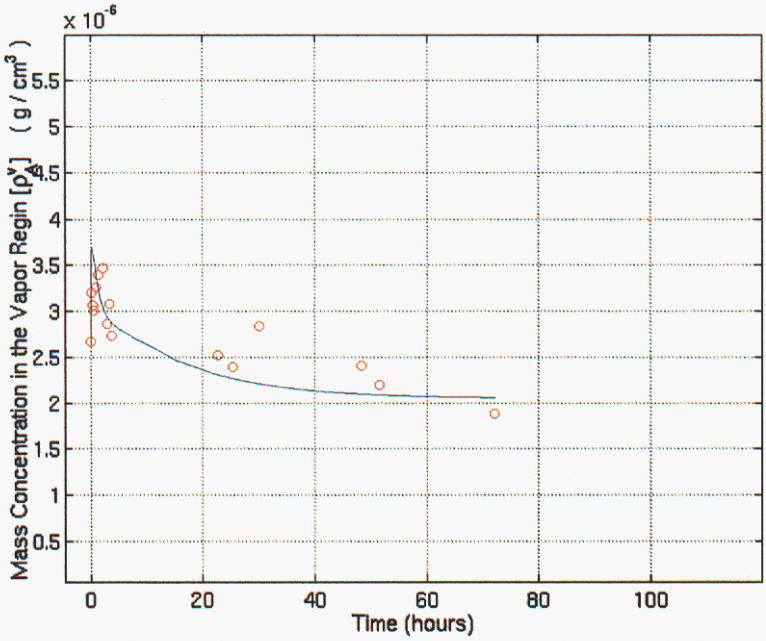

Figure 44: Observed and predicted vapor phase concentration with getter using one drop of H_2O

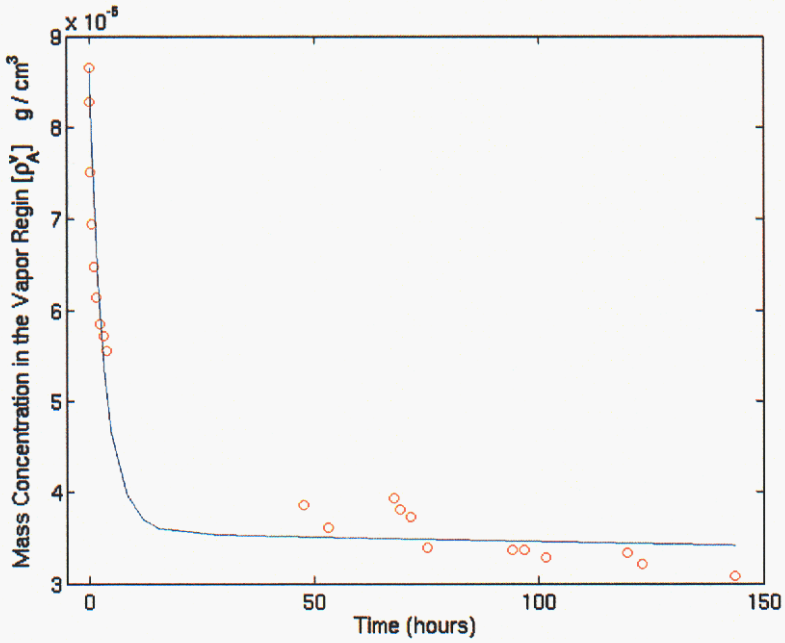

Figure 45: Observed and predicted vapor phase concentration with getter using one drop of EtOH

Experiment	$k_A^{(G)}$ hr^{-1}	$\rho_A^{(G)\max}$ g / cm^3
H_2O (1 drop)	45	1.9257E-4
H_2O (4 drops)	20	1.9258E-4
EtOH (1 drop)	0.244	2.7985E-4
EtOH (4 drops)	0.199	6.0769E-4

Table V: Estimated getter rate ($k_A^{(G)}$) and getter capacity ($\rho_A^{(G)\max}$) for PMA getter.

As in the previous control experiments, several drops of contaminant were added to the cell over the course of the experiment. Similar to the above analysis, the time scale was re-initialized for each drop so they could be analyzed separately. Between drops, the entire cell is opened to the atmosphere, changing the boundary conditions in the manner explained previously. As in Eq. (72), the initial condition in the getter region is specified in terms of the steady state value reached in the previous drop:

$$t^k = 0 \qquad \rho_A^{k(G)} = \rho_{A-SS}^{(k-1)(G)} . \tag{81}$$

Here it is assumed that the initial concentration in the getter region for the kth drop is the steady state concentration reached in the previous drop. This condition seems reasonable since contaminant held within the getter material is irreversibly reacted rather than being reversibly adsorbed. The results are shown graphically in Figure 46 for the sequential drops of water and in Figure 47 for the sequential drops of EtOH. Overall, the relationship between the experimentally observed quantities and those predicted by the model are quite satisfactory given the simplicity of the developed model.

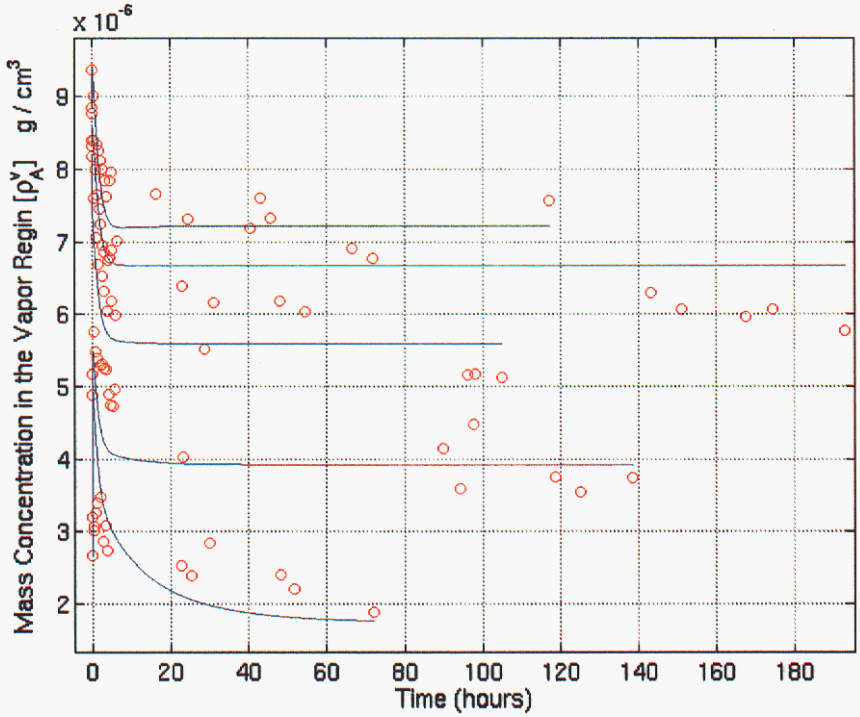

Figure 46: Observed and predicted vapor phase concentration with getter using five drops of H_2O.

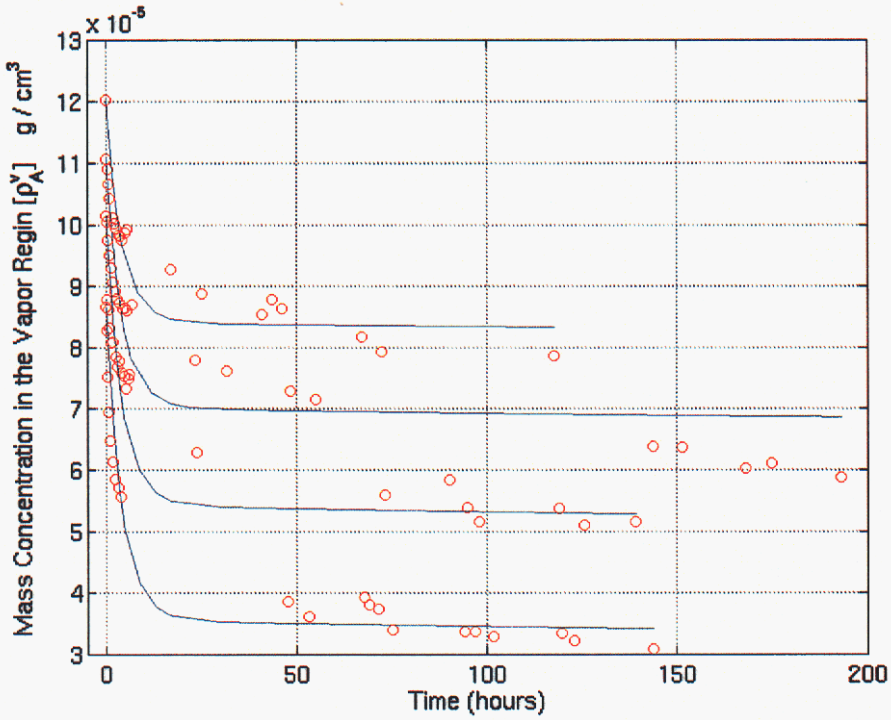

Figure 47: Observed and predicted vapor phase concentration with getter using four drops of EtOH.

5. Project Summary and Future Work

In anticipation of future microsystem packaging concerns, we have explored several potential getters that could be used to ensure an ultra-clean environment. These getters rely on a new approach by taking advantage of strong covalent chemical bonds. To help guide experiments and predict system performance, numerical transport models were also developed.

Absorption based getters for non-reactive volatiles were evaluated by solid phase micro-extraction (SPME). Polydimethylsiloxane and a high surface area carbon in polydimethylsiloxane coatings on the SPME fibers were used to evaluate a particular carbon as an absorption based getter for the model compounds hexamethyl disiloxane (HMDS), perfluorohexane (PFH), ethylbenzene (EB) and 1,1,1-trichloroethane (TCE). The carbon-loaded fiber showed continued desorption of ethylbenzene as the injection port temperature was raised to 250°C, indicating a higher affinity or thermal stability for the carbon-ethylbenzene association. The temperatures required to desorb the ethylbenzene is a positive sign that this carbon, and possibly others, will hold on to hydrocarbons fairly well as part of a getter system.

One poly isocyanate based polymer **1** and two anhydride based polymers, poly (maleic anhydride-*alt*-1-octadecane) **(PMA) 2** and poly (ethylene-*alt*-maleic anhydride) **(PEMA) 3** were evaluated as moisture and alcohol getters. Each of these getters functioned as predicted by chemically reacting out volatile species in sealed environments with varying efficiencies. PEMA **3** performed best as a getter material for two reasons: 1) PEMA **3** did not require a catalyst to activate the polymer for reaction with water as was observed for both **1** and **2**, and 2) PEMA **3** inherently possessed the best theoretical gettering capacity with calculated values of 14.3, 36.5, and 47.6% weight change for reaction with water, ethanol, and iso-propanol, respectively. PEMA **3** was proven to be an excellent getter for water and ethanol as shown by weight change values upon exposure to these species. For both water and ethanol, PEMA **3** reached its theoretical conversion capacity after 1 and 2 months, respectively, under saturated exposure conditions. Although PEMA **3** reaction with iso-propanol occurred at a much slower rate, gettering occurred steadily upon exposure. IR spectroscopy was used to evaluate the extent of reaction for each of the getter materials with water, ethanol and iso-propanol under saturated conditions. The technique was ideal for monitoring characteristic functional group changes over time.

Infrared spectroscopy was used to test PEMA, 5Å molecular sieves, Ricon, PEMA in Ricon, 5Å molecular sieves in Ricon, GA2000, and Hicap for their ability to remove a limited supply of gas phase water or ethanol from a closed reaction cell. Deuterated isotopes of water and ethanol were used to eliminate common interferences in the IR spectra allowing for accurate measurement of their gas phase concentration. The commercial getters GA2000 and Hicap worked well at removing water, but are not rated for other contaminates such as alcohols. PEMA **3** and 5Å molecular sieves also proved effective at removing water and, at a slower rate, ethanol.

Each getter absorbed the contaminants at a rate that decreased as the getter was loaded up. Since the liquid drop provided a constant source of contaminant, the amounts of gas phase contaminates were seen to increase although the getter was still functioning. Over time, the contaminate levels are expected come down. Additionally, mixing the PEMA or 5Å molecular

sieves with Ricon (polybutadiene) slowed the absorption of water and ethanol. Such an effect is beneficial in that it allows more time to apply the getter to a specific microsystem before it can be substantially filled with residual contaminants present during packaging. Future tests should examine the getters performance at removing the actual contaminants that are expected in a particular microsystem, as well as the effect of combining PEMA for irreversible gettering and 5Å molecular sieves to absorb non-reactive compounds into a single getter.

In the modeling portion of this work we have developed and applied one- and two-dimensional numerical models of contaminant species transport within a representative microsystem package consisting of an open gas-filled volume adjacent to a polymer layer containing embedded particles of microporous gettering material. The one-dimensional model assumes a homogeneous distribution of gettering material within the polymer/getter slab, as appropriate when getter particles are much smaller than the slab thickness. The complementary two-dimensional model features explicit representation of the individual getter particles, as necessary when the particle size is comparable to the layer thickness.

The one-dimensional results clearly illustrate that contaminant transport within the vapor phase is extremely rapid compared to that within the polymer/getter layer, such that the contaminant concentration is always nearly uniform within the gas volume. Thus, getter placement within the microsystem only becomes important when some regions of the vapor volume are poorly connected to the primary gas volume. Nevertheless, it is recommended that the getter material be collocated with the entry point of a contaminant leak path or adjacent to those items that require greatest protection if possible.

Gettering rates are generally controlled either by the reaction kinetics of the bare getter material or by diffusion through the polymer binder. Diffusion within the getter particles is not a rate limiting process because the diffusivity within the particles greatly exceeded that of the surrounding polymer binder. The relative rates of reaction and polymer diffusion are characterized by the dimensionless parameter, N, defined in Eq. (34). When a Ricon polymer binder is used in a water gettering system, the parameter N takes a value of about 267, indicating that the reaction rate is much faster than the polymer diffusion rate. In this instance diffusion is clearly the rate limiting process. However, in getting of ethanol, we estimate $N = 0.3$ which implies that both the reaction rate and diffusion play an important part in system dynamics. Several example calculations were presented to illustrate the influence of the parameter N on gettering performance.

A two-dimensional mathematical model was also developed and used to study the effects of differing diffusivities and differing volume fractions of the getter and polymer phases. To first order, it was found that the overall time required for loading of the getter to full capacity was nearly the same for getter particle volume fractions of 20% and 40%. Apparently the doubling of getter capacity was offset by the increased transport through the getter phase that has diffusivity far greater than that of the polymer binder. However, it is not expected that this invariance of loading time will hold when the imbalance between volume fractions of the two phases becomes more extreme.

Application of the developed models to specific microsystems and getter materials requires characterization of the transport and reactive properties of the system. Computational methodologies for deducing these properties from experimental data were developed and tested. In Section 4.4.1, a technique for determining the diffusion coefficient of a particular contaminant through a polymer material was developed and used to obtain diffusion coefficients for ethanol and water through the polymer binder material, Ricon. In Section 4.4.2, a methodology for quantitative analysis of getter reactive properties was developed and used to estimate reactive parameters for PEMA, the particular getter of interest. This methodology utilized least squares fitting of predicted values to measured data, taking into account the evaporation rate of test droplets, and adsorption on experimental hardware surfaces, as well as the targeted process of reaction and adsorption on bare getter surfaces.

While much was accomplished in the areas of model development, experimental data analysis, and parameter estimation, these activities also serve as the foundation for future expansion of databases and future studies of system design and performance. A wealth of information remains to be extracted from many of the experiments described in Section 3. In addition, the developed models can play an important role in evaluating the sensitivity of current microsystem packages to various design parameters and storage conditions as well as aiding in the design and optimization of new systems.

Model calculations can provide guidance in optimal placement of the getter material, particularly in complex packages having partially isolated regions and multiple ingress passages. In addition, numerical analysis can be used to design new systems having tailored gettering kinetics - perhaps controlled by the choice and thickness of low diffusivity polymer binder layer. Using the models, unique gettering strategies can also be analyzed without the need for costly laboratory experiments. For example, a system having multiple layers of getter material and or polymer matrix could be evaluated and the reactive and transport properties of the system tailored to yield some desired objective. One such system might include a relatively fast and reversible getter and a slower, but irreversible getter. One could imagine that this system would handle contaminant bursts very well in that the fast reversible getter would quickly absorb the bulk of the contaminant to protect the microsystem in the short term. Then, as the contaminant is desorbed from the reversible getter, it would be adsorbed irreversibly into the other getter material. A large number of potential layouts could be evaluated in a reasonable amount of time at a relatively low cost.

The life-cycle performance of a specific system can also be simulated using the developed models. Either the one or two-dimensional models can be implemented using alternative boundary conditions to describe typical lifecycle events. The amount of getter loading suffered during packaging would first be evaluated. The possible consequences of unintended isolated or episodic events such as several short bursts of influx can be readily evaluated, as well as the expected internal concentrations and dew point corresponding to a steady influx through a partially sealed surface or the steady desorption of contaminant molecules from internal surfaces, organics, or trapped vapor spaces within the package.

In any case, the developed analysis methodologies help form a framework for continued work and analysis in designing and evaluating microsystems of the future.

This page intentionally left blank

6. Acknowledgements

The authors would like to thank summer student Seth Carmody (formerly of Dept 8762, currently at Ithaca College) for his experimental work in Sections 3.3 and 3.4 of this work. Additionally, we would also like to acknowledge the significant contributions by Serge Tchikanda in the Fluid and Thermal Science Department (8752) and his work on the computational aspects of the problem using MATLAB. We would also like to thank Steve Thornburg (1812) for his contribution on measuring concentrations in actual microsystems and for the photo presented in Figure 18.

This work was supported by Laboratory Directed Research and Development (LDRD) funding. For this, the authors are grateful.

This page intentionally left blank

7. References

1. Brinkman Report-Physics Survey Committee of the National Research Council, (1986).

2. Thornberg, S. and Borek, T., "W80 Gas Analysis Report" SAND99-0157, February (1999).

3. Olah, G., Fung, A. and Miedar, D, Synthesis, 280, (1981).

4. Yu, L.; Li, J.; Wang, P. G., J. Org. Chem. (1997), vol *62*, 3575.

5. Ko, Wen H. Packaging of Microfabricated Devices and Systems, Materials Chemistry and Physics 42 (1995) pp. 169—175.

6. M. M. Visser, S. T. Moe, and A. B. Hanneborg, Diffusion at Anodically bonded interfaces, J. Micromech. Microeng. 11 (2001) pp. 376—381.

7. Gillen, Kenneth T. Green, Peter F., Moisture Permeation of Environmental Seals Used in Weapons, SAND REPORT SAND92-2651 Feb 1993.

8. S. Mack, H. Baumann, U. Gosele, H. Werner, and R. Schlogl, Analysis of Bonding-Related Gas Enclosure in Micromachined Cavities Sealed by Silicon Wafer Bonding, J. Electrochem. Soc. Vol 144, No. 3. March (1997) pp. 1106—1110.

9. W. H. Weber, M. Zanini-Fisher, and M. J. Pelletier, Using Raman Microscopy to Detect Leaks in Micromechanical Silicon Structures, Applied Spectroscopy, Volume 51, Number 1, (1997) pp. 123—129.

10. Keenan, M. R., Moisture Control in Sealed Electronic Packages, SAND REPORT, SAND89-2106 February 1990.

11. George, Soney C., and Thomas, Sabu, Transport phenomena through polymeric systems, Prog. Polym. Sci. 26 (2001) pp. 985--1017

12. Salazar, Michael R., Thompson, Shelley L., Laintz, Kenneth E., and Pack, Russell T., Degradation of a Poly(ester urethane) Elastomer. I Absorption and Diffusion of Water in Estane 5703 and Related Polymers, Journal of polymer science. Part B, Polymer Physics (2002) vol 40 issue 2 pp. 181—191.

13. Taqvi, Syed M. Yishnoi, Anurag, and Levan M. Douglas, Effects of Macropore Convection of Mass Transfer in a Bidisperse Adsorbent Particle, Adsorption 3, (1997) pp. 127—136.

14. Marais, S, Nguyen, Q. T., Devallencourt, C, Metayer, M, Nguyen, T. U., and Schaetzel, P., Permeation of Water through Polar and Nonpolar Polymers and Copolymers: Determination of the Concentration-Dependent Diffusion Coefficient, Journal of Polymer Science: Part B: Polymer Physics, Vol. 38 (2000), pp 1998—2008.

15. Yoon, Jin-San, Hung Hae-Won, Kiim, Mal-Nam, and Park, Eun-Soo, Diffusion coefficient and Equilibrium Solubility of Water Molecules in Biodegradable Polymers, Journal of Applied Polymer Science, Vol 77 (2000) pp. 1716—1722

8. Distribution

1	MS-FJ39	Jim Schicker Honeywell Int'l Federal Manufacturing & Technologies 2000 E. 95th Street, M/S FJ39 Kansas City, MO 64131-3095 Attn: J. Schicker, D/MF3,
1	MS 0866	S. M. Thornberg, 1812
1	MS 0886	M. J. Kelly, 1822
1	MS 0886	M. R. Keenan, 1812
1	MS 1076	A. D. Oliver, 1745
1	MS 1078	K D. Hanselmann, 1314
1	MS 1310	F. W. Sexton, 1762
1	MS 1310	F. J. Peter, 2614
1	MS 9001	M. E. John, 8000 Attn: R. H. Stulen, 8100 D. R. Henson, 8200 W. J. McLean, 8300 P. N. Smith, 8500 K. E. Washington, 8900
1	MS 9042	C. D. Moen, 8752
1	MS 9042	P. A. Spence, 8774
1	MS 9161	W. R. Even, 8760
1	MS 9161	E.-P. Chen, 8763
1	MS 9161	D.L. Medlin, 8761
1	MS 9401	J. E. M. Goldsmith, 8751

1	MS 9401	S. W. Tchikanda, 8752
1	MS 9402	C. H. Cadden, 8772
1	MS 9402	J. C. F. Wang, 8773
1	MS 9402	S. K. Griffiths, 8752
4	MS 9402	J. T. Hollenshead, 8752
2	MS 9402	R. H. Nilson, 8752
1	MS 9403	T. J. Shepodd, 8762
10	MS 9403	L. L. Whinnery, 8762
5	MS 9403	J. R. McElhanon, 8762
1	MS 9403	G. M. Buffleben, 8762
1	MS 9403	T. Zifer, 8762
1	MS 9403	P. M. Dentinger, 8762
1	MS 9404	G. D. Kubiak, 8750
1	MS 9405	J. M. Hruby, 8700
1	MS 9405	K. L. Wilson, 8770
1	MS 9409	W. C. Replogle, 8771
1	MS 9409	J. R. Garcia, 8754
1	MS 0323	D. Chavez, LDRD Office, 1011
3	MS 9018	Central Technical Files, 8945-1
2	MS 0899	Technical Library, 9616
1	MS 9021	Classification Office, 8511 for Technical Library, MS 0899, 9616 DOE/OSTI via URL